Molecular Mechanisms of Heart Development and Trabeculation

GOETHE
UNIVERSITÄT
FRANKFURT AM MAIN

MAX-PLANCK-GESELLSCHAFT

Dissertation
zur Erlangung des Doktorgrades
der Naturwissenschaften

vorgelegt beim Fachbereich 15
der Goethe-Universität
in Frankfurt am Main

von
Filomena Ricciardi
aus Frankfurt am Main

Frankfurt 2015
(D30)

Vom Fachbereich   der

Goethe Universität als Dissertation angenommen.

Dekan:

Gutachter:

Datum der Disputation:

SUPERVISED BY

Prof. Dr. Felix B. Engel
Experimental Renal and Cardiovascular Research
Department of Nephropathology
Institute of Pathology
Friedrich-Alexander-Universität Erlangen-Nürnberg (FAU)
Erlangen, Germany

Prof. Dr. Didier Y. Stainier
Department of Developmental Genetics
Max Planck Institute for Heart and Lung Research
Bad Nauheim, Germany

Eidesstattliche Erklärung:

Hiermit versichere ich, dass ich die Dissertationsschrift selbstständig verfasst und keine anderen als die angegebenen Quellen und Hilfsmittel benutzt habe, alle Ausführungen, die anderen Schriften wörtlich oder sinngemäß entnommen wurden, kenntlich gemacht sind und die Arbeit in gleicher oder ähnlicher Fassung noch nicht Bestandteil einer Studien- oder Prüfungsleistung war.

Filomena Ricciardi

"Ein Gelehrter in seinem Laboratorium ist nicht nur ein Techniker; er steht auch vor den Naturgesetzen wie ein Kind vor der Märchenwelt"

Marie Curie, Physikerin und
Chemikerin 1987-1934

Contents

I Abbreviations

ALPM	Anterior Lateral Plate Mesoderm
AMP	Adenosine mono phosphate
AP	Alkaline phosphatase
aPKC	atypical Protein Kinase C
ATP	Adenosine 5'tri phosphate
BSA	Bovine serum albumin
CCV	Common Cardinal Vein
cDNA	Complementary DNA
cds	coding sequence
Cfl1	Cofilin-1
clo	cloche
CRISPR	Clustered Regularly Interspaced Short Palindromic Repeats
CT	Carboxy-Terminal
DAPI	4,6-diamino-2-phenylindole
DC	Duct of Cuvier
DEPC	Diethylpyrocarbonate
dH$_2$O	Distilled water
DIG	Digoxigenin
DMSO	Dimethyl sulfoxide
DNA	Deoxyribonucleic acid
dNTP	Deoxyribonucleotidtriphosphate
dpf	Days post fertilization
DTT	Dithiothreitol
dus	duesentrieb
E.coli	*Escherichia coli*
ECL	Enhanced chemiluminiscence
ECM	Extra Cellular Matrix
EDTA	Ethylenediaminetetraacetic acid
EGFP	Enhanced green fluorescent protein
EGTA	Ethylene glycol tetraacetic acid
EMT	Epithelial Mesenchymal Transition
ErbB2	V-Erb-B2 Avian Erythroblastic Leukemia Viral Oncogene Homolog 2
EtBr	Ethidium bromide
F-actin	Filamentous actin
FAK	Fokal Adhesion Kinase
Flii	Flightless I
g	Acceleration of gravity

g	Gram
G-actin	Globular actin
GalT	Galactosyltransferase
GAPDH	Glyceraldehyde-3-phosphate dehydrogenase
gRNA	guide RNA
HCl	Hydrochloric acid
HEPES	4-(2-hydroxyethyl)-1-piperazineethanesulfonic acid
hpf	Hours post fertilization
HRS	Horseradish peroxidase
ICC	Immunocytochemistry
IHC	Immunohistochemistry
IPTG	Isopropyl-D-1-thiogalactopyranoside
KCl	Potassium chloride
kDa	Kilodalton
KH$_2$PO$_4$	Potassium dihydrogen phosphate
l	Liter
LPM	Lateral Plate Mesoderm
LRR domain	Leucine Rich Repeat domain
M	Molar
MAB	Maleic acid buffer
Memo1	Mediator of cell motility 1
mg	Milligram
MgCl$_2$	Magnesium chloride
min.	Minute
ml	Milliliter
mM	Millimolar
mmol	Millimol
MO	Morpholino
MOPS	3-[N-morpholino] propanesulfonic acid
mRNA	Messenger RNA
MT	Microtubuls
Na$_2$HPO$_4$	Disodium hydrogen phosphate
Na$_2$HPO$_4$	Disodium hydrogen phosphate
NaCl	Sodium chloride
NaN$_3$	Sodium azide
NaOH	Sodium hydroxide
ng	Nanogram
NICD	Notch Intra Cellular Domain

Abbreviations

NP40	Nonidet P40
Nrg1	Neuregulin 1
OD	Optical density
p-Pax	Phospho Paxillin
PAGE	Poly Acryl Gel Electrophoresis
Par6	6 Family Cell Polarity Regulator
Pax	Paxillin
PBS	Phosphate buffered saline
PCR	Polymerase chain reaction
pg	Picogram
pH	Negative logarithm of hydrogen
PMSF	Phenylmethanesulfonyl fluoride
POD	Peroxidase
PTU	N-phenylthiourea
PVDF	Polyvinylidenfluorid
RNA	Ribonucleic acid
Rnase	Ribonuclease
rpm	Revolutions per minute
rt	room temperature
RT-PCR	Reverse transcription followed by polymerase chain reaction
SDS	Sodium dodecyl sulfate
sec	Second
SSC	Saline-sodium citrate

t-tubuls	Transverse Tubuls
TAE	Tris-acetate-EDTA
Taq	*Thermus aquaticus*
TBE	Tris-borate-EDTA
TBS	Tris buffered saline
TE	Tris-EDTA
Tln	Talin
tnnt2	Troponin T type 2 (cardiac)
Tricaine	Ethyl-3- aminobenzoate methanesulfonate
tRNA	Transfer RNA
U	Unit
UTR	Untranslated Region
UTR	Un-translated region
UV	Ultraviolet
V	Volt
v/v	Volume/volume
Vcl	Vinculin
w/v	Weight/volume
WB	Western blot
wea	weak atrium
wt	wild type
X-gal	5-bromo-4-chloro-3-indolyl—D-galactopyranoside

1 Introduction

1.1 Heart Development

Animal development is an inconceivably complex process. From a single fertilized egg an independently viable organism is formed from interconnected organs, which are composed of highly specified cells. The underlying developmental processes are orchestrated in time and space in order to allow morphogenetic changes to occur in a well-defined sequence. In vertebrates the heart is the first organ to develop and function in order to establish blood flow and oxygen supply throughout the developing embryo (Stainier and Fishman, 1992; Yelon et al., 1999). While fulfilling this essential function the heart develops and undergoes morphogenetic changes in order to adapt to the conditions in the growing embryo. These changes however are dependent on the functionality and the workload of the heart itself. Likewise, non-contracting hearts will not undergo certain developmentally important morphological changes that are dependent on contractility and blood flow (Berdougo et al., 2003; Sehnert et al., 2002). In mammals early developmental defects affecting heart function and blood circulation lead to prenatal death due to oxygen deprivation in the developing organs (Chan et al., 2002; Kuo et al., 1997; Lee et al., 1995; Lyons et al., 1995; Molkentin et al., 1997; Tanaka et al., 1999).

In order to study heart development and essential gene functions the zebrafish has proven to be a very useful animal model. Even though the zebrafish heart is two-chambered and might seem very different form a mammalian four-chambered heart, the molecular mechanisms of heart development are highly conserved (Burggren and Crossley, 2002; Opitz and Clark, 2000).

The two-chambered zebrafish heart starts developing in the segementation period from a ventrally located bilateral region of the embryo, the anterior lateral plate mesoderm (ALPM; primary heart field). At around 16 hours post fertilization (hpf) the lateral plate mesoderm (LPM) has already established an asymmetric expression pattern which differentiates the ALPM from the surrounding tissue (Yelon, 2001). Coordinative migration of the bilateral primordia towards the embryonic midline is the prerequisite of

early heart formation and failure of this process leads to the formation of two independent heart tubes, the so-called cardia bifida (Alexander and Stainier, 1999; Schier et al., 1997). Fusion of these areas starts around 19 hpf from posterior, building a v-shaped structure which closes up anteriorly to form the heart cone (Glickman and Yelon, 2002).
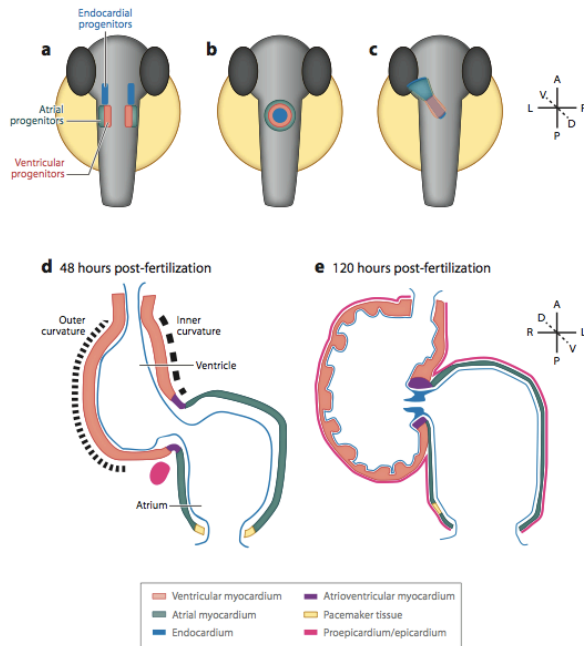
Figure 1.1: Schematic of early zebrafish heart developmental stages.

a-c) Heart development from 12-24 hours post fertilization (hpf). Embryos are shown in a dorsal view. a) At 12 hpf the first heart progenitors are found in the anterior lateral plate mesoderm (ALPM). Ventricular progenitors are located medially from atrial progenitors and both lie dorsally from endocardial progenitors in the ALPM. b) The lateral fields migrate to the midline where they meet to form the heart cone at 19 hpf. c) This cone involutes and elongates asymmetrically in respect to the body axis to form the heart tube, which starts contracting at around 24 hpf. d-e) Heart sections from a ventral view. d) At 48 hpf the two chambers of the heart have started ballooning and looping and the endocardium now lines the lumen of both chambers. The chambers are connected by the atrioventricular myocardium. e) The atrioventricular myocardium forms the atrioventricular canal in which the valves are formed in order to prevent retrograde blood flow. At 120 hpf ventricular chamber specific trabeculae have formed. Figure adapted from (Staudt and Stainier, 2012).

At this stage the heart primordium is already patterned with medially located ventricular precursors expressing the markers cardiac myosin light chain 2 (*cmlc2*) and ventricular myosin heavy chain (*vmhc*); and laterally located atrial precursors positive for *cmlc2* but not *vmhc* (Yelon and Stainier, 1999). After the cardiac fusion is completed the cone extends into a linear heart tube where the ventricular apex of the cone elongates dorsally and becomes tilted to the right side of the embryo (Yelon et al., 1999) (Fig. 1.1 A-C). Parallel to the cone extension the endocardial cells start spreading out, lining the

lumen of the heart primordium (Stainier et al., 1993). The elongated linear tube then starts bending at the atrio-ventricular boundary (AV-boundary) between 24 hpf and 48 hpf and obtains a S-shaped morphology. This looping of the heart causes the ventricle to finally lie on the right side of the atrium (Chen et al., 1997). During the process of morphogenesis the heart starts its function with peristaltic contractions of the entire heart tube as early as 24 hpf. Later, at 36 hpf the two distinct heart chambers contract sequentially (Fishman and Chien, 1997). The heart valves, which prevent retrograde blood flow, start forming at 48 hpf through the formation of endocardial cushions at the atrio-ventricular canal (AVC). By the end of zebrafish embryonic- and the beginning of the larval stages valve flaps will replace these cushions during further morphogenetic changes. From 80 hpf onwards cells of the ventricular wall start to form muscular luminal protrusions, so called trabeculae. The ventricular chamber specific morphogenetic process of trabeculation will allow the heart to adapt to the increasing demands of the growing embryo (Fig.1.1 D,E)

1.2 Trabeculation

Trabeculation is essential for the heart's function. During this phase the heart increases its number of ventricular cardiomyocytes in order to form a strong ventricular wall that is capable of pumping blood throughout the developing organism. Before trabeculation starts the heart chambers resemble simple balloons with a smooth inner surface, which is lined by a single layer of endocardial cells. The first trabeculae appear at around 80 hpf at the outer curvature of the ventricle. They form ridges inside the ventricular wall, which become a highly complex meshwork over time. However, the precise mechanism that initiates trabeculation is unknown.

Different hypotheses have been proposed describing active invagination of cardiomyocytes into the lumen; the endocardium actively evaginating into the myocardial wall; or passive buckling of the chamber wall producing the ridges (Icardo and Fernandez-Teran, 1987; Marchionni, 1995; Sedmera and Thomas, 1996).

Some insights into the molecular mechanism have been provided by the function of signaling pathways involving interactions between the endocardium and the myocardium. Notch1, predominantly expressed in the endocardium at the base of

trabeculating cells, drives expression of bone morphogenetic protein 10 (BMP10) and EphrinB2 (Grego-Bessa et al., 2007). Ablation of the Notch1 intracellular domain (NICD)-inhibitor Fkbp1a leads to hypertrabculation in Fkbp1a endocardial-specific knockout mice (Chen et al., 2013). Similarly, ablation of Numb/Numblike leads to increased Notch2 expression with strong upregulation of BMP10 also leading to hypertrabeculation (Yang et al., 2012). BMP10 regulates cardiomyocyte proliferation independent of EphrinB2, which drives cardiomyocyte differentiation via neuregulin1 (Nrg1) expression (Grego-Bessa et al., 2007).

Neuregulins are growth factors that bind and activate ErbB-receptor tyrosine kinases promoting basic cell functions such as cell survival, proliferation and differentiation. In mouse, Nrg1 is expressed by the endocardium whereas the receptors (ErbB2 and ErbB4) are expressed by myocardial cells. Lack of neuregulin signaling leads to reduced or absent trabeculation in mouse and zebrafish (Liu et al., 2010; Ozcelik et al., 2002). The presence of endocardial cells and the activation of ErbB2/4 receptors are necessary for the initiation of trabeculation in zebrafish larvae. Likewise, cloche mutants (clo) lacking the endocardium do not form trabeculae (Stainier et al., 1995), suggesting that the lack of signaling molecules from the endocardium, such as neuregulin, are essential for this process. Similarly, ErbB-receptor-deficiency leads to the lack of trabeculae in zebrafish and mouse (Liu et al., 2010; Meyer et al., 1997), demonstrating that neuregulin/ErbB2 signaling is essential for the initiation of trabeculation. However, how ErbB2 downstream signaling leads to the invagination of only a subpopulation of ventricular wall cardiomyocytes is unknown.

The characterizations of zebrafish mutants that affect the contractility of the heart and or the blood flow through the heart have provided additional insight into the process of trabeculation. *Thin-filament contractile protein cardiac Troponin T* (*tnnt2*) is essential for sarcomere assembly and cardiac contractility. Zebrafish *silent heart* mutants carrying mutations in the *tnnt2* gene fail to trabeculate (Chi et al., 2008; Sehnert et al., 2002).

The blood flow through the heart itself is important for a variety of cardiac developmental processes, including the formation of AV endocardial-cushions (Hove et al., 2003), the enlargement and elongation of outer curvature cardiomyocytes (Auman et al., 2007) and the maturation of the conduction system (Chi et al., 2008; Sedmera et al.,

2005). Zebrafish weak atrium (wea) mutants carry mutations in the *atrial myosin heavy chain (amhc)* gene (Berdougo et al., 2003). These mutant animals have non-contractile atria and therefore substantially reduced blood flow in the ventricle. The gene mutation does not affect the contractility of the ventricle itself, nevertheless these animals fail to trabeculate, proving, that blood flow is essential for this process.

Taken together, trabeculation is a complex morphogenetic process that is based on the ability of contractile cardiomyocytes to respond to mechanical forces and extracellular matrix (ECM) changes by changing their epithelial like character in order to move out of the compact myocardial layer. This process is based on subcellular functions requiring a highly flexible cytoskeleton, tight control of cell polarity and finally aspects of cell migration.

1.3 Cytoskeleton

The cytoskeleton is, unlike other skeletons, highly dynamic and undergoes constant renewal in order to adapt to the cell's necessities. Forming a complex network throughout the cell, it is involved in almost all cell functions. This network is composed of different kinds of filaments, which in are made of different protein subunits and fulfill distinctive cellular functions, adding to its complexity. The three main components are Microtubules (MTs), Intermediate filaments and Microfilaments.

The largest intracellular filaments are MTs. They are part of the main vesicle transportation system of the cell, establishing apico-basal cell polarity (Bornens, 1991; Ginzburg, 1991; Nelson, 1991). Often, MTs extend from the nucleus, where they nucleate, to the cell edges where they play a significant role in cell migration (Olmsted and Borisy, 1973; Watanabe et al., 2005). Furthermore, they play an essential role in cell division, forming the spindle apparatus, which is the driving force for chromosome segregation into the daughter cells (Inoue, 1981; Inoue and Sato, 1967; Nicklas, 1971). MTs are composed of alpha- and beta-tubulin dimers, which build polarized protofilaments with alpha-tubulin at the minus end and beta-tubulin at the plus end providing MTs directionality. These filaments can only grow on their plus ends by the attachment of another heterodimer. Mature MTs are hollow cylindrical structures with a

width of approximately 28 nm, formed by the conglomeration of thirteen protofilaments forming the tube (Mitchison and Kirschner, 1984; Nogales et al., 1998).

Filamentous Actin (F-actin), on the other hand is composed of globular Actin monomers (G-actin), which polymerize and form polarized microfilaments (6 nm diameter). Similar to MTs they are involved in cell migration, allowing the cell to form protrusions and providing the actual force together with the ATP-dependent motor protein Myosin. But also in dividing cells it is F-actin together with Myosin that forms the constricting ring between the two daughter cells carrying out cytokinesis (Otterbein et al., 2001; Pelham and Chang, 2002). Proteins that bind Actin play a major role in regulating the Actin cytoskeleton-dependent on the cell's status. They are involved in Actin nucleation (Arp2/3 complex) (Pollard, 2007), polymerization (Profilin, Formins) (Baarlink et al., 2010), F-actin stabilization (CapG, CapZ) (Edwards et al., 2014), cross-linking (alpha-Actinin), and destabilization (Gelsolin, Cofilin) (Vavylonis et al., 2005).

Specialized cells however, have specific demands on the composition of their cytoskeleton as well as on its plasticity. Likewise, striated muscle cells develop a highly specialized cytoskeleton that enables them and the organs they form to contract. The basis for this contractility is provided by the sarcomeres, which are highly complex units, composed of many different proteins (Fig. 1.2). The main components however, are F-actin and Myosin. Repetitive sarcomeric units form so called myofilaments, which are organized in myofibrils forming an almost crystalline arrangement (Epstein and Fischman, 1991; Gautel, 2011).
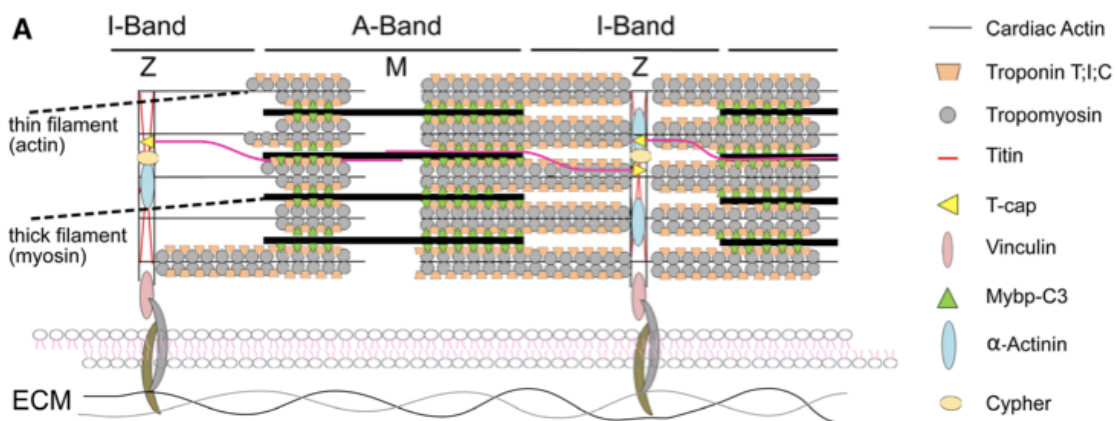
Figure 1.2: Simplified schematic of a sarcomere.

Sarcomeres are the smallest contracting unit of striated muscles. The main components are thin filaments (F-actin) and thick filaments (myosin) which interact in an ATP-dependent manner providing the force for contraction. Vinculin anchors the sarcomeres to the extracellular matrix (ECM) by connecting them to transmembrane proteins. Further stabilization of the sarcomeres is provided by proteins of the z-disc (Titin, T-cap, alpha-Actinin) which, cap and cross connect f-actin filaments. Furthermore proteins like Troponins and Tropomyosins, which are components of thin filaments and are involved in force regulation. Figure from (Reischauer et al., 2014).

The formation of these structures is important for the differentiation of precursor cells into functional muscle fibers of myocytes in skeletal muscle and the heart (McNally and Dellefave, 2009; Telley and Denoth, 2007).

Amongst these and other functions F-actin plays a significant role in the formation focal adhesions. These structures attach the cells to the substratum/basal membrane and promote mechanosensation, allowing cells to respond to changes in the ECM and the cellular environment (Kopecki et al., 2011).

1.4 focal adhesion

Focal-adhesions are complex, macromolecular structures that form at the plasma membrane. The key mechanosensing proteins in these complexes are Integrins, heterodimeric, integral membrane proteins, which can become activated at their extracellular and intracellular domains, therefore being able to transmit signals bidirectionally (Goldmann, 2014).
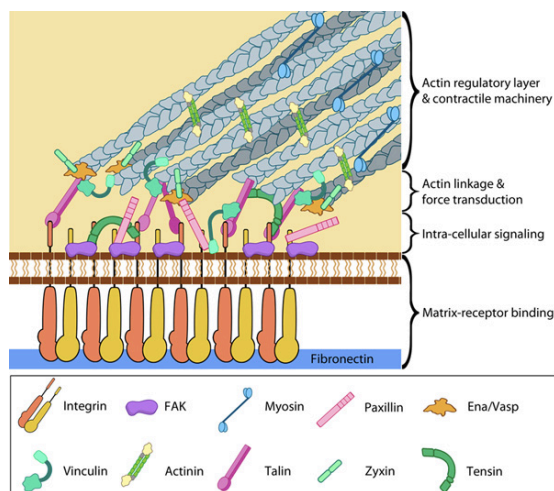
Figure 1.3: Schematic of focal adhesions of migrating cells. Integrins, extracellularly bound to fibronectin, extend through the plasma membrane. Intracellular signaling of integrins is mediated by tyrosine kinases like Focal adhesion kinase (FAK), which can phosphorylate Paxillin upon activation. Ena/Vasp capped and alpha-Actinin-crosslinked, Actin filament bundles extend to focal adhesion sites and become

connected to integrins via Talin, Tensin and Vinculin forming functional mechanosensory units.
http://www.mechanobio.info/topics/methods/super-resolution-microscopy-intro/7_super-resolution-microscopy

This bidirectional signaling allows focal adhesions to modify the structure and rigidity of the ECM. Binding of Talin to the intracellular domain of Integrins leads to a conformational change of their extracellular domains into an active state. This 'inside-out' signaling is important for the formation of cell adhesions (Hirata et al., 2014).

Intracellularly, Talin-activated Integrins are then connected to F-actin through the proteins Vinculin and alpha-Actinin, forming functional focal adhesions. Vinculin is an essential component for the mechanosensation, regulating the recruitment and release of core focal adhesion proteins in a force-dependent manner (Carisey et al., 2013). Focal adhesion-mediated intracellular signaling is in part conducted by protein tyrosin kinases such as Focal Adhesion Kinase (FAK) and Src, which become recruited to focal adhesion sites after extracellular integrin activation (Fig. 1.3, Fig. 1.4, D). Phosphorylation of proteins like the signal transduction adaptor protein Paxillin allows cells to respond appropriately to their environment switching from an adhesive to a motile state and vice versa (Brown and Turner, 2004; Schaller, 2004).
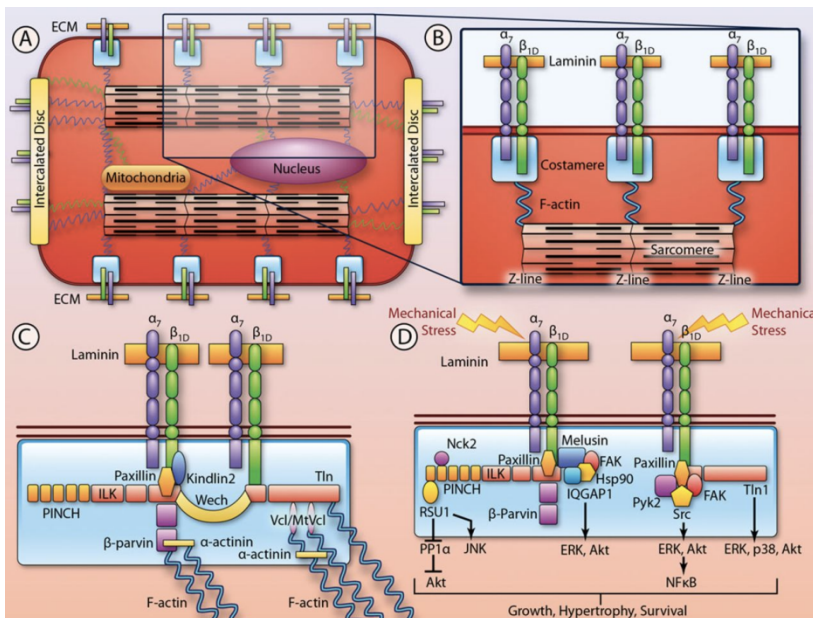
Figure 1.4: Costameric mechanotransduction in cardiomyocytes.

A,B) Simplified schematic of costamreres, myocyte specific focal adhesions sites. A) Integrins are located in the sarcolemma transducing mechanical information from the ECM to the Actin cytoskeleton and the contractile apparatus. B) Closer view of costameres. Integrins connect the sarcolemma to the underlying z-line (z-disc) of sarcomeres by the formation of costameres. C,D)

Costamere components and mechanosensation. C) Integrins, extracellularly bound and activated by Laminin, recruit focal adhesion core complex proteins (Paxillin, Kindlin2, Talin (Tln), beta, Parvin, Vinculin (Vcl) and alpha-Actinin) to the plasma membrane and form functional costameres. D) Upon Integrin activation trough mechanical stress signaling cascades become activated, which regulate cell survival, call growth and hypertrophy. (Israeli-Rosenberg et al., 2014)

In contracting muscle cells, in vivo, structures that resemble focal adhesions are present and form in a specialized way in order to meet the cell's high mechanical burden. These structures are called costameres and are composed of the same core proteins, as classical focal adhesions (Samarel, 2005; Tidball, 1991) (Fig. 1.4, A).

Adapted to muscle cell demands these structures overlay with myofibrillar structures, connecting the contractile apparatus to the sarcolemma (striated-muscle cell membrane) and the ECM (Fig. 1.4, B). These contacts allow muscle cells to respond to changing hemodynamic loads. The sarcolemma of muscle fibers forms transverse tubules (t-tubules) reaching into the fibers allowing fast conduction of action potentials. These t-tubules overlay with costameres and z-discs forming muscle specific focal adhesion which are important for cell survival, growth and differentiation (Brette and Orchard, 2003; Judice et al., 2009; Sorrentino and Gerli, 2003).

1.4.1 Flightless I

The Flightless I (Flii) protein is a component of classical focal adhesion core complexes (Hopkinson et al., 2014). *Flii* null mutations are embryonic lethal due to defective gastrulation associated with disorganized Actin cytoskeleton (Campbell et al., 2002). Mild mutations in this gene however, cause indirect flight-muscle degeneration in *Drosophila melanogaster* (Campbell et al., 1993). Interestingly, it represents the only Gelsolin family member composed of a Leucine-Rich Repeat (LRR) domain, which promotes protein-protein interactions and Gelsolin, an Actin binding domain. Indeed, has been shown to bind G- and F-actin. However, unlike the protein Gelsolin itself, Flii also binds to the DAD domain of Diaphanous-Related Formins, Daam1 and mDia1, via its Gelsolin domains G4-6, regulating their activity in a RhoA-dependent manner (Higashi et al., 2010). Formins are proteins that promote F-actin assembly in order to allow fast changes in cytoskeletal structures. The reduction of Actin polymerization efficiency can

lead to a deficiency in adhesion site turn over and reduced cell migration abilities (Goley and Welch, 2006; Goode and Eck, 2007; Woychik et al., 1990). Fibroblasts overexpressing Flii show reduced Paxillin phosphorylation and increased alpha-Actinin expression, which causes impaired focal adhesion site turnover (Kopecki et al., 2011), suggesting a role for Flii in focal adhesion homeostasis.

Another important role of Flii is its function in wound repair. It has been shown that Flii is a negative regulator of wound healing in mice. Heterozygous *Flii* knockout animals have enhanced wound healing compared to wild type (wt) animals. These, increased wound repair abilities are most likely attributed to improved turnover of adhesion structures, resulting in improved cellular migration and proliferation. This goes in hand with the observation, that cells with reduced *Flii* expression migrate more quickly into the denuded area in a cell scratch assay. Furthermore, the number of adhesions that contained activated beta1 Integrin and Vinculin was 50% reduced in migrating *Flii* knockdown cells compared to wt cells (Kopecki et al., 2011; Mohammad et al., 2012). As in the fruit fly and mouse, mutations in the zebrafish *flii* gene, are lethal. Mutants develop but display skeletal fast-twitch muscle degeneration with impaired burst swimming behavior from 48 hpf onwards (Campbell et al., 1993; Naganawa and Hirata, 2011).

1.5 Cell Polarity (Golgi)

The control and maintenance of cell polarity is important for a verity of cell functions and cell survival. Generation of two distinct surfaces, one facing the outside world (the apical domain) and the other contacting the neighboring cells and basal-extracellular matrix (ECM, basolateral domain), is the most fundamental property of epithelial cells (Manninen, 2015). Polarity is maintained by several factors including the composition of the ECM, the communication between cells and the integration of this information inside of the cell.

Likewise, the organization of MTs along the apico-basal axis of the cell is crucial since it determines the directionality of vesicle transportation by motor-proteins like Kinesins (anterograde or plus-end transport) and Dyneins (retrograde or minus-end transport) (Mitchison, 1986). In turn vesicles containing certain types of membrane proteins might be selectively delivered to the apical or basal side, respectively, thereby

establishing polarization of the cell membranes. Not only the transportation of vesicles but also the localization of the Golgi-apparatus is organized along MTs. This dependence was first shown by fragmentation of the Golgi into several mini-stacks after treatment with MT-depolymerizing drug nocodazole (Rogalski and Singer, 1984). The Golgi-apparatus, which in mammalian cells is a single-copy organelle, fulfills important cellular functions. Besides posttranslational modification of proteins and vesicle formation, it plays an important role in apoptosis, mitosis and cell migration (Millarte and Farhan, 2012). The orientation of the Golgi-apparatus in the cell is dependent on the cell type and status. Epithelial cells classically present an apical localization of the Golgi in respect to the nucleus (Fig.1.5).
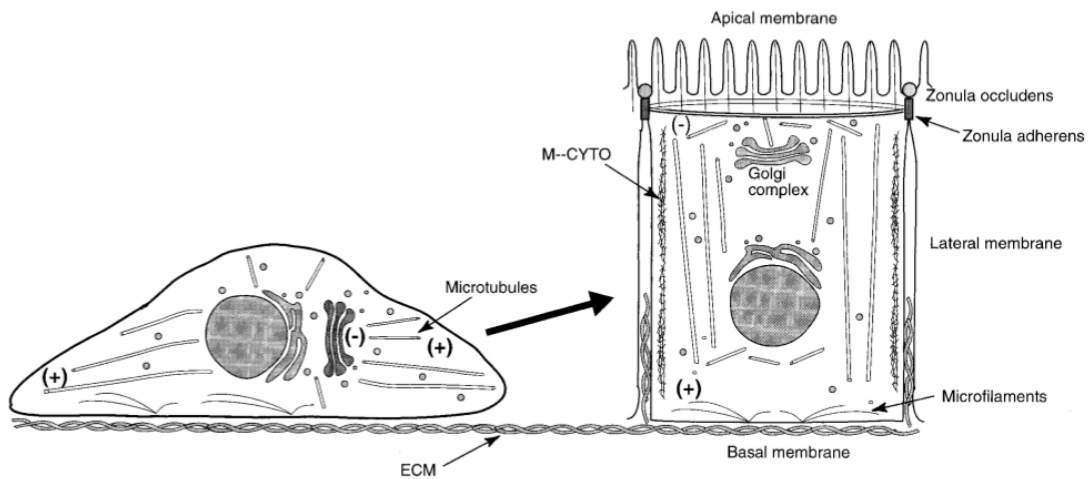
Figure1.5: Schematic of cell polarization in a migrating mesenchymal cell and an epithelial cell. Migrating cells locate their Golgi-apparatus towards the direction of migration in respect to the nucleus. The microtubule network originates from the nucleus and extents, with their plus ends to the cell edges. The formation of a single layered epithelium is primarily driven by the formation of cell-cell contacts. The cell reorient their cytoskeleton in order to establish an apical and a baso-lateral side. The Golgi-apparatus is localized towards the apical surface, and microtubules reach from the basal side (plus end) to the apical side (minus end) allowing unidirectional transport of vesicles in order to maintain the apical and baso-lateral identity of the cell membranes. Figure from (Yeaman et al., 1999)

However, epithelial cells, transforming into carcinoma, often lose their polarized epithelial organization. In breast carcinoma acini (glandular epithelial cells, organized

around a lumen), activation of ErbB2 leads to the disruption of the apico-basal cell polarity with the loss of apical Golgi localization in a Par6/aPKC-dependent manner (Fig1.6). (Aranda et al., 2006)
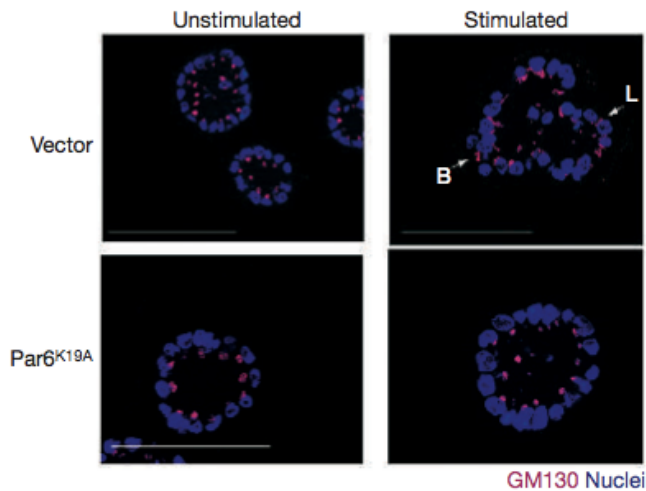
Figure 1.6: Cross sections through day 20 acinar structures. Acinar structures have been stained for nuclei (DAPI) in blue and the cis-Golgi (GM130) in red. Upper left panel: Unstimulated acini co expressing ErbB2 and wt Par6 show uniform localization of the Golgi-apparatus towards the luminal side of the cell in respect to the nucleus. Upper right panel: After stimulation with dimerizer, the acinar structure is lost and the Golgi-apparatus is not longer restricted to a specific localization (B=basal; L=lateral). Lower panels: Expression of a mutant form of Par6 (Par6K19A), which is defective for the binding to atypical PKC (aPKC) inhibits the loss of cell polarization after stimulation. This suggests that the interaction of Par6-aPKC is required for ErbB2-induced disruption of apico-basal cell polarity. Figure from (Aranda et al., 2006).

To date there is not much known about cell polarity of cardiomyocytes *in vivo*. Studies from mouse hearts have shown, that signaling of the small GTPase Rac1 is important for cardiomyocyte polarity in the embryonic heart. Deficiency of Rac1 leads to impaired elongation and cytoskeletal organization of cardiomyocytes (Leung et al., 2014).

Furthermore, it has been shown, that ventricular cardiomyocytes of mouse embryonic hearts are coordinated locally, showing a biased centrosome-nucleus and cell division plane parallel to the heart surface (Le Garrec et al., 2013).

Interestingly, cardiomyocytes of zebrafish hearts show differences in the distribution of cytoskeletal/contractile fibers. Atrial cardiomyocytes start forming a fine meshwork of Actin fibers, which is localized solely on the basal (luminal) side of the

cells at 22 hpf. At 3.5 dpf the myofibril architecture of ventricular cardiomyocytes is distinctive between the basal side, mainly containing thick, cortical sarcomeres, whereas the apical side is mainly comprised of fine sarcomeric structures. These observations indicate an apico-basal cell polarization of cardiomyocytes in the developing vertebrate heart.

1.6 Cell migration

Cell migration is a prerequisite for animal development. The ability of a cell to migrate is dependent on an orchestrated process that involves sensing and transmitting information form the extracellular environment and the rearrangement of cell-adhesions and the cytoskeleton. There are different modes of cell migration dependent on the cell type. 'Amoeboid', highly motile cells like immune cells have weak adhesions and a less complex cytoskeleton. In contrast, cardiomyocytes have highly organized sarcomeric structures as well as strong cell-cell / cell-ECM adhesions, in order to exert and withstand the forces of contraction. However, to move out of the, initially mono-layered, myocardium during trabeculation, the cells have to transition into a motile state.

4D observations of beating hearts prior and during trabeculation have revealed, that cardiomyocytes are able to renew cell-cell contacts by forming luminal protrusions along neighboring cell-cell junctions. Subsequent to protrusion formation, some cells start to constrict their abluminal membrane surface, moving their cell bodies towards the ventricular lumen (Staudt et al., 2014).

ErbB2-activation leads to trans-differentiation of epithelial cells into a motile, mesenchymal state (Aranda et al., 2006). This process plays a pivotal role during animal development and is known as epithelial-mesenchymal transition (EMT). Depending on the tissue and the signaling contexts, epithelial cells may lose only some characteristics or may show some epithelial and mesenchymal properties, considered as partial EMT (Lamouille et al., 2014). Cells that undergo trabeculation, upon ErbB2-activation, lose their epithelial-likel shape. However, cardiomyocytes do not de-differentiate during their maturation, always keeping their myocyte characteristics, suggesting a partial EMT as the underlying process (Liu et al., 2010).

1.6.1 Memo1

Memo1 (*mediator of Erbb2 driven cell motility*) has been shown to bind selectively to phosphorylated ErbB2 receptors in migrating cells (Jiang et al., 2013; Marone et al., 2004). After activation of the receptor, Memo1 translocates to the cell membrane and enables MTs to be captured at the edge of lammelipodia. The extension of MTs within these forward protrusions is important to sustain cell polarity and to promote adhesion site turnover. Through the inhibition of GSK3 Memo1 allows the relocalization of APC and CLASP2, known MT associated proteins, to the membrane and to ruffles (Zaoui et al., 2010). Furthermore, ACF7, which has been shown to be necessary and sufficient for MT capturing at the membranes, also translocates in a Memo1 depended manner (Zaoui et al., 2010). The lack of Memo1 in migrating breast carcinoma cells leads to defective localization of alpha-Actinin-1 and a reduced number of short-lived adhesion sites . Furthermore, translocation of proteins important for Actin polymerization, like the small GTPase RhoA and mDia1, to the lammelipodial membrane is dependent on Memo1 (Zaoui et al., 2010). It has been shown, that Memo1 is essential for the maintenance of directionality during ErbB2-induced tumor-cell migration by enhancing Cofilin1-dependent Actin depolymerization and severing activity (Meira et al., 2009).

Recently, Memo1 has been shown to play an important role in mouse vascular development through cell autonomous Sphingosine-1-Phosphate signaling, which is implicated in cell survival and migration. Animals deficient for Memo1 develop hemorrhages and edema and die before birth at embryonic day E18.5. (Kondo et al., 2014).

1.7 Aim of the study

Memo1 functions as a sensor for activated ErbB2 receptors in migrating cancer cells. Through its ability to relocalize protein complexes to the leading edge of the cell, it allows a directed response to extracellular stimului. The activation of ErbB2 receptors is involved in the disruption of epithelial apico-basal cell polarity and Golgi relocalization in acinar structures. Similar to cancer cells, ErbB2-activated, trabecular cells become motile and need to exert a certain degree of flexibility in order to intrude the ventricular

lumen. This flexibility of the cytoskeleton and of adhesion sites however needs to be tightly regulated in order to allow migration while sustaining myocyte contractility.

In order to better understand vertebrate heart trabeculation we were interested in studying the molecular mechanisms involved in this process. Combining the knowledge gained from previous studies of cancer cells and vertebrate heart development we formulated the following hypotheses:

"Flightless I function in cytoskeletal organization and mechanosensation and Memo1 mediated ErbB2 signaling are essential for the initiation of ventricular trabeculation in the zebrafish heart."

In order to test these hypotheses we had the following aims:

Aim 1: Analyzing the function of Flii in zebrafish skeletal muscle and heart by studying Flii-deficient animals.

Aim 2: Assessing the function of Memo1 during zebrafish heart development by utilizing Memo1-deficient animals.

Aim 2.1: Determining the subcellular localization of Memo1 in cardiomyocytes.

Aim 3: Studying the Golgi-apparatus in cardiomyocytes.

2 Materials

2.1 Equipment

2.1.1 Miscellaneous equipment

Table 1: List of used equipment

Equipment	Model	Supplier
aliqouting pipette	Repeater Plus	Eppendorf
accuracy balance	ALC 80.4	Acculab Sartorius
agarose gel electrophoresis chamber	B2 Separationssystem	OWI
zebrafish aquatic system		Tecniplast
bacterial incubator	InnOva 4200	New Brunswick Scientific
balance	ALC 3100.2	Acculab Sartorius
belly dancer	The belly dancer	Stovall
chemical hood	Vinitex Air	Vinitex
CO_2 incubator	Galaxy R	New Brunswick Scientific
CO_2 incubator	Innova co-170	New Brunswick Scientific
heating block	Digital Heatblock	VWR
homogenizer	Ultra turrax T8	IKA Werke
hybridization oven	HB 1000 Hybridizer	UVP Laboratory Products
injection pump	Pneumatic PicoPump PV820	World Precision Instruments
laminar flow	Hearasafe KS	Heraeus
luminescent image analyzer	LAS-4000	FujiFilm
magnetic heating plate	Combimag RCT	IKA Werke
magnetic stirrer	Stirrer	VWR
micromanipulator	MM33-right	World Precision Instruments
microwave	European Style 722	MWG
pH Meter	pH 221 Microprocessor pH Meter	HANNA Instruments
pipettes 2,5µL; 10µL; 100µL; 200µL 1000µL	Research	Eppendorf

plate reader	NanoQuant	Tecan
powersupply	EV243; EV231	Consort
roller mixer	SRT6	Stuart
rotator	SB3	Stuart
SDS-PAGE electrophoresis chamber	X Cell Sure Lock	Invitrogen
spectrophotometer	NanoDrop 2000c	PeqLab
thermo-mixer		HLC
transfer chamber	X Cell II Blot Module	Invitrogen
transilluminator	Gel ix DNA and Protein imager	itas
vacuumpump	Diaphragma Vacuum pump	Vacuubrand
vortex	VV3	VWR
waterbath	U3	Sulabo

2.1.2 PCR cycler

Table 2: List of used PCR machines

Type	Model	Supplier
PCR cycler	Mastercycler pro	Eppendorf
Real-time PCR cycler	Eco	Illumina

2.1.3 Microscopes

Table 3: List of used microscopes

Microscopes	Model	Supplier
microscope	Axiovert 25	Zeiss
stereo microscope	SMZ25	Nikon
confocal microscope	LSM 700	Zeiss
confocal microscope	LSM 780	Zeiss
Spinning disc microscope	Observer Z.1	Zeiss

2.1.4 Centrifuges

Table 4: List of used centrifuges

Centrifuge	Model	Supplier
cooling centrifuge	Centrifuge 5424R	Eppendorf
cooling table top centrifuge	Centrifuge 5810R	Eppendorf
table top centrifuge	Centrifuge 5424	Eppendorf

2.1.5 Protein Separation

Table 5: List SDS PAGE and protein blotting equipment

Western Blot Equipment	Supplier
Criterion SDS PAGE Chamber	Bio Rad
Trans-Blot Turbo	Transfer Chamber
ChemiDoc MP	Gel and Blot Doc

2.2 Miscellaneous materials

2.2.1 Disposables

Table 6: List of disposable materials

Materials	Type	Supplier
aliquoting pipette tips	Combitips Plus 5 ml; 10 ml	Eppendorf
bacterial culture tubes	14 ml PP Tube Sterile	Greiner bio-one
cell culture dishes	10 cm	Greiner bio-one
cell culture plates	24 Well Cell Culture Plate, Cell Star	Greiner bio-one
cell culture plates	6 Well Cell Culture Plate, Cell Star	Greiner bio-one
cell scraper	Cell Scraper	Greiner bio-one
coverslips	24x50 mm	Menzel Gläser
coverslips	12 mm diameter	Menzel Gläser
filter paper		Whatman

Materials	Type	Supplier
capillaries		World Precision Instruments
latex gloves	SATIN PLUS	KIMTECH
microscope slides	frosted, beveled, 76x26 mm	Knittel Glaser
microscope slides	SUPER FROST ULTRA PLUS 25x75x1.0 mm	Menzel Gläser
nitril gloves	Activ Aloe	BLOSSOM
nitrocellulose transfer membrane	Protran Nitrocellulose	Whatman
PCR tubes	0.5 ml	Eppendorf
pipette filter tips	FT10; FT100; FT200; FT1000	Greiner bio-one
pipette tips	10 µl; 200 µl; 1000 µl	Greiner bio-one
plastic pipettes	2 ml; 5 ml; 10 ml; 50 ml cell star	Greiner bio-one
reaction tubes 1,5mL; 2mL	Save Lock Tubes	Eppendorf
reaction tubes 15mL; 50mL	Cell Star TUBES	Greiner bio-one
thin pipette tips for kapillary filling	20 µL Physio Care Concept	Eppendorf
transfer pipettes	Transfer Pipettes	Sarstedt

2.2.2 Non disposables

Table 7: List of non-disposable materials

Materials	Type	Supplier
glass beaker	DURAN	SCHOTT
forceps	Inox.4	DUMONT
glass bottles	DURAN	SCHOTT
glass erlenmeyer flasks	DURAN	SCHOTT
glass measuring cylinder	DURAN	Hirschmann
glass pipettes	2 mL; 5 mL; 10 mL; 25 mL	BRAND
micro scale	1 mm in 100	Novex
Neubauer chamber	0.1 mm depth; 0.0025 mm^2	Marienfeld
optical dishes	Glass Bottom Culture Dishes (35 mm dish, 14 mm microwell)	MatTek

2.3 Chemicals

Table 8: List of used chemicals

Chemicals	Supplier
acetic acid	Sigma
agarose	Roth
agarose low melting	Molwkula
ampicillin	Calbiochem
B-Block	Roche
bicine	Fluka
BM purple AP substrate, percipitating	Roche
β-mercaptoethanol	Merck
bovine serum	ATCC
bromophenol blue	Merck
BSA	Roth
CHAPS	Sigma
chloroform	Roth
DAB-Substrate	Roche
deoxycholate	Sigma
DEPC	Roth
dNTPs	Invitrogen
DTT	Roth
dulbecco's PBS	PAA Laboratories
EDTA	Sigma
EGTA	Sigma
EMEM	ATCC
entellan / xylol based	Merck
eosin	Chroma
ethanol	Roth
ethidium bromide	Fisher Sceintific
Fast Red Tablets	Roche
fetal bovine serum gold	PAA Laboratories
formaldehyde	Polyscience

Chemicals	Supplier
formalin	Sigma
formamide	Roth
glycerol	Sigma
glycine	Roth
H_2O_2	Sigma
HCl	Roth
hemalum	Chroma
heparin	Fluka
HEPES	Roth
IPTG	Sigma
isopropanol	Roche
kaiser's glycerol gelatin / water based	Merck
kanamycin	Serva
KCl	Roth
KH_2PO_4	Roth
LB-Agar	Sigma
LB-Medium	Sigma
Levamisole	Fluka
methanol	Roche
$MgCl_2*6H_2O$	Roth
Moviol	Sigma
Na_2HPO_4	Roth
NaCl	Roth
NaH_2PO_4	Fluka
NaN_3	Sigma
NaOH	Roth
nonidet P40	Sigma
N-phenylthiourea	Sigma
para-formaldehyde	Sigma
penicillin/streptomycin	Sigma
phenol red	Sigma
PMSF	Sigma
propanolol	Roche

Chemicals	Supplier
protease inhibitor cocktail	Thermo sceintific
RNase inhibitor	Roche
SDS	Fluka
sodium acetate	Roth
sodium citrate	Roth
SYBR Safe	Life technologies
Tricane	MP Biomedicals LLC
Tris base	Roth
Triton X-100	Sigma
Trizol	Invitrogen
trypsin/EDTA	Gibco
Tween 20	Sigma
x-gal	Fluka
xylol	Roth
yeast tRNA	Roche

2.4 Buffers and solutions

Table 9: List of used solutions

Solution	Formulation
agarose gel loading buffer (6x)	bromophenol blue 0.25% [w/v]
	xylene cyanol FF 0.25%[w/v]
	Ficoll 400 15% [v/v] in dH$_2$O
ampicilin solution	100 mg/ml
DIG-block (blocking solution)	2% blocking reagent
	dissolve in MABT
	at ca. 68°C under strirring
	add few drops of NaOH
	store in 10 ml aliquots at -20°C
DEPC-H$_2$O	DEPC 0.01%
	incubate overnight at RT; autoclave
deyolking buffer	NaCl 55 mM

	KCl 1.8 mM
	NaHCO$_3$ 1.25 mM
	in dH$_2$O
egg water	Instant ocean 0.3 g/l
	Calcium sulfate 0.75 g/l
Evans Blue	0.1% (w/v)
formaldehyde 3.5%	formaldehyde 3.5% in PBS [v/v]
goat serum 5%	goat serum 5% in PBS [v/v]
glutaraldehyde 25%	glutaraldehyde 25% in dH$_2$O [v/v]
Glycerol 30%, 50%, 70%	Glycerol in PBS
Hyb- (hybridization mixture)	formamide
	20x SSC
	blocking reagent
	RNase free water 10.9 ml
	dissolve at 65°C and cool to RT
	EDTA 0.5 M; 1 ml
	Tween-20 100 µl
	CHAPS 10%; 1ml
	heparine 5mg/ml; 2ml
	DEPC-H2O ad 90 ml
	store in 9 mL aliquots at -20°C
	add fresh: yeast tRNA 10 mg/ml; 1 ml/9 ml

Hyb+ (hybridization mixture with yeast tRNA)

25% Hyb-	Formamide 125 ml
	20x SSC 100 ml
	20% Tween20 5 ml
	H$_2$O ad 1 l
kanamycin	20 mg/ml
KCM buffer	KCl 500 mM
	CaCl$_2$ 150 mM
	MgCl$_2$ 250 mM
Levamisole (1 M)	241 mg Levamisole in 1 ml TBS-T
5x MAB	Maleic acid 58.04 g

	NaCl 43.83 g
	NaOH pellets 38 g
	pH 7.5 (with NaOH)
	H_2O ad 1 l
	filtrate through 0.22 µm pore filter
MABT	5x MABT; 200 ml
	20% Tween20; 5 ml
	H_2O ad 1 l
mounting medium	Moviol 4 g in
	Tris HCl 0.2 M pH 8.5; 20 ml
	65°C on a shaker 4 hours
	after cooling
	glycerol 10 ml
	DABCO 750 mg
	spin 15 min 15,000 rpm
	aliquot and store at -20°C
NTMT Buffer	NaCl 5 M; 1 ml
	20% Tween20; 2.5 ml
	Tris 2 M pH 9.5; 2.5 ml
	Levamisole 1 M; 100 µl
	H_2O ad 50 ml
PBS	NaCl 137 mM
	KCl 2.7 mM
	Na_2HPO_4 10 mM
	KH_2PO_4 1.76 mM
	pH 7.4
	distilled H_2O ad 1 l
PBS-0,1% NP40	PBS with 0.1% Nonidet P40
PBS-T	PBS with 0.1% Tween-20
PBS-T-glycine	glycine 2 mM; in PBS-T
PFA 4% in PBS	PFA 4 g
	PBS 100 ml
	add few drops of 10 M NaOH
	heat at 55°C until dissolved; cool on ice

	pH 6-7 (adjust with HCL)
RIPA	SDS 2.5 ml
	NaCl 5 M; 15 ml
	NP40 5 ml
	deoxycholate 25 ml
	EDTA 0.5 M; 1 ml
	Tris 1 M pH 8; 25 ml
	DEPC-H_2O ad 500 ml
20x SSC	NaCl 175.3 g
	sodium citrate 88.2 g
	H_2O ad 1 l
	pH 6.0 (adjust with citric acid)
2x SSCT	20x SSC;200 ml
	20% tween20;10 ml
	H_2O ad 2 l
0.2x SSC	20x SSC; 20 ml
	20% Tween20; 10 ml
	H_2O ad 2 l
TAE running buffer (1x)	Tris base 0.04 M
	EDTA*$2H_2O$ 0.002 M
	in dH_2O
TBS (10x)	NaCl 8 g
	KCl 0.2 g
	Tris 1 M pH 7.5; 25 ml
	dH_2O ad 100 ml
TBS-T (10x)	10x TBS with 1 ml Tween-20
TSB	PEG-3500 10
	DMSO 5 ml
	$MgCl_2$ 1 M; 1 ml
	$MgSO_4$ 1 M; 1 ml
	LB-medium pH 6.1 ad 100 ml
	sterile filtrate with 0.45 µm filter
	store at 4°C
wash buffer	NaCl 110 mM

KCl 3.5 mM

CaCl$_2$ 2.7 mM

Tris HCl 1 M, pH 8.5; 500 µl

dH2O ad 50 ml

2.5 Growth media

Table 10: List of used media

Media	Application	Formulation
LB-agar	propagation of bacteria	35 g in 1l H$_2$O
LB-medium	propagation of bacteria	20 g in 1l H$_2$O

2.6 Zebrafish feed

Table 11: List of zebrafish feed

Feed	Fish age	Supplier
Brine shrimp	5 dpf to 12 dpf	Special Diets Services
SDS100 (granule size 80-200 µm)- SDS400 (granule size 500-800)	12 dpf-adult (≥3 month)	Special Diets Services
Topical breeder mix (flakes)	adult (≥ 3 months)	Special Diets Services

2.7 Kits

Table 12: Kits used in this study

Kit	Application	Supplier
Bio Rad DC^{TM} Protein Assay Kit	protein concentration	Bio Rad
Bio Rad Criterion TGX Stain Free	Protein Gel 4-20%	Bio Rad
Bio Rad Trans Blot Turbo	Transfer Pack	Bio Rad
Bio Rad 10x Tris/Glycine/SDS Buffer	Protein Gel Running Buffer	Bio Rad
DIG RNA Labeling Kit (SP6/T7)	*in situ*	Roche
FuGENE	transfection reagent	Promega

GeneJet Gel Extraction Kit	DNA extraction from agarose gel	Thermo Scientific
GeneJet PCR Purification Kit	PCR product clean up	Thermo Scientific
GeneJet Plasmid Miniprep Kit	plasmid purification	Thermo Scientific
MEGAshortscript T7 Kit	T7 RNA polymerase for RNA synthesis	Ambion
mMESSAGE mMACHINE Sp6 Kit	SP6 RNA polymerase for capped mRNA production	Ambion
PureLink	plasmid purification	Invitrogen
RNeasy® Mini Kit	RNA isolation	Qiagen
SuperSignal West Femto	chemiluminescene	PIERCE
Clean & Concentrator -5	RNA clean up	ZYMO RESEARCH

2.8 Plasmids

Table 13: Used plasmids

Plasmid	**Application**	**Supplier**
pAcGFP1-N2	mammalian expression voector	Clontech
pGEM-T Easy	cloning vector/probe synthesis	Promega
pCS2+	mRNA synthesis/mammalian expression voector	RZPD

2.9 Antibodies

Table 14: Used antibodies

Antibody	**Application and Dilution**	**Isotype**	**Supplier**
Primary Antibodies			
Anti-Pan-Actin	WB 1:1000	Rabbit polylconal	Cell Signaling
anti-Myc Tag clone 4A6	WB 1:500; ICC 1:100	mouse monoclonal IgG	Millipore
anti-GFP	WB 1:1000; ICC 1:100	rabbit polyclonal	Invitrogen
anti Digoxigenin-AP, Fab fragments	ISH 1:5000		Roche

anti-Flightless I	WB 1:200	rabbit polyclonal	Novus Biologicals
anti Flightless I	WB 1:200	rabbit polyclonal	Naganawa et al.
Secondary Antibodies			
Alexa Fluor 488 anti-Rabbit	ICC 1:200	goat IgG	Invitrogen
Alexa Fluor 594 anti-Rabbit	ICC 1:200	goat IgG	Invitrogen
Alexa Fluor 488 anti-Mouse	ICC 1:200	goat IgG	Invitrogen
Alexa Fluor 594 anti-Mouse	ICC 1:200	goat IgG	Invitrogen
ECL anti-Rabbit IgG HRP-linked	WB 1:10.000	donky IgG	GE Health care UK limited
ECL anti-Mouset IgG HRP-linked	WB 1:10.000	sheep IgG	GE Health care UK limited
Fluorescent Stains			
Rhodamine Phalloidin	1:100	-	Invitrogen

2.10 Enzymes

Table 15: Used enzymes

Enzyme	Supplier
Cold Fusion	SBI
DNase	Roche
DyNAmoColor Flash	Thermo Scientific
KAPA2G Fast ReadyMix+dye	KAPABIOSYSTEMS
PCR Master Mix (2x)	Thermo Scientific
Phusion High-Fidelity DNA Pol	NEB
Proteinase K	Invitrogen
RNase	Roche
SP6 RNA Polymerase	Roche
SuperScript II Reverse Transcriptase	Invitrogen
T3 RNA Polymerase	Roche
T4 DNA Ligase	Promega
T7 RNA Polymerase	Roche
ApaI	NEB
BamHI	NEB
EcoRI	NEB
HindIII	NEB
NotI	NEB
SacII	NEB
SalI	NEB
SpeI	NEB
XhoI	NEB
ApaI	NEB

2.11 Size markers

Table 16: Markers and Standards used in this study

Size Markers and Standards	Supplier
Precision Plus Protein Standard	BioRad
GeneRuler 100 bp plus	Thermo Scientific
GeneRuler 1 kb	Thermo Scientific

2.12 Oligonucleotides

Table 17: Used Oligonucleotides

Oligo name	Sequence (5'-3')	Gene name	Species	Supplier
flii genotyF	GGATAAGAACCTGGAGAAGCCT	*flightless I*	*Danio rerio*	Sigma
flii genotyR	GACATTTGGACAAACAGCGA	*flightless I*	*Danio rerio*	Sigma
fliiseq	CTGGAGAAGCCTCAGCTGGA	*flightless I*	*Danio rerio*	Sigma
flii ISH pGEM-T	CCTCTAAAAGCATCCTCACTCGA	*flightless I*	*Danio rerio*	Sigma
flii ISH pGEM-T	GAACTTGGATTTGAAGACCTGGC	*flightless I*	*Danio rerio*	Sigma
flii for pcDNA3.1 myc/HIS F	GCACAGTGGCGGCCGCTCGAGATA TCCCGAATTAGACATG	*flightless I*	*Danio rerio*	Sigma
flii for pcDNA3.1 myc/HIS R	GAAGGGCCCTCTAGACTCGAGTGC GGGTGCCGTCTTGAAG	*flightless I*	*Danio rerio*	Sigma
flii qPCR F1	AATGCCAGGTCTTCAAATCC	*flightless I*	*Danio rerio*	Sigma
flii qPCR R1	TTTCATCTGGTCCTTCTGCT	*flightless I*	*Danio rerio*	Sigma
flii qPCR F2	GGCTACTTTGCTGTATCAGAG	*flightless I*	*Danio rerio*	Sigma
flii qPCR R2	TTGAATATAGACCTGACAAGCC	*flightless I*	*Danio rerio*	Sigma
M13 forward20	GTAAAACGACGGCCAGT	-	-	-
mi372 genotyF	CTGCAGGCATGACTTAACTTC	*flightless I*	*Danio rerio*	Sigma
mi372 genotyR	CATGTTTCTGGAGTTCTCCAAG	*flightless I*	*Danio rerio*	Sigma
memo HRMA F	CCCACCGACGAGGTTTTATTG	*memo1*	*Danio rerio*	Sigma
memo HRMA R	GGTCTCTGGCTCTACCTGAG	*memo1*	*Danio rerio*	Sigma
memo mRNA F	CAACTCTGCCAGCCCAGTTTCTCTG	*memo1*	*Danio rerio*	Sigma

memo mRNA R	GGGGTCATATTTGCTGAGCACTGTATTTG	*memo1*	*Danio rerio*	Sigma
memoPromoter F	GGAGAGTGTAGCACCAAAGCTTG	*memo1*	*Danio rerio*	Sigma
memoPromoter R	CGCCTATCTTGGTCCAATAAAACC	*memo1*	*Danio rerio*	Sigma
actc1b:vinculin-GFP F	TTTGTCCTGCACAGACCAAGGATGCCAGTTTTCCATACCAA	*vinculin*	*Danio rerio*	Sigma
actc1b:vinculin-GFP R	CCTTGAATTCTTACTTGTACATTACTTGTACAGCTCGTCCATG	*vinculin*	*Danio rerio*	Sigma

2.13 Morpholinos

Table 18: Morpholinos used in this study

Morpholino Binding Position	Sequence 5'-3' antisense
Memo1 start codon ATG	TCTGCACACCATCCGGTTCGACATC
Memo1 5'UTR ATG	ACGCGAGACATATAACTGACGATAC
Flightless I start codon ATG	AGCCATGTCTAATTCGGGATATGG

Table 19: CRISPR gRNAs

gRNA Binding Position	Sequence 5'-3' antisense
Memo1 gRNA F	CGCCGGCAGCTGGTACACGG
Memo1 gRNA R	CCGTGTACCAGCTGCCGGCG

2.14 Strains

2.14.1 Bacterial strains

Table 20: Used bacteria

Bacterial strain	Specification	Supplier
DH5α	E. coli	Invitrogen

2.14.2 Zebrafish lines

Table 21: Studied Zebrafish lines

Fish Line	Specification	Reference
Tuebinger	wild type	MPI-Tübingen
Tg(myl7:galT:mCherry)^{bns5}		AB
Tg(myl7:LifeAct-GFP^{Js974} / Tg(myl7:nucDsRed)		AB
Tg(myl7:memo1-EGFP)^{bns4}		AB
Tg(kdrl:GFP)		AB
Tg(memo1:EGFP)^{bns1}		AB

2.15 Computer software

Table 22: Used software

Software
Microsoft Office Excel, Word, PowerPoint
Adobe Photoshop, Illustrator, Reader
Image, J FiJi
Tracker
Graph Pad Prism
Imaris
Geneious

3 Methods

3.1 Zebrafish husbandry and microinjection

3.1.1 Maintenance

WT and transgenic zebrafish were maintained at 26°C water temperature and 27°C room temperature on a 14-hour light and 10-hour dark cycle in an aquarium tank system from Tecniplast. This system is composed of fish tanks placed in metal, racks interconnected to a common fresh water reservoir and a central water recycling system. The biological filters of the recycling system are made of a foamy material which provides a large surface area for the growth of aerobic denitrifying bacteria (*Nitosomonas* and *Nitrobacter*), which detoxify the ammonium compounds excreted by the fish. pH (pH 7) and conductivity (180 µS) of the water are under permanent control. Approximately 20% of the water in each tank is exchanged every 24 hours. The water is sterilized by UV-light before re-entering the fresh water reservoir. Wild type (wt), transgenic or injected embryos were cultured in 10 cm dishes in a 28°C incubator until 5 dpf and were then transferred into the Tecniplast system.

3.1.2 Breeding

Animals were bred in special mating tanks having egg-permeable insets. Couples were set up in the late afternoon by placing them together in a mating tank separated through a transparent barrier. On the next morning the barrier was removed. After around 15 minutes the females started to spawn with immediate fertilization by the males. The fertilized eggs fell through the permeable insets to the bottom of the tank. Fertilized zebrafish eggs were taken out of the breeding tanks by pouring the whole content of the tank through a fine sieve. The eggs were then washed with E3 medium and transferred to a 10 cm dish containing approximately 10 ml of E3 medium.

3.1.3 Microinjection

Preparation of injection plates

For the preparation of agarose plates 2% agarose in E3 medium was heated in a microwave until the agarose was completely dissolved. A first layer of about 4 mm agarose was poured into the 10 cm plastic petri-dish. After solidification a mold was placed on top of the layer and a second approx. 4 mm layer of agarose was poured in such a way as to build the boundaries of the future cavities. After complete solidification of both layers the mold was removed carefully with the help of a blade.

Preparation of injection needles

A glass capillary was fixed into the pulling machine under tension. After closing the lid of the "puller" the start button was pressed and the center of the glass capillary was heated. By reaching the melting point of the glass capillary its tension was released and the fixed ends of the capillary pinched apart. This stretching of the capillaries results in two very thin needles which can be used for micro-injection.

For micro-injection up to 6 µl of solution was pipetted into the injection-needle by using a very thin and long 20 µl Eppendorf pipette tip and subsequent the needle was fixed into the micromanipulator. A very small part of the needle's tip was broken off with tweezers and a droplet of solution was injected into a drop of Halocarbon oil 27 (Sigma) on the top of a micro-scale in order to measure the drop-size. A drop of solution was produced with a preset pressure time of about 450 ms as a starting point for a 20 nm diameter drop. Then again a small part of the needle was broken off in order to adjust the drop to 20 nm. Since the width of the needle opening varies and cannot be broken to perfectly fit the drop size the pressure time has to be change accordingly but not to any extend since the needle width is critical for the injection of the embryos, a thin needle would not be able to penetrate the chorion whereas a thick needle would destroy the embryo. After needle preparation, the fertilized eggs were arranged on the injection plate as shown in (Fig 3.1)
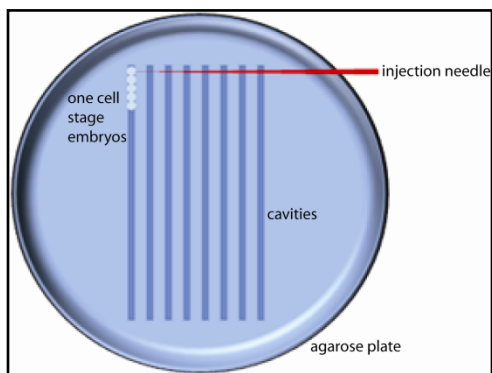
Figure 3.1: Injection plate illustrating arrangement of embryos

For transient expression or knockdown of genes mRNA or morpholinos were injected into the yolk of one-cell stage embryos. plDNA along with IsceI or transposase mRNA for transgene incorporation into the zebrafish genome were injected into the cell of a one-cell stage embryo.

3.2 Bacteria-based techniques

3.2.1 Propagation of E. coli

E.coli DH5α were cultivated in LB-medium or on solid agar-plates containing the appropriate antibiotic at 37°C overnight. For the cultivation on agar-plates bacterial suspension was spread with a Drigalski-spatula and incubated top-down in a bacterial incubator. For analytical preparations of plasmid DNA (plDNA) 2 ml of LB-medium inoculated with a single bacterial colony were shaken at 180 rpm. For the preparations of large amounts of plDNA 100 ml of LB-medium were inoculated with 50 µl of bacterial suspension and incubated at 100 rpm.

3.2.2 Generation of chemically competent E. coli

A single colony of *E. coli* strain DH5α was inoculated in 5-6 ml LB-medium and cultured overnight at 37°C under shaking. 4 ml of grown culture was added into fresh 250 ml LB and grown to early logarithmic phase (OD_{600}=0.3-0.6). The culture was then centrifuged for 10 minutes at 2500 rpm at 4°C in a tabletop centrifuge. The bacterial pellet was resuspended in 25 ml cold TSB buffer (1/10th volume of the bacterial suspension) and incubated on ice for 10 minutes. Competent cell suspension was aliquoted into cold Eppendorf tubes (100 µl and 200 µl) and quick-frozen in liquid nitrogen. Aliquoted, frozen competent bacteria were stored at -80°C.

3.2.3 Transformation od competent E. coli

For the transformation of chemically competent *E. coli* 1-10 ng of plDNA or 1-5 µl of a ligation reaction was added to 20 µl of 5x KCM buffer in a total volume of 100 µl H_2O. At the same time competent bacteria were thawed on ice and 100 µl cell suspension were added to the reaction and mixed by flicking of the tube. After incubation on ice for 20 minutes and room temperature for 10 minutes, 1 ml of SOC-medium was added to the mixture. The bacterial suspension was shaken vigorously for 1 hour at 37°C and then centrifuged for 4 minutes at 3000 rpm in a tabletop centrifuge. Approximately 1 ml of the supernatant was removed and the pellet was resuspended carefully and plated as described before.

3.2.4 Isolation of plDNA from E. coli

The isolation of plDNA from *E. coli* was performed with the GeneJet Plasmid Miniprep Kit (Thermo Scientific) for small amounts of plDNA and PureLink HiPure Palsmid Filter Midiprep Kit (Invitrogen) for large amounts, according to manufactures' instructions.

3.3 DNA-related methods

3.3.1 Amplification of DNA

DNA was amplified by the polymerase chain reaction (PCR) using a DNA-dependent DNA polymerase. This enzyme synthesizes a new DNA-strand complementary to a single-stranded DNA template. For the binding of the polymerase to template DNA starter-oligonucleotides (oligos) are needed. These oligos are precisely designed to bind the ends of the forward and reverse strand of the template and hence restrict the size of the future product.

The chain reaction is composed of three steps: denaturing of the DNA, annealing of the oligonucleotides and elongation of those by adding deoxynucleotidetriphosphates (dNTPs). The temperatures of these steps and the composition of the reaction mixture can vary depending on the enzyme and the oligos used (Table 23-26). PCRs were run on Eppendorf vapo protect master cycler pro PCR machines.

Table 23: Reaction mixture for PCR

Kapa	Concentration
2x MasterMix (with dye)	1x
Forward oligo	10 pmol
Reverse oligo	10 pmol
Template	(gDNA 1/plDNA)
Water	accordingly

Table 24: PCR conditions for Kapa

Temperature	Time	Step of PCR
95°C	5 minutes	initial denaturation
95°C	15 seconds	**denaturation**
55-65°C	30 seconds	**annealing**
72°C	10 seconds / kbp	**elongation**
		repeat three steps 23-38x
72°C	7 minutes	final elongation
4°C	∞ minutes	storage

Table 25: Reaction mixture for PCR

Phusion	Concentration
5x Buffer	1x
Forward oligo	10 pmol
Reverse oligo	10 pmol
Template	1x
10 mM dNTPs	0.2 mM
DNA Polymerase	0.5-1 µl
Template DNA	(gDNA/plDNA)
Water	accordingly

Table 26: Touchdown PCR conditions for Phusion (for oligos with long overhangs)

Temperature	Time	Step of PCR
98°C	5 minutes	initial denaturation
98°C	15 seconds	denaturation
50°C	30 seconds	annealing
72°C	1 minute / kbp	elongation
98°C	15 seconds	denaturation
64°C	30 seconds	annealing
72°C	1 minute / kbp	elongation
98°C	15 seconds	denaturation
62°C	30 seconds	annealing
72°C	1 minute / kbp	elongation
98°C	15 seconds	denaturation
59°C	30 seconds	annealing
72°C	1 minute / kbp	elongation
98°C	15 seconds	denaturation
58°C	30 seconds	annealing
72°C	1 minute / kbp	elongation
		repeat three steps 31x
72°C	7 minutes	final elongation
4°C	∞ minutes	storage

3.3.2 DNA restriction

For cloning and restriction analyses DNA was digested with restriction endonucleases at 37°C for 2 hours or overnight in a heating block (VWR) depending on the amount of DNA and the enzyme used. ApaI digestions were done at 25°C in a heating block overnight (Table 27).

Table 27: DNA restriction mixture

Component	Concentration
10x Buffer	1x
10x BSA (if necessary)	1x
DNA	max.-10 µg
Enzyme 20 U/µl	2 U/µg DNA
H$_2$O	ad 20 µl < 3 µg / ad 50 µl

3.3.3 Purification of DNA

The purification of DNA samples like PCR-products and linearized plasmids was done with GeneJet PCR Purification Kit following maufactures' instructions.

3.3.4 Agarose gel electrophoresis

Gelelectrophoresis was used to separate DNA fragments according to their size by running through an agarose gel in an electric field. For this purpose gels were made using 1-2% agarose dissolved in 1x TAE buffer containing 1 µl ethidium bromide or 2.5 µl SYBR Safe per 50 ml. The DNA samples were prepared by the addition of 1x colored loading buffer (6x). The gels were run at 80 V for approximately 40 minutes in 1x TAE buffer and the ethidium bromide intercalated DNA bands were detected under UV-light ($\lambda = 260$ nm). Digital pictures were taken with the "Gel ix Protein imager". If SYBR Safe was used, bands were detected with blue-light transilluminator and pictures were taken with the Bio Rad Gel Doc EZ imager.

3.3.5 Extraction of DNA from agarose gels

DNA bands were cut out from agarose gels with a scalpel and DNA was extracted by using the GeneJet Gel Extraction Kit following the manufactures' instructions.

3.3.6 Measurement of nucleic acid concentrations

The concentration of DNA- and RNA-samples was measured with the Nanodrop® ND-2000 spectrophotometer by placing 1 µl of sample onto the optical pedestal. Absorption at 260 nm was measured and the concentration was calculated by the program according to the Lambert-Beer law: $A = \varepsilon bc$ where $\underline{A}$ is absorbance, $\underline{\varepsilon}$ is the molar extinction coefficient, $\underline{b}$ is the path length, and $\underline{c}$ is the sample concentration. The molar extinction coefficient for double stranded DNA (dsDNA) is 50, for RNA it is 40 $[cm^{-2} \times M^{-1}]$. The path length is 1mm.

3.3.7 DNA ligation

DNAs with 3' and 5' overhangs (sticky ends) were ligated with the T4-DNA Ligase. The enzyme connects the 5' phosphate of one fragment to the 3' hydroxyl group of the other fragment under the consumption of ATP. The reaction was incubated for 2 hours at room temperature or overnight at 4°C. For an estimation of negative clone percentage a self-ligation control was carried out in which no insert was added to the ligation reaction (Table 28).

For cloning of PCR products pGEM-T easy has been used. The vector is linear and provides dTMP overhangs whereas the PCR-product carries dAMP overhangs produced by the DNA polymerase, which allows the fragments to be ligated to each other.

Table 28: DNA ligation mixture

Component	Concentration	For self-ligation control
10x Buffer	1x	1x
Insert	molar ratio 1:3 (vector to insert)	-
Vector	200 ng	200 ng
T4-DNA ligase	1 µl	1 µl
H₂O	ad 10 µl	ad 10 µl

3.3.8 Sequencing of DNA

In order to verify the sequence inserted into vectors, plDNA was sequenced by Seqlab according to the Sanger chain termination method.

3.4 RNA-related methods

3.4.1 RNA isolation from mammalian cells

Total RNA from mammalian cells was isolated with TRIZOL$^®$ according to the manufactures' instructions.

3.4.2 RNA isolation from zebrafish

RNA from fish embryos was isolated using the RNeasy$^®$ Mini Kit (Qiagen). Zebrafish embryos were dechorionated and washed twice in PBS. Subsequently 350 µl buffer RLT containing β-mercaptoethanol was added to the pooled fish (20-30). Carefully and without creating bubbles the fish were passed through a 24 gouge-needle and afterwards loaded on a QIAShredder$^®$ (Qiagen) column. For all further steps manufactures' instructions were followed.

3.4.3 cDNA "first strand" synthesis

The cloning of genes and gene expression analyses require the production of complementary-DNA (cDNA) from mRNA. For this purpose a "first strand" of DNA was synthesized by a reverse transcriptase. This enzyme synthesizes DNA in a RNA-dependent manner producing RNA/DNA hetero-duplexes, which can be used as a template for PCR and real-time quantitative PCR (qPCR). The Maxima First Strand cDNA Synthesis Kit for RT-qPCR (Thermo Scientific) was used for the reverse transcription of 0.5 µg RNA using Oligo(dT)$_{18}$ and random hexamer primers (Invitrogen) following manufactures' instructions in an total volume of 10 µl.

3.4.4 Real-time PCR

Quantitative PCR (qPCR) was done to analyze gene expression levels relative to an endogenous control. The conditions for this quantitative method were precisely adjusted. For example, the amplicon length was always chosen to be smaller than 200 bp in order to reliably duplicate the molecules in each cycle. Furthermore, gene specific exon-spanning oligonucleotides were designed that target a part of the mature mRNA that on genome level is separated by an intron. This prevents the amplification of genomic DNA (gDNA), which might be present in low amounts after RNA isolation and will be still present in the cDNA samples.

SYBR Green (2x DyNAmo color flash, Thermo Scientific), which intercalates dsDNA, was used as fluorescent-dye for the quantification of PCR products and melt curves on the Eco qPCR cycler (Illumina). The measurement of dsDNA amount, which increases after each elongation step, is based on the characteristic light absorbtion at $\lambda =$ 484 nm and light emission at $\lambda =$ 521 nm of the SYBR Green/dsDNA-complex. Each sample was measured in triplicates for the gene of interest and for a housekeeping gene as endogenous control (Table 29-30).

Table 29:qRT-PCR mixture

Component	Concentration
cDNA (12,5ng/µL)	2 µl
Primer Forward	5 pmol
Primer Reverse	5 pmol
SYBR Green 2x	5 µl
H_2O	Ad 10 µl

Table 30: qRT-PCR protocol

Temperature	Time	Step
95°C	3 minutes	denaturation
95°C	10 seconds	denaturation
59°C	10 seconds	annealing
72°C	30 seconds	elongation

The successful amplification of a single product was confirmed via the melt-curve, which was monitored after the last cycle of each qPCR-reaction. Since the melting thermodynamics of a dsDNA are characteristic, a single melt-peak can be correlated to a specific product (appendix). The threshold cycle $(C_{(t)})$ of each amplification was determined by a threshold which is automatically set to the log-phase of the amplification curve. The mean values of triplicates were employed for the calculations of the $2^{-\Delta\Delta C(t)}$.

$$\Delta\Delta C_{(t)}=(C_{(t),} \textit{YFG} - C_{(t),} \textit{HKG})_{\textbf{individual sample}}- (C_{(t),} \textit{YFG} - C_{(t),} \textit{HKG})_{\textbf{mean of WT}}$$

The resulting values represent the fold-change relative to non-injected fish.

3.5 Capped mRNA synthesis

Capped mRNA was synthesized for rescue experiments in morpholino-injected zebrafish embryos using the mMESSAGE mMACHINE® kit (Ambion).

3.5.1 Preparation of template plDNA for mRNA synthesis

For capped mRNA synthesis 5 µg of pCS2+ vector containing the whole coding sequence (cds) of the gene of interest was linearized by digestion with the appropriate restriction endonuclease at 37°C in a heating block overnight. The restriction digest was stopped by the addition of "Ammonium Acetate Reaction Stop Buffer" containing 1/20th volume of 0.5 M EDTA, 1/10th volume of 3 M Na acetate and 2 volumes of ethanol. After mixing and incubating for 15 minutes at -20°C the DNA was pelleted in a table top centrifuge at maximum speed. The supernatant was removed completely and the invisible pellet was resuspended in 10 µl of nuclease-free water. Subsequently the DNA concentration was measured.

3.5.2 mRNA synthesis

The transcription reaction was carried out using the SP6 RNA-polymerase. mRNA was synthesized from 1 µg linearized plDNA. The reaction mixture was incubated at 37°C for 2 hours in a heating block (Table 31).

Table 31: mRNA synthesis mixture

Component	Concentration
Linearized plDNA	1 µg
2x NTP/CAP	1x
10x Reaction Buffer	1x
Enzyme mix	2 µl
Nuclease free H$_2$O	ad 20 µl

3.5.3 plDNA removal and RNA precipitation

For the removal of residual plDNA 1 µl of TURBO DNase was added directly to the freshly synthesized mRNA. The reaction was incubated for 15 minutes at 37°C in a heating block. Thereafter, the capped mRNA was precipitated by the addition of 30 µl nuclease-free H$_2$O and 30 µl of LiCl precipitation solution and incubation at -20°C for 30 minutes. The mRNA was pelleted by centrifugation in a tabletop centrifuge for 15 minutes at maximum speed. Subsequently, the pellet was washed in 1 ml 70% ethanol, again centrifuged for 10 minutes, dried at room temperature and dissolved in 20 µl nuclease-free H$_2$O. Finally 0.5 µl of RNase inhibitor was added and the RNA concentration was measured. Capped mRNA was aliquoted in 3 µl aliquots in order to avoid freeze-thaw cycles and was stored at -80°C.

3.5.4 mRNA clean up

For in vitro synthesized RNA clean up ZYMO RESEARCH RNA Clean & Concentrator columns were used following the manufactures' instructions.

3.6 Whole-mount in situ hybrididzation

Whole-mount *in situ* hybridization was performed to analyze the expression of genes in time and space throughout the early development of the whole zebrafish.

3.6.1 RNA probe synthesis

RNA-probes were synthesized for the detection of gene expression in *in situ* hybridization experiments. Digoxygenin (DIG)- and fluorescin-labled sense- and antisense-probes were made by the use of the DNA-dependent T7, T3 or SP6 RNA-

polymerases depending on the vector. As template 1 µg of linearized plDNA containing the gene of interest was added to the RNA-Probe synthesis reaction (Table 32). After 2 hours of incubation at 37°C in a heating block the plDNA was degraded by the addition of RNase free DNase (Invitrogen) for one additional hour at 37°C (Table 33). Subsequently the freshly synthesized RNA was purified by salt-precipitation with ethanol and afterwards washed with 70% ethanol to remove the salt from the pelleted probe (Table 34). The dried pellet was dissolved in 40 µl RNase free H_2O plus 1 µl of RNase inhibitor and the concentration was determined. For long-term storage the RNA-probes were kept at -80°C.

Table 32: RNA probe synthesis mixture

Component	Amount
10x Buffer	1x
DIG / Fluorescin labeled dNTPs	2 µl
RNase Inhibitor	1 µl
plDNA	1 µg
T7, T3, SP6 RNA-Polymerase	2 µl
RNase free H_2O	ad 20 µl
Mix by flicking the tube / short spin down / incubate for 2 hours at 37°C	

Table 33: DNAse treatment

Component	Amount
Sample	20 µl
10x DNase Buffer	2.5 µl
DNAse	2.5 µl
Incubate 1 hour at 37°C (keep 2 µl for a control gel)	

Table 34: RNA probe purification

Component	Amount		
Sample	23 µl	Ethanol 100%	86 µl
EDTA 0,2 M	2.3 µl	Mix components and add to sample	
LiCl 5 M	2.3 µl	**Application**	**Duration**
		-80°C	40 min
		spin 14,000 rpm, 4°C	10 min

150 µl 70% EtOH	wash pellet
-20°C	20 min
spin 17,000 rpm, 4°C	10 min

3.6.2 Zebrafish embryo preparation

Zebrafish embryos were dechorionated and up to 60 individuals were pooled per 2 ml tube. Subsequently, they were washed three times in RNase-free PBS and fixed in 4% PFA/PBS for 2 hours at room temperature or at 4°C overnight. Following fixation the embryos were washed two times 30 minutes in PBS-T to remove the PFA and passed through several dehydration steps (series of methanol:PBS-T solutions: 25:75; 50:50; 75:25; 100% methanol) which were each carried out at room temperature for 10 minutes. Dehydrated embryos can be stored at -20°C in methanol for several months. If the procedure was continued on the same day the dehydrated embryos were kept at -20°C for at least 2 hours. Afterwards, fish were rehydrated through a reversed series of ice-cold methanol:PBS-T solutions (75:25; 50:50; 25:75) on ice for 10 minutes and twice in PBS-T. Embryos older than 40 hpf were treated with 6% hydrogen peroxide for 30 min at 4°C in order to bleach the red blood cells which have already been developed at this stage. After bleaching, the fish were washed three times for 5 minutes in PBS-T.

Prior to permeabilization the embryos were fixed for 30 minutes in 4% PFA/PBS with three subsequent washes in PBS-T. The embryos were then treated with 10 µg/ml proteinase-K (Invitrogen) in order to permeabilize the tissue and thus facilitate probe-entry.

Depending on the developmental stage of the embryos tubes were agitated on the rotator SB3 (Stuart) for different time periods (Table 35). Proteinase-K was inactivated by washing the embryos twice for 5 minutes in PBS-T/glycine and twice in PBS-T. WT and morphant fish older than 45 hpf were additionally treated with RIPA-buffer for 10 minutes under agitation on the rotator with subsequent removal and washing three times for 5 minutes in PBS-T.

Table 35: Zebrafish proteinaseK treatment

Developmental stage	Duration of proteinase-K treatment
1 cell stage - 1 somite	30 seconds at room temperature (r.t.)
1 - 8 somite	1 minutes (r.t.)
9 - 18 somite	3 minutes (r.t.)

18 somite - 24 hpf	10 minutes (r.t.)
36 hpf - 5 d	30 minutes (r.t.)

After permeabilization animals were once more fixed in 4% PFA/PBS containing 0.2% glutaraldehyde/PBS-T for 20 minutes under agitation. Glutaraldehyde, which is a cross linker of proteins, helps fixating the tissue. Subsequently the fish were washed three times for 5 minutes in PBS-T. After finishing all preparative steps the embryos were selected and transferred into 1.5 ml "safe lock"-tubes (Eppendorf) for the incubation with different RNA-probes.

3.6.3 Hybridization

Prior to hybridization the embryos were washed once in Hyb- buffer for 10 minutes at room temperature. Fresh Hyb+ buffer was added and embryos were incubated at 68°C for 2 hours.

For hybridization of the animals with the RNA-probe, the latter was prepared in a concentration of 0.3 µg/ml - 1 µg/ml in Hyb+ buffer and denatured at 100°C for 5 minutes in a heating block (Digital heat-block; VWR). Embryos were mixed with 0.5 – 1 ml of this mixture and incubated under agitation overnight at 68°C.

For the removal of residual unbound probe fish were washed extensively in a series of buffers (Table 36). Unbound probe in the specimen results in unspecific and/or high background staining.

Used probe mixtures can be collected, stored at -20 and reused.

Table 36: Probe removal

Buffer	Conditions
Hyb-	68°C; 5 minutes
25% Hyb-	68°C; 3x 10 minutes
2x SSCT	68°C; <5 minutes
0.2x SSCT	68°C; 2x 30 minutes
50% 0.2x SSCT in MABT	RT; 5 minutes
MABT	RT; 5 minutes or 4°C; ON

3.6.4 Detection

Embryos were incubated in DIG-block for 1 hour at room temperature in order to minimize the background of unspecific bound antibody. At the same time conjugated antibodies were pre-adsorbed in DIG-block. Subsequently, fish were incubated in blocking solution containing antibody (Table 37) overnight at 4°C. For the removal of unbound antibodies the embryos were washed in MABT at room temperature for 3x 5 minutes and subsequently incubated over night at 4°C.

Table 37: ISH antibody dilutions

Antbody	Final concentration
Anti-Digoxigenin-AP Fab fragments	1:5000 in 2% Dig Block
Anti-Fluorescein-AP Fab fragments	1:1000 in 2% Dig Block
Anti-Fluorescein-POD Fab fragments	1:50 in 2% Dig Block

In order to prepare the embryos for the staining they were washed in freshly prepared alkaline-phosphatase buffer (NTMT) at room temperature for 2x 15 minutes. Subsequently they were incubated in 500 µl staining solution (BM-Purple, alkaline-phosphatase substrate; Roche) in the dark at room temperature for 2-6 hours, or overnight at 4°C. The time for color development (blue precipitate) varies depending on the probe and the gene to be detected. The dephosphorylation of the BM-purple substrate by the enzyme finally produces the purple, insoluble precipitate from the initially yellow solution. After the blue color had developed the embryos were washed in NTMT buffer in order to reduce the background. Subsequently they were washed twice for 5 minutes in PBS-T to stop the reaction. Afterwards the embryos were post fixed and treated as described in Table 38.

For staining with Fast Red, one Fast Red tablet was dissolved in 3 ml of 1 M Tris/HCl pH8,2, filtrated through a 0,22 µm pore filter and kept in the dark until use. Embryos were washed in 0,1 M Tris/HCl pH8,2 for 15 minutes prior to the incubation in Fast Red solution. After the red color had developed the embryos were washed post fixed and transferred to glycerol (Table 38).

For a peroxidase staining the embryos were washed twice in PBS. Subsequently, they were incubated under agitation at room temperature with freshly prepared 1x

DAB/metal enhanced substrate/peroxide buffer (Roche) in the dark until the precipitation of the color complex became visible.

The time for color development (brown precipitate) varies depending on the probe and the gene to be detected.

Table 38: Treatment after Fast Red staining

Buffer	Conditions
0.1 M Tris/HCl pH 8.2	15 min
PBS-T	2x 15 min or ON at RT
4% PFA/PBS	30 min RT
PBS-T	2x 15 min
30% Glycerol	until embryos settle down
50% Glycerol	until embryos settle down
70% Glycerol	until embryos settle down, refresh glycerol

If the embryos were to be stained in a second reaction for a second probe, the embryos were post-fixed and then transferred in to tubes, heat inactivated at 70°C for 1 hour, washed in MABT and blocked again in 2% DIG-block for 1 hour. At this point the protocol was repeated as previously by using the antibody against the second probe.

3.6.5 Preparation for imaging

Stained fish were washed once in 100% and twice in 70% ethanol. Subsequently the ethanol was exchanged by 50% glycerol/H_2O for long-term storage at 4°C. For imaging stained fish were either embedded in 1.5% low-melting agarose/egg water on an optical-dish (MatTek) or directly placed on a depression-slide containing a drop of 50% glycerol

3.7 Protein-related methods

3.7.1 Protein isolation from zebrafish

Total protein was isolated from 50 to 60 pooled, dechorionated embryos. At first the yolk-sack was removed by shearing the embryos by pipetting up and down in deyolking buffer using a 200 µl pipette and shaking them twice for 3 minutes at 1100 rpm on a thermo-mixer (HLC). Subsequently, deyolked embryos were washed in washing buffer under shaking for 3 minutes at 1100 rpm. After pelleting the embryos at 300 rpm and 4°C for 1 minute in a cooling tabletop centrifuge the supernatant was removed and 100 µl

RIPA-buffer were added for tissue-lyses. For the complete homogenization of the tissue the lysate was passed through a 24 gouge needle and was subsequently centrifuged at 10,000 rpm and 4°C for 10 minutes in order to remove RIPA-buffer-insoluble cell debris. The supernatant and the pellet fraction were stored separately at -20°C.

3.7.2 Protein concentration measurement

Protein concentration of extracts was measured with the BioRad DC^{TM} Protein Assay Kit. This colorimetric assay is based on the Lowry method of protein concentration measurement. A bovine serum albumin (BSA) standard curve and the protein samples (5 µl protein extract plus 5 µl H$_2$O) were prepared with subsequent addition of 20 µl Reagent A and 200 µl Reagent B (Table 39). After 15 minutes of incubation at room temperature the absorbance was measured at λ=740 nm in a Tecan Genios plate reader. The concentration of the samples was estimated according to the standard curve.

Table 39: BSA standard curve

	Concentration of BSA					
[mg/ml]	0	0.2	0.5	1	2	4
H$_2$O ad	5 µl	5 µl	5 µl	5 µl	5 µl	5 µl
µl RIPA	5 µl	5 µl	5 µl	5 µl	5 µl	5 µl

3.7.3 Mass spectrometry

A binary buffer system was used for peptide separation on the High Pressure Liquid Chromatography (HPLC) system "Easy Nanoflow" (Thermo Fisher Scientific). The HPLC was coupled via a "nano ESI" source to the mass spectrometer "QExactive". Peptides were eluted from the 20 cm columns by adjusting the ratio between the binary buffer system within 240 minutes at a temperature of 45 °C. MS spectra in a mass range of 350-1650 *m/z* were acquired using an AGC target of 3E6 at a resolution of 35000 at 200 *m/z*.

The Data was analyzed using MaxQuant (1.4.1.2) and the Andromeda search engine. For protein assignment ESI-MS/MS fragmentation spectra were correlated to the Uniprot zebrafish database (*D. rerio*, 40368 entries). A maximum of two

missed cleavages and a mass tolerance of 4.5 ppm and 7pp for MS/MS first and main search were set respectively.

Follow up data analysis and visualization was performed with Perseus and the statistical environment R.

3.7.4 Denaturing polyacrylamide gel electrophoresis

Proteins can be separated on denaturing polyacrylamide-gels (PAGE) in an electric field. The presence of reducing agents such as DTT or β-mercaptoethanol in the sample helps to denature the proteins by destroying tertiary and quaternary (oligomeric) structures. Being denatured and negatively charged through the binding of the anionic detergent SDS, which is present in the sample buffer, the gel and the running buffer, the proteins run towards the positively charged electrode (anode). The proteins run according to their electrophoretic-mobility, which is proportional to their molecular weight.

Protein extracts with SDS Sample Buffer and were heated at 95°C for 5 minutes and loaded on pre-casted 4-20% gradient criterion TGX stain free gels (BioRad). Additionally 3 µl protein standard (PrecisionPlus, BioRad) were loaded in one slot for the subsequent size estimation. In a PAGE chamber (Criterion, BioRad) filled with 1x Tris/Glycine/SDS Buffer (BioRad) the gels were run first at 75 V for 30 minutes to concentrate the samples in the stacking gel in order to assure the same running distance for all proteins present in a sample. Then the gels were run at 150 V for 1.5 hours for the actual separation of the proteins.

3.7.5 Western blot

Western blots were performed to detect specific proteins. The proteins separated in the gel were transferred on a PVDF membrane (Trans Blot Turbo Transfer Pack) where they were bound tightly through hydrophobic interactions. For this purpose the membrane was placed on top of the gel and placed between filter papers Bubbles were removed from each layer by gentle pressure. Thereafter an electric field between cathode and anode was applied and the proteins were transferred from the gel to the membranes in 7-10 minutes using Trans Blot Turbo (BioRad). After transfer the membranes were blocked in 5% skim milk in 1x PBS-T for 1 hour at room temperature on a orbital shaker. For the immuno-detection of specific proteins primary antibodies were diluted in a minimum of 4 ml skim

milk solution or 5% BSA in TBS-T and membranes were incubated overnight at 4°C on a roller mixer SRT6 (Stuart). For the removal of unbound antibodies membranes were rinsed three times with PBS-T and additionally washed three times for 10 minutes in PBS-T at room temperature on an orbital shaker. Subsequently, horseradish-peroxidase-conjugated secondary antibodies were diluted 1:10,000 in PBS-T and membranes were incubated for 1 hour at room temperature. After washing in PBS-T as described before the membranes were covered with chemiluminescent solution SuperSignal West Femto (PIERCE) and pictures were taken with the ChemiDoc MP (BioRad).

### 3.8 Generation of zebrafish mutants

Zebrafish mutants were generated by with the clusterd, regularly interspaced, short palindromic repeat (CRISPR) technology.

3.8.1 CRISPR-Cas9

The CRISPR technology is based on RNA guided nucleases such as Cas9, which cause DNA double strand breaks (DSBs). These DSBs can be repaired by nonhomologous end-joining (NHEJ). NHEJ often leads to the formation of insertion/deletion mutations (indels) which can cause frame shifts und thus lead to the formation of null-mutants for the desired gene.

3.8.2 CRISPR design

Guide RNAs (gRNAs) for the gene locus of interest allow to generate targeted DSBs. Specific gRNAs were designed using http://crispr.mit.edu/ CRISPR design tool. DNA oligomers corresponding to the selected gRNA sequences were purchased from Sigma Aldrich as standard de-salted oligos. The oligos that were designed for Memo1 are shown below.

```
5`- TAGGCCGTGTACCAGCTGCCGGCG          -3`
3`-      GGCACATGGTCGACGGCCGCCAAA     -5`
```
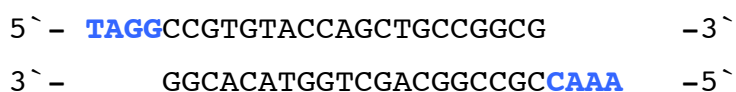
The overhangs will facilitate ligation of the annealed oligos to the destination vector backbone. The oligos were annealed by simply mixing equal amounts of complementary oligos and heating them up to 95°C for 3 min and then cooling them

down slowly at room temperature for approximately 1 hour. The destination vector DR274 was previously digested with BsaI (NEB) so that annealed oligos with complementary overhangs can be ligated to it. The ligated product was the used for transformation of bacteria. Positive clones were screened by sequencing with M13 forward primer. Synthesis of the gRNA was performed with the MEGAshortscript T7 kit (Ambion) following the manufactures' instructions, using *Dra*I digested gRNA expression vector as template.

Cas9 nuclease mRNA was transcribed from *Pme*I-digested Cas9 expression vector using the mMESSAFE mMACHINE T7 ULTRA kit (Ambion). Zebrafish embryos were injected with a mixture of 25 pg gRNA and 150 pg Cas9 mRNA.

3.8.3 Identification of mutants and genotyping (HRMA)

To analyze animals for genomic insertions / deletions (indels) at the CRISPR binding locus, genomic DNA (gDNA) was isolated from individual embryos or from fin clips of adult zebrafish. To do so, animals / fin clips were heated at 95°C for 10 min in 25 μl Tris/EDTA buffer and subsequently proteinaseK was added to a final concentration of 2 mg/ml. The samples were incubated a 55°C for two hours and then heated at 95°C for 10 min, to inactivate the proteinaseK. After centrifugation 1 μl of the lysate was applied to each high-resolution melt analysis (HRMA) PCR reaction. For the PCR reaction mixture 5 μl 2x DyNAmo color flash SYBR green master mix (thermo Scientific) and 5 pmol of forward and reverse primer were used (Table 40).

Table 40: HRMA PCR protocol

Temperature	Time
95°C	10 minutes
95°C	10 seconds
60°C	15 seconds
	repeat two stepts x40
High-resolution melt-curve	
95°C	15 seconds
55°C	15 seconds

95°C	15 seconds

3.9 Zebrafish imaging techniques

3.9.1 Life imaging (spinning disc)

Blood flow velocity as a measure of heart performance was measured by spinning disc life imaging. Blood flow of zebrafish was recorded by imaging the dorsal aorta below the 8th -10th segmental vessel by using a spinning disc microscope, which allows high-speed recording. Larva were kept in egg water containing 0.02% Tricaine (5, 6 dpf) until they were touch irresponsive. Subsequently they were mounted in low melting agarose on a glass bottom slight, so they could be imaged in a lateral view. Videos were taken at 400 frames/second for a total length of 2 seconds. Blood flow velocity and acceleration were measured by blood cell tracking using a particle tracking software (Tracker).

Heartbeats of transgenic zebrafish larva were imaged using the spinning disc microscope. Zebrafish were mounted in low melting agarose on a glass bottom dish, so they could be imaged in a ventral view. Z-stacks of beating hearts were imaged at 400 frames/second.

3.9.2 Life imaging (LSM700/LSM780)

Hearts and skeletal muscle of life or fixed zebrafish larva were imaged using confocal microscopy. Embryos/larva were mounted in low melting agarose on glass bottom dishes, so they could be imaged in a lateral or ventral view, respectively. Optical sections were 1.4 μm thick.

3.9.3 Whole mount immuno-staining

For whole mount immuno-staining zebrafish were incubated in 0,05% Tricaine to stop and relax the heart. Subsequently fish were fixed in "fish-fix" or 4% PFA (Thermo scientific) in PBS over night at 4°C. Next day the fish were washed with PBS and treated with 10 μg/ml proteinaseK for 30 min at room temperature. Subsequently they were washed in PBS and post fixed in "fishfix" or 4% PFA/PBS for 1 hour at room temperature and then permeabilized in PBS containing 0.5 % triton x-100 at 4°C over night. Fixed and permeabilized zebrafish were then blocked in 5% goat serum until

evening and incubated in 5% goat serum containing primary antibody over night at 4°C. Removal of excessive primary antibody was achieved by washing in permeabilization buffer for 3 short and three long washes over several hours. Finally the embryos/larva were incubated in secondary antibody (Alexa fluor, Invitrogen)) diluted 1:100 in 5% goat serum over night at 4°C. Phalloidin (Invitrogen) stainings were similarly performed 1:100 in 5% goat serum over night at 4°C. After extensive washing zebrafish were mounted and imaged.

3.9.4 "Evans Blue" membrane integrity staining

Evans Blue staining was performed to analyze membrane integrity of zebrafish skeletal muscle cells. Evans Blue (Sigma) was dissolved at 0.1% (w/v) in egg water. Live zebrafish larva were incubated in the solution for 60 min and subsequently washed in egg water. Fish were mounted and imaged with the Nikon SMZ25 stereomicroscope.

4 Results

4.1 Flightless

4.1.1 Flightless I, the causative gene in *duesentrieb* mutants, is expressed in the zebrafish heart.

To study the relevance of cytoskeletal integrity in heart trabeculation we were interested in genes that encode proteins, which associate to structural proteins such as Actin. Previous studies have shown that the Actin binding protein Flightless I (Flii) is important for skeletal muscle development and swimming behavior in zebrafish.

In order to investigate the role of *flii* in the zebrafish heart an *in situ* hybridization detecting *flii* mRNA expression was performed (Fig.4.1, A). *Flii* is expressed in the heart, in the brain and the fin buds of zebrafish larvae at 72 hpf. At 7 dpf *flii* expression is still found in the heart whereas the expression in the brain is reduced. However, expression in skeletal muscle was below the detection limit at any time point and under the conditions applied in these experiments. To further analyze the expression of *flii* in zebrafish its overall temporal expression at different time points was analyzed by qRT-PCR (Fig. 4.1, B). *Flii* is maternally contributed and expressed throughout the embryonic development until 72 hpf. Taken together, *flii* is expressed at least until 7 dpf in a variety of organs including the heart.

In a previous study the *duesentrieb* (dus^{tg250}) phenotype has been described, exhibiting skeletal muscle fiber disorganization with reduced touch responsive swimming ability (Granato et al., 1996). Due to the phenotypical similarity between the *dus* mutants and the $flii^{mi372}$ mutants, that had been previously described, a sequence analysis for *flii* was performed. Sequencing of the *flii* gene in dus^{tg250} mutants revealed a homozygous point mutation in exon 12 in position 1581 (C/A), leading to a premature stop-codon (Tyr/ochre) (Fig. 4.1, D, E).
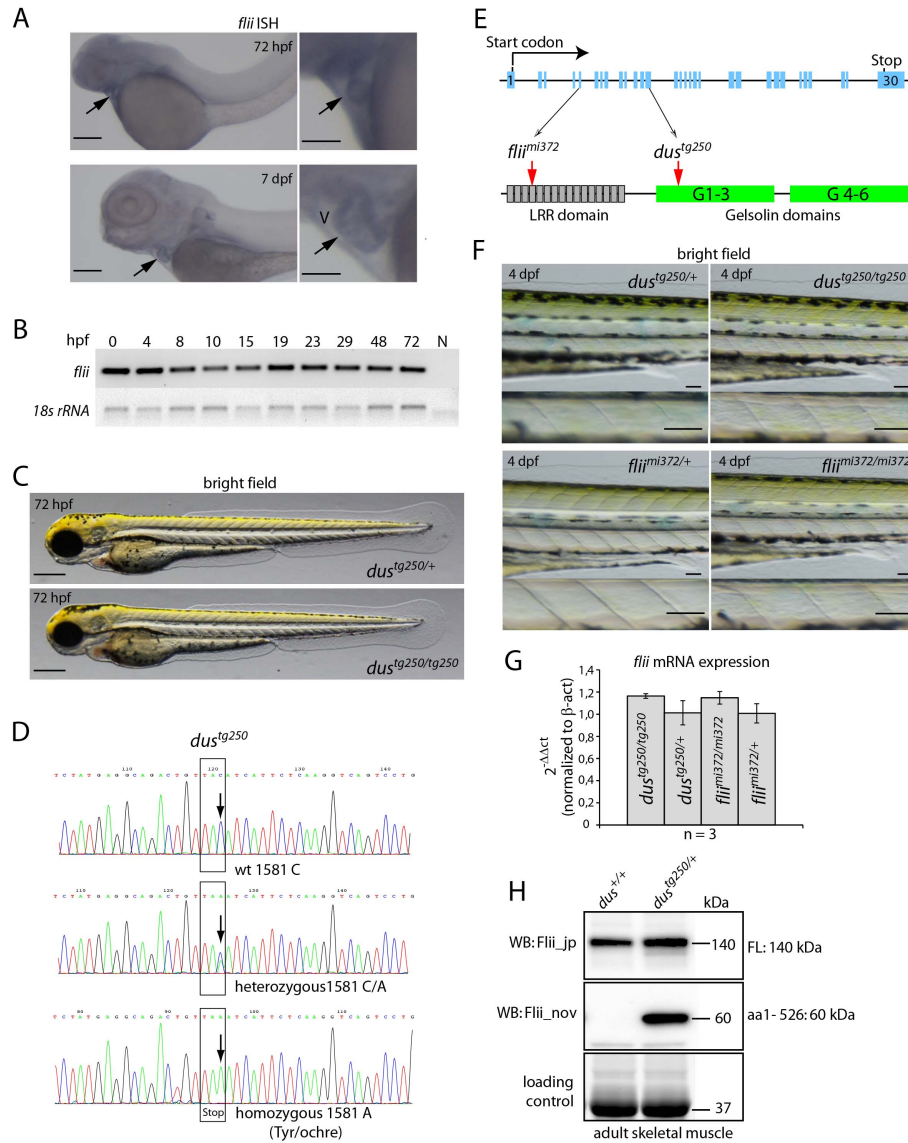
Figure 4.1: Allele $dus^{tg250/tg250}$ corresponds to a mutation in the flightless I gene.

A) *In situ* hybridization for flightless I in zebrafish larvae. Flightless I is expressed in in the heart at 72 hours post fertilization (hpf) and at 7 days post fertilization (dpf) in the ventricle. Arrows mark the position of the heart. Scale bars: 250 µm, in magnifications 100 µm. **B)** Temporal expression for *flii* by qRT-PCR. *flii* is maternally contributed and expressed at all developmental time points tested from 4 hpf to 72 hpf. 18S rRNA expression was analyzed as housekeeping gene (loading control). N is the negative control. **C)** Bright field images of zebrafish larvae at 72 hpf. Dus^{tg250} mutants are phenotypically indistinguishable from siblings. Scale bars: 250 µm. **D)** Sequence analysis of animals carrying the dus^{tg250} allele. The dus^{tg250} allele corresponds to a C/A mutation at position 1581 in the *flii* gene leading to a premature Stop codon (Tyr/ochre). Arrows mark position of the mutation in wild-type (wt), heterozygous and homozygous mutant animals. **E)** Scheme of *flii* gene and protein structure. *Flii* is composed of 30 coding exons. The protein is composed of 16 LRR-domains and 6 gelsolin domains (green bars represent Gelsolin domains G1-3 and G4-6). The two alleles $flii^{mi372}$ and dus^{tg250} are located on different exons. Allele $flii^{mi372}$ is located in exon 5 and leads to a frame shift in the fourth LRR-domain. Allele dus^{tg250} is located on exon 13 and leads to premature STOP in the first gelsolin domain. **F)** Bright field pictures of zebrafish trunk area at 4 dpf. Trunk somites, yolk extension and cloaca develop normal in mutants and siblings. Enlargement of ventral somites shows rough surface appearance in mutants compared to siblings. Scale bars 50 µm. **G)** QPCR for *flii* mRNA expression at 72 hpf. Mutant animals for two different alleles dus^{tg250} and $flii^{mi372}$ show slight but not significant increase in *flii* mRNA levels compared to siblings. Measured values were normalized to b-Actin expression. **H)**

68

Western blot detecting Flii protein in adult zebrafish skeletal muscle extracts. Flii_jp (courtesy from Hiromi Hirata, Japan) detects a band at 140 kDa. Flii_nov (purchased from Novus) antibody detects a band at 60 kDa only in extracts from heterozygous animals. Loading control corresponds to a whole protein staining using TGX Stain-Free^{TM} gels (BioRad).

The *flii* gene is composed of 30 exons encoding two different types of domains, a leucine-rich-repeat domain (LRR-domain) and six gelsolin domains. The six gelsolin (G) sub-domains form two functional gelsolin domains, an amino-terminal (NT) domain composed of G1-3 and a carboxy-terminal (CT) domain composed of G4-6 (Fig. 4.1, E). The *dus^{tg250}* mutation leads to a putative truncation of the protein in the first gelsolin domain, whereas the *flii^{mi372}* mutation, which is located in exon 5, leads to a premature stop codon in the corresponding fourth LRR-domain.

Both mutants display the previously described fast twitch muscle deficient swimming behavior at 48 hpf (data not shown). However, *dus^{tg250}* mutants develop morphologically indistinguishable from siblings until 72 hpf (Fig. 4.1, C). In order to confirm the skeletal muscle phenotype, bright filed images of the trunk region above the yolk extension where taken at 4 dpf. The trunks of mutant animals and siblings appear normal (Fig. 4.1, F). In a higher magnification of the ventral somites of *dus^{tg250}* and *flii^{mi372}* mutants, however, a rough appearance of the somite surface is visible compared to siblings, most likely reflecting the muscle fiber malformation.

In order to analyze if the mutant *flii* mRNA is stable or if it becomes degraded, RT-PCR using gene specific primers was performed. *flii* mRNA from *dus^{tg250}* and *flii^{mi372}* mutants is not targeted for degradation. Mutants have a slight but not significant increase in *flii* expression compared to siblings (Fig. 4.1, G).

Since the *flii* mRNA is stably expressed we were interested in analyzing if a truncated protein becomes translated from the mutant mRNA. Proteins isolated from adult skeletal muscle of *dus$^{tg250/+}$* and wt animals were analyzed on immuno-blots using anti-Flii antibodies (Fig. 4.1, H). Anti-Flii_jp antibody detects a band corresponding to the full-length protein with a size of ~140 kDa. Whereas Anti-Flii_nov (Novus Biologicals) detects a band of ~60 kDa. This 60 kDa band is only present in the heterozygous animals, and presumably corresponds to the mutated allele (amino acids 1-526) leaving a truncated LRR-domain containing Flii protein fragment (Fig. 4.1, E, H).

This result suggests that the mutated *dus^tg250* mRNA is stable and becomes translated into a truncated Flii protein, which might be able to fulfill partial protein function.

Although the mutant animals appear morphologically normal, they fail to inflate their swim bladder at around 4 dpf and most probably die due to reduced feeding ability at the time they become transferred to the aquatic system.

To further analyze the skeletal muscle phenotype a phalloidin staining, which marks Actin fibers, was performed. Trunk skeletal muscle of 48 hpf *dus^tg250/+* zebrafish embryos display an organized striated pattern (Fig. 4.2. A). In contrast, *dus^tg250/tg250* mutant animals show mostly disorganized myofibrils. Magnifications of specific areas and z-planes corresponding to either fast or slow twitch muscle cells reveal that the fast twitch muscle fibers of *dus* mutants at 48 hpf and 6 dpf are affected (Fig. 4.2, B). Interestingly, slow twitch muscle cells of 48 hpf and 6 dpf old animals appear unaffected (Fig. 4.2, C, D).

To examine if slow twitch muscle fibers are generally unaffected in zebrafish *dus* mutants, craniofacial muscles, which have been demonstrated to be slow muscle myosin-positive, were analyzed. Interestingly, craniofacial muscles are affected and have a similar corrugated appearance as observed in fast twitch muscle fibers of *dus* mutant zebrafish trunks (Fig. 4.2, F), suggesting that Flii function is not restricted to fast twitch muscle fibers.
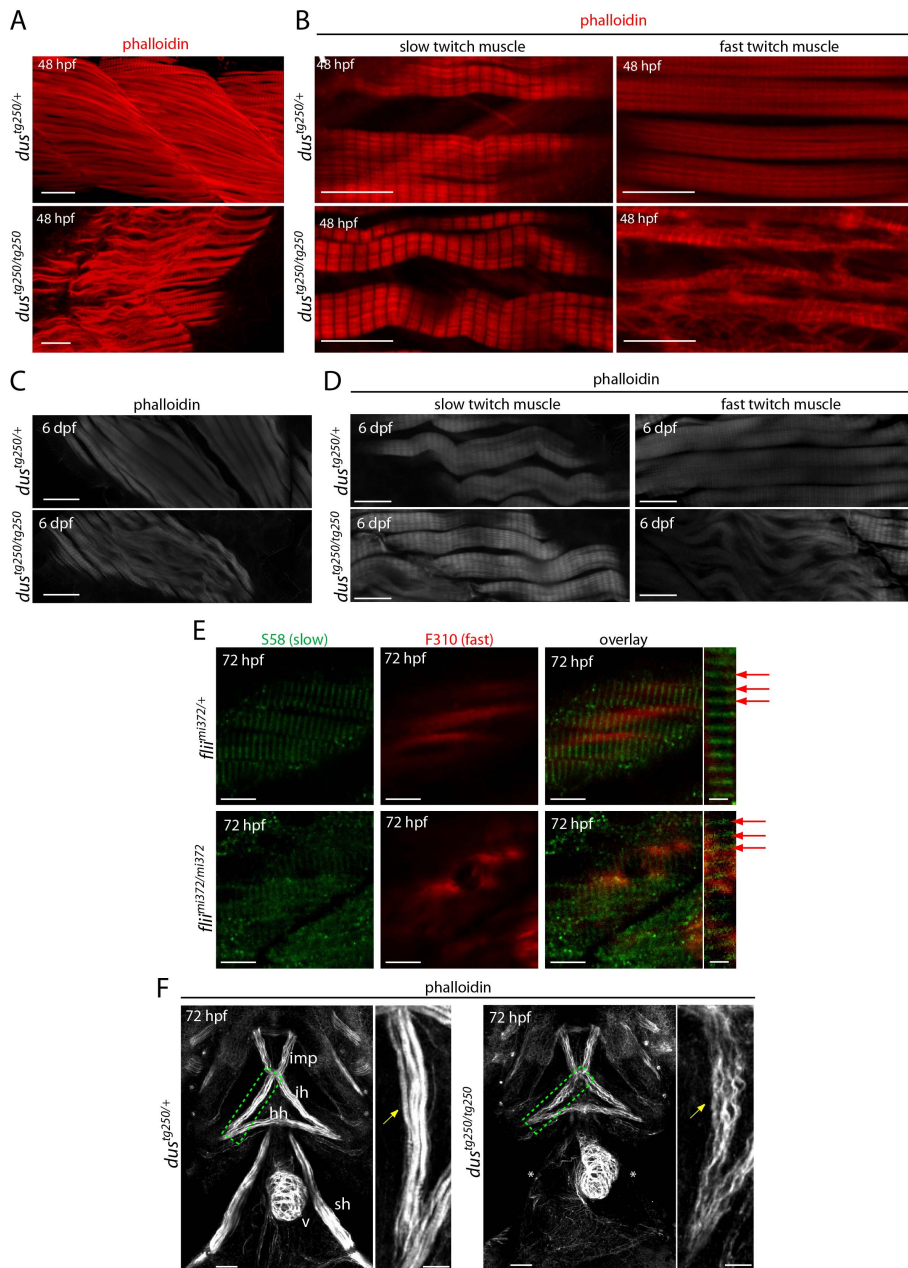
Figure 4.2: Fast and slow twitch skeletal muscle fibers are affected in *dus^tg250* mutant animals.

A-D) Confocal projections of phalloidin stained zebrafish trunk skeletal muscle showing muscle fibers. **A,C)** Phalloidin staining at 48 hpf and 6 dpf, respectively, show disorganized appearance of muscle fibers in *dus^tg250* mutants compared to heterozygous siblings. **B,D)** Left panel: slow twitch skeletal muscle fibers look similar in *dus^tg250* mutants and heterozygous siblings at 48 hpf and 6 dpf. Right panel: fast twitch skeletal muscle is affected in *dus^tg250* mutants compared to heterozygous siblings.

Scale bars A, C: 25 µm; B, D: 10 µm. **E)** Whole mount staining of zebrafish larvae at 72 hpf showing slow and fast twitch muscle specific staining. Slow twitch fibers (anti-avian slow myosin heavy chain 2 and 3; clone S58) in green and fast twitch fibers (anti-myosin light chain 1 and 3f; clone F310) in red. *flii^mi372* siblings show organized striated pattern in muscle fibers for slow muscle myosin. *flii^mi372* mutant animals show weaker slow myosin striations and disorganized staining. Fast muscle myosin staining shows bundled fast twitch muscle fibers in *flii^mi372* siblings, which appear disorganized in homozygous mutants. **F)** Confocal projections of phalloidin stained zebrafish at 72 hpf. View on jaw muscles and magnification of the interhyoideus, corresponding to the area in the green box. The arrows point at the muscle fibers of the interhyoideus, which appear disorganized in *dus^tg250* mutant animals compared to siblings. Asterisks mark the position of the sternohyoideus present but not visible in this projection. Scale bars: 25 µm, in

magnification 10 μm; hh = hyohyoideus, ih = interhyoideus, imp = intermandibularis posterior, sh = sternohyoideus, v = ventricle.

A more detailed analysis of *flii^mi372* animals was performed in order to confirm that the slow twitch trunk skeletal muscle fibers are unaffected. For this reason whole mount immunostaining's for slow (F58) and fast (F310) muscle myosin were analyzed (Fig. 4.2,E). As expected fast muscle myosin (red) appeared disorganized in *flii^mi372* mutants compared to siblings. Slow muscle specific myosin (green) shows an organized striated pattern in *flii^mi372* siblings. However, mutants display partially disorganized slow muscle fibers, suggesting that the slow twitch trunk skeletal muscle fibers are as well affected by Flii deficiency.

4.1.2 Vinculin localization to cell-matrix adhesions is affected in skeletal muscle cells of *duesentrieb* mutants.

Muscular dystrophies, like Duchenne, are caused by mutations in the gene encoding dystrophin, a protein involved in adhesion site formation (Hoffman et al., 1987). Since Flii has been shown to play a role in focal adhesion formation we were interested if *dus* mutants exhibit hallmarks of muscular dystrophies. Evans blue dye is a marker for the disruption of the sarcolemma and therefore provides insight into the pathogenesis underlying the *duesentrieb* phenotype. *Dus* mutants do not show any Evans blue-positive trunk muscle cells indicating that the cells are intact and therefore the dye cannot enter and stain the muscle fibers (Fig. 4.3, F). This result suggests that *dus* might rather resemble a myopathy than a muscular dystrophy (Cardamone et al., 2008; Chawla, 2011).

To further understand the function of Flii in focal adhesions we analyzed the subcellular localization of Vinculin-GFP in skeletal muscle cells. Vinculin is a focal adhesion core protein, which interacts with several proteins in order to link the Actin cytoskeleton to the cell membrane at the position of a focal adhesion (Carisey et al., 2013). In muscle cells Vinculin is associated to costameres, connections between sarcomeres and the sarcolemma, and to somite boundaries (Tidball, 1991).
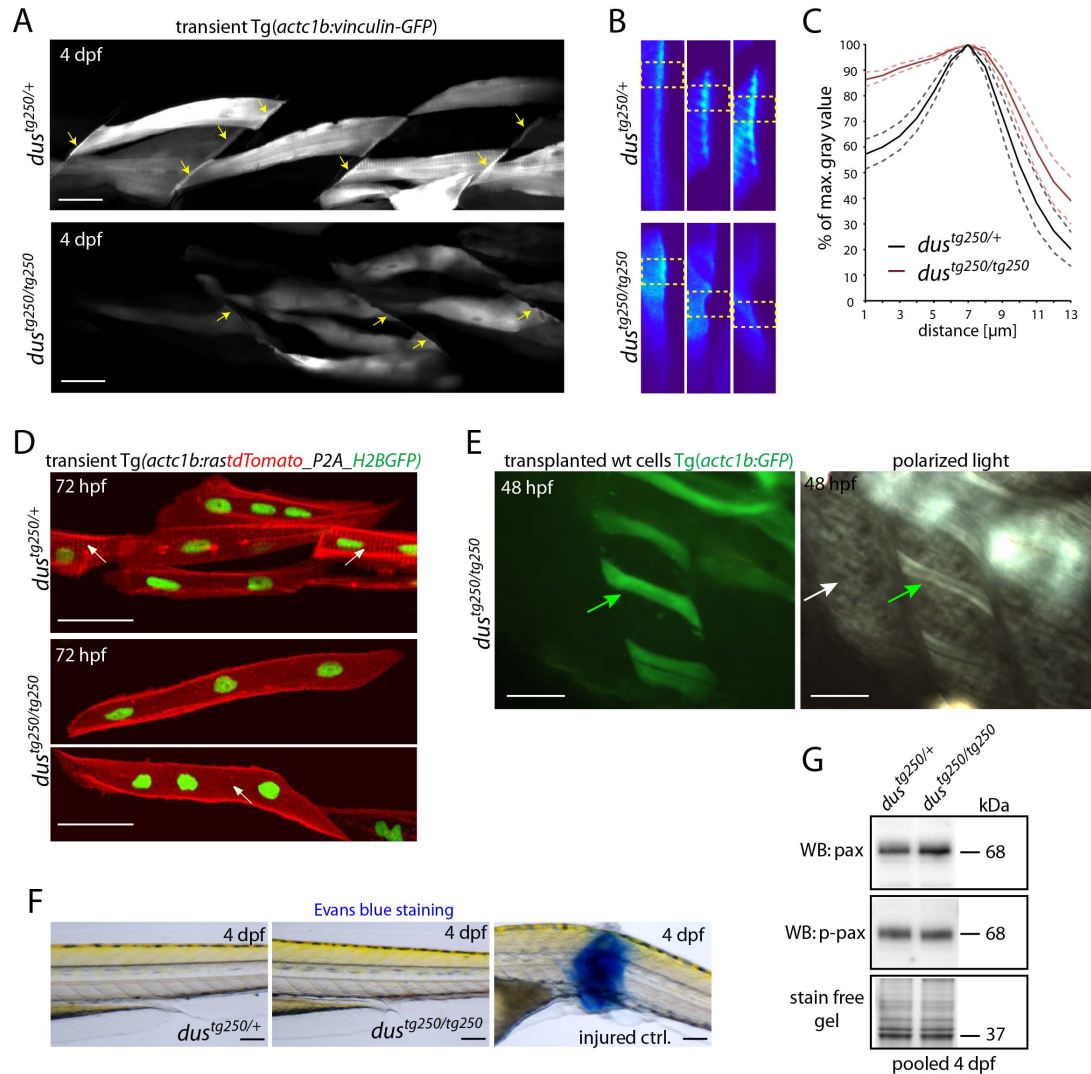
Figure 4.3: Impaired vinculin localization in *dus^tg250^* mutant animals.

A, B) Confocal projections of transient *Tg(actc1b:vinculin-GFP)* expressing zebrafish at 4 dpf. **A)** View on trunk fast twitch muscle cells. Arrows show cell edges on the somite boundaries. Scale bars 25 µm. **B)** Heat map of the confocal projections from three optical sections. Vinculin-GFP localization at cell edges appears reduced in *dus^tg250/tg250^* mutants compared to siblings. **C)** Averaged fluorescence intensity quantification of boxed areas in B. *dus^tg250^* siblings show 57% (+/-6%) fluorescence intensity in cytosol relative to the cell edge (black line) while mutants show 86% (+/- 3%) fluorescence intensity in cytosol relative to the cell edge (red line). Dotted lines represent standard errors. **D)** Confocal projections of transient *Tg(actc1b:rastdTomato_P2A_H2B-GFP)* expressing zebrafish at 72 hpf. Views on trunk fast twitch muscle cells showing striated pattern in *dus^tg250^* siblings, which are not detectable in the mutant animals, yellow arrows. Membranes are red and nuclei are green. Scale bars 25 µm. **E)** Confocal projections of zebrafish trunks showing transplanted wt *Tg(actc1b:GFP)* expressing fast twitch muscle cells at 48 hpf. Transplanted cells appear unaffected (green arrows) in *dus^tg250^* mutant background (white arrow). The right panel shows images of the same trunks taken with polarized light. Scale bars 50 µm. **F)** Bright field images of Evans blue stained zebrafish larvae at 4 dpf. No Evans blue-positive cells are visible in trunks of *dus^tg250/+^* or *dus^tg250/tg250^* animals. As positive control for Evans blue staining injured zebrafish were used. Scale bars 100 µm **G)** Western blot detecting Paxillin (Pax, 68 kDa) and

phospho Paxillin (p-pax, 68 kDa) in protein extracts from pooled 4 dpf zebrafish trunks. Pax and p-Pax are expressed in dus^{tg250} siblings and mutants. Pax expression in the mutants appears slightly increased compared to siblings.

Indeed, $dus^{tg250/+}$ zebrafish expressing a skeletal muscle-specific Vinculin-GFP construct exhibit a striated GFP pattern and localization to the somite boundaries (Fig. 4.3, A). In contrast, mutants do not show a subcellular localization of Vinculin-GFP to specific structures. Magnifications of cell edges indicate that there is an accumulation of Vinculin-GFP at the somite boundaries of *dus* siblings compared to the cytoplasm (Fig. 4.3, B). Quantifications of the gray values of these areas revealed that $dus^{tg250/+}$ siblings display 57% (+/-6%) fluorescence intensity in cytosol relative to the somite boundaries (black line) whereas mutants display 86% (+/- 3%) fluorescence intensity in cytosol relative to the somite boundaries, suggesting that mutants might fail to localize Vinculin to focal adhesion sites, or that the focal adhesions might be disrupted. (Fig. 4.3, B, C)

To further explore the status of focal adhesions we were interested, if another core complex protein Paxillin is also affected in *dus* mutants. Western blot analysis revealed that zebrafish trunk extracts from 4 dpf *dus* mutants have a slight increase in Paxillin concentration compared to mutants (Fig. 4.3, G). Paxillin is a signal transduction adaptor protein, and becomes phosphorylated by Focal Adhesion Kinase (FAK) and Src upon integrin activation. It has been previously shown, that Paxillin phosphorylation is reduced in Flii overexpressing fibroblasts (Kopecki et al., 2011). Western blot analysis for p-Pax revealed no difference in the amount of phosphorylated Paxillin in *dus* mutants compared to siblings (Fig. 4.3, G).

4.1.3 Skeletal muscle cells of *duesentrieb* mutants lack t-tubular structures.

In order to understand if membrane structures that are associated with sarcomeres are per se affected we analyzed the presence of transverse-tubules (t-tubules), which are formed by the sarcolemma. These structures are associated with the underlying z-discs of myofibrils, and allow efficient propagation of action potentials in muscle fibers (Brette and Orchard, 2003). Skeletal muscle-specific overexpression of palmitoylated Ras-tdTomato, which localizes to cell membranes, revealed that myofibrils of 72 hpf *dus* siblings display the striated pattern characteristic for t-tubles (Fig. 4.3, D). However, these striations are not detectable in fast skeletal myofibrils of $dus^{tg250/250}$ animals.

These results suggest, that myofibrils of *dus* mutants might lack t-tubular structures rendering them dysfunctional.

4.1.4 Cardiac myofibril formation / bundling is disrupted in *duesentrieb* mutants.

Since the main Goal of this study is to understand the role of Flii during heart development we characterized cardiac myofibrils in *dus* mutant animals. To do so we generated a line carrying the *dus^{tg250}* allele in a *Tg(myl7:LifeAct-GFP)^{s974}* background, which enables visualization of F-actin. Analysis of live zebrafish embryonic hearts at 24 hpf exhibit a fine meshwork of F-actin only at the luminal side of the cardiomyocytes, in both *dus* mutants and sibling (Fig. 4.4, A). This localization of F-actin to the basal side represents an early sign for polarization of the cells. At 72 hpf the hearts are looped and ballooned and thick myofibrils have formed in both cardiac chambers of *dus* siblings (Fig. 4.4, B, D). Hearts of mutant animals appear slightly delayed in cardiac looping (Fig. 4.4, C). Myofibrils are formed in mutant animals, however they appear to be thinner compared to siblings in both ventricles and atria (Fig. 4.4, B', B'', C', C''). Hearts of compound heterozygous (*flii^{mi372}/dus^{tg250}*) animals at 4 dpf are slightly delayed and posses overall thinner myofibrils compared to siblings (Fig. 4.4, F-F'', G-G'')

4.1.5 *Duesentrieb* mutants fail to form trabeculae in the ventricular lumen.

To observe later morphogenetic changes occurring in the heart we analyzed hearts of zebrafish larvae at 5 dpf, at this stage trabeculae have formed in the ventricles of siblings (Fig. 4.5, A). The magnification of a trabecular cell in the projection displays thick myofibrils, which stretch through the entire presumptive cell. In hearts of mutant animals clear trabecular cells are missing, and the magnified projection image shows thinner and less bundled myofibrils (Fig. 4.5, B). Ventricular cardiomyocytes show a specific subcellular distribution of thick and thin myofibrils. The abluminal (apical) side is mainly occupied by thin fibers (Fig.4.5, A', B'), whereas the basal side contains thick fibers (Fig. 4.5, A'', B''). This specific distribution is not altered in *dus* mutant animals compared to siblings. Single planes of the ventricular chambers however clearly show a reduced amount of thick fibers in the mutants. Furthermore the myofibrils of mutant animals appear less tensed, almost slack (Fig. 4.5, A''', A'''', B''', B'''').
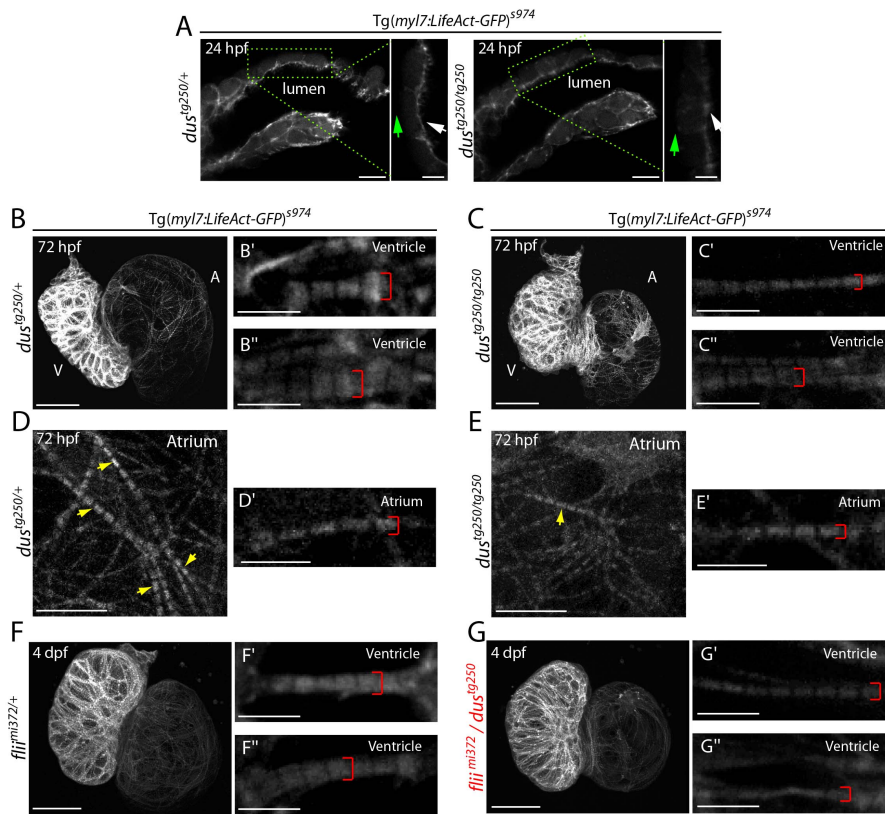
Figure 4.4: Impaired cardiac myofibril formation / bundling in *dus^{tg250}* mutant animals.

A) Confocal projections of zebrafish atrial heart chambers expressing *Tg(myl7:LifeAct-GFP)^{s974}* at 24 hpf. LifeAct-GFP binds to filamentous Actin (F-actin). GFP-positive Actin meshwork can only be detected at the luminal side of the cardiomyocytes (white arrows) in both *dus^{tg250}* mutants and siblings. Green arrows denote the abluminal side of the cardiomyocytes. Scale bars 10 µm, magnifications 5 µm. **B-G)** Confocal projections of *Tg(myl7:LifeAct-GFP)^{s974}* zebrafish hearts at 72 hpf and 4 dpf respectively. Visualization of LifeAct-GFP, which is bound to F-actin in cardiac myofibrils. **B,C)** Hearts of *dus^{tg250/+}* and *dus^{tg250/tg250}* are looped and ballooned. Panels B', B'' and C', C'' show examples of ventricular myofibrils. Mutants (C) appear to have thinner fibrils compared to siblings (B). **D,E)** Myofibrils of atrial chambers. D) Siblings show more thick myofibrils compared to mutant (E) animals (arrowheads). D', E') Magnifications of myofibrils shows similar thickness for both siblings and mutants. Scale bars of whole hearts 50µm, Atrium 10 µm, magnifications 5 µm. **F,G)** Hearts of compound heterozygous animals *flii^{mi372/+}/dus^{tg250/+}* are looped and ballooned at 4 dpf. Panels F', F'' and G', G'': compound heterozygous animals appear to have thinner ventricular myofibrils (G) compared to *flii^{mi372/+}* siblings (F). Scale bars of whole hearts 50µm, magnifications 5 µm. V = Ventricle A = Atrium.

At 5 dpf the atria of *dus* mutants are strongly affected showing only few and thin myofibrils compared to siblings and the atrial cardiomyocytes appeared inflated (Fig. 4.5, D). Analysis of single ventricular planes revealed that *dus* mutant animals failed to form trabeculae at 5 dpf (Fig. 4.5, C). These results suggest, that Flii is necessary for myofibril formation or maintenance; its deficiency leading to thinner and sparse myofibrils. Furthermore Flii-deficiency leads to a lack of trabeculation in zebrafish hearts at 5 dpf.
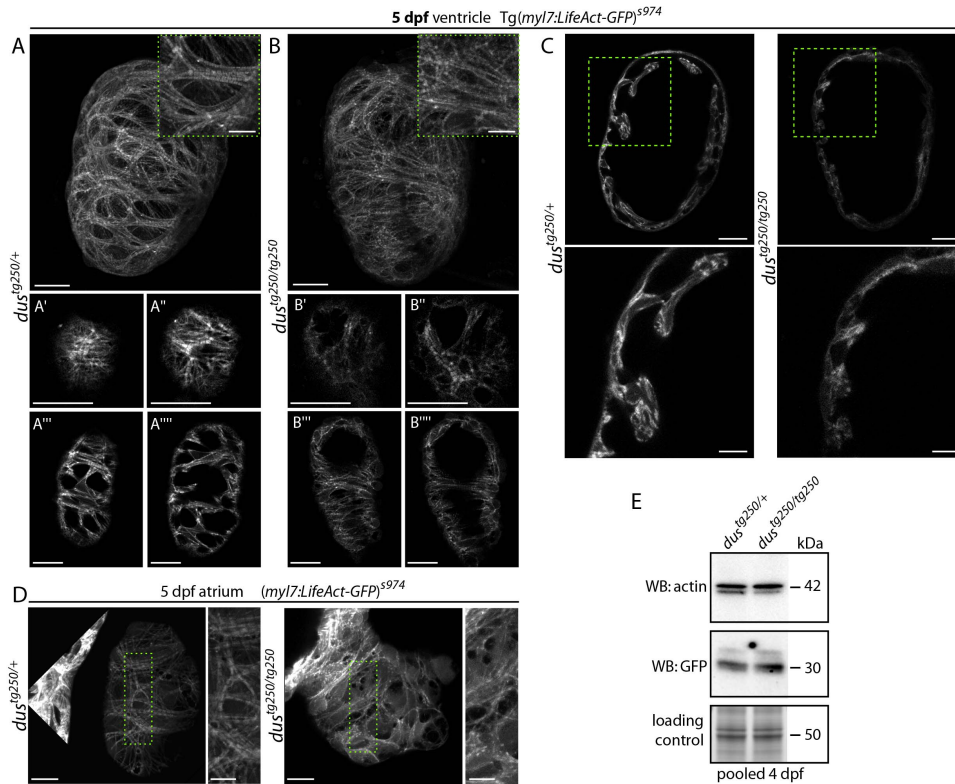
Figure 4.5: Impaired cardiac trabeculation in *dus^{tg250}* mutant animals.
A-C) Confocal projections and single planes of *Tg(myl7:LifeAct-GFP)^{s974}* zebrafish hearts at 5 dpf. **A)** View on the outer curvature of heart ventricles. Magnification shows bundled myofibrils in *dus^{tg250/+}* while *dus^{tg250/tg250}* animals show aberrant bundling, compare green boxes. Single optical sections of different planes of the ventricular chamber. A' and B' show thin fibers of the abluminal side of the cardiomyocytes in both *dus^{tg250/+}* and *dus^{tg250/tg250}* animals. A'' and B'' show thick fibers at the luminal side of the cells in both *dus^{tg250/+}* and *dus^{tg250/tg250}*. A''', A'''' and B''', B'''' represents the meshwork that directly underlies the ventricular wall. *dus^{tg250/tg250}* appear to have a reduced number and size of contractile fibers compared to siblings. Scale bars of projection 25 μm, magnifications 10 μm, single planes 25 μm. **B)** Projections of atria show aberrant appearance of chamber surface in *dus^{tg250/tg250}* animals compared to siblings. Mutants also show reduced number and size of contractile fibers compared to siblings (magnification of the green boxes). Scale bars 10 μm, magnifications 5 μm. **C)** Single planes: ventricular trabeculae are visible in the lumen of the chamber. Magnifications from the areas in the green boxes from the above respective panels show that *dus^{tg250/tg250}* lack these trabecular structures. Scale bars 25, magnifications 10 μm. **E)** Western Blot detecting Actin and LifeAct-GFP in zebrafish trunk extracts at 4 dpf. Protein levels of Actin and LifeAct-GFP are similar in *dus^{tg250/+}* and *dus^{tg250/tg250}* animals. Loading control corresponds to a whole protein staining using TGX Stain-Free^{TM} gels (BioRad).

In order to unravel if the myofibrillar phenotype is due to reduced availability of Actin building blocks we analyzed Actin levels. Actin protein levels were not changed in extracts from 4 dpf *dus* mutants compared to siblings. Furthermore expression of LifeAct-GFP was measured in order to exclude the possibility that the reduced myofibrill appearance was due to reduced availability of LifeAct-GFP. Protein levels of LifeAct-
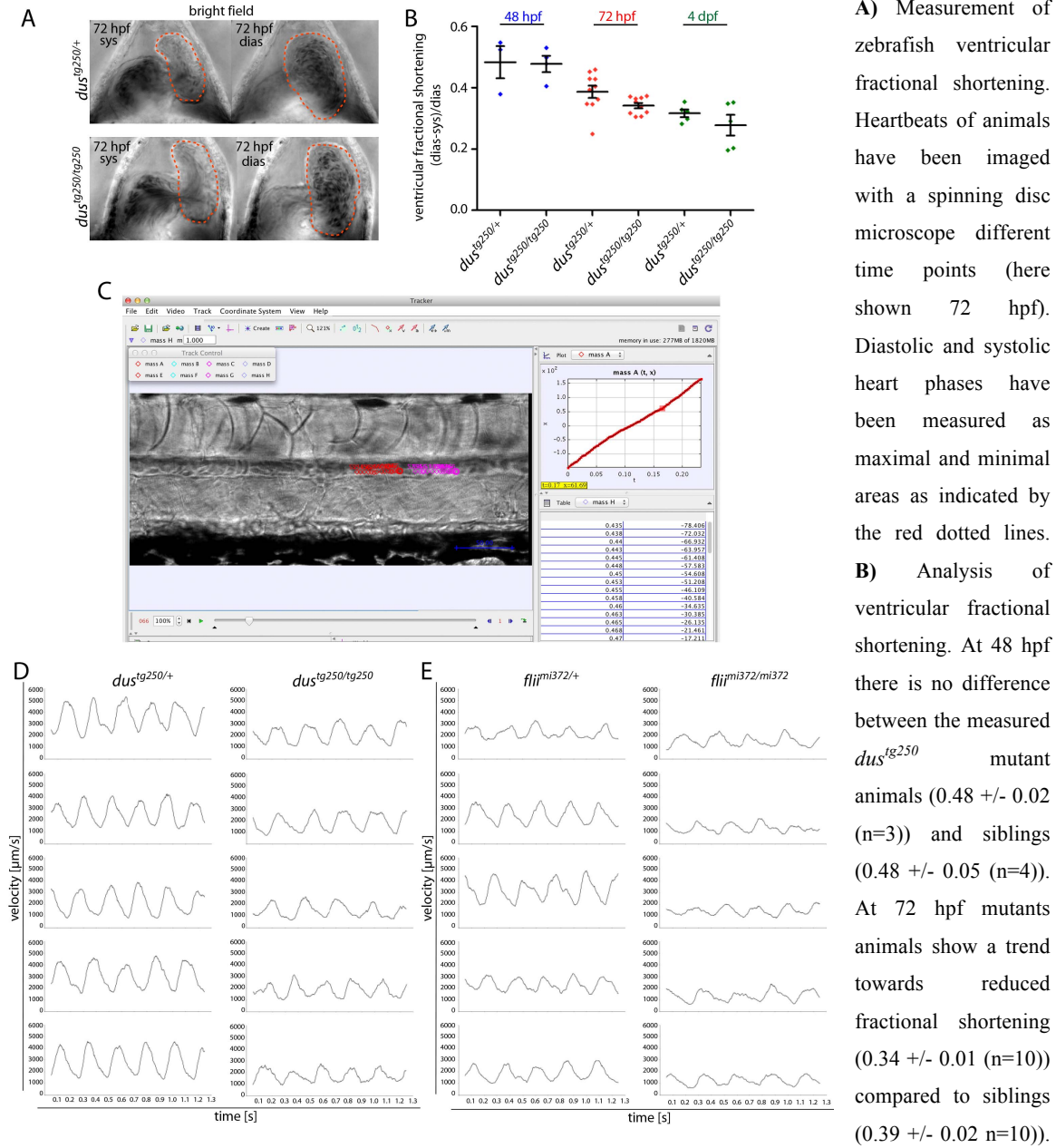
GFP were similar in mutants and siblings analyzed by western blot using anti-GFP antibody.

4.1.6 Cardiac performance is reduced in *duesentrieb* mutants.

To examine cardiac performance we studied ventricular fractional shortening, which compares the systolic and the diastolic phases of heart contraction. Hearts of zebrafish at three developmental time points were imaged with a spinning disc confocal microscope. The areas of systolic and diastolic hearts were measured (Fig. 4.6, A) and the fractional shorting was calculated. *Dus* mutant animals displayed a trend towards a reduction in fractional shortening at 72 hpf and at 4 dpf, but not 48 hpf compared to siblings (Fig. 4.6, B), suggesting that the phenotype might be progressive.

To better characterize the heart function, we measured blood flow velocity as a read out for heart performance. Zebrafish embryos were imaged with a spinning disc confocal microscope so that blood flow could be observed in the dorsal aorta. For the analysis individual blood cells were tracked over time (Fig. 4.6, C). The calculation of the velocity of the blood cells over time shows the characteristic sinus curve of the heartbeat. Both *dus* and *flii* mutants show reduced maximum velocity of the blood cells in the dorsal aorta compared to their corresponding siblings (Fig. 4.6, D, E). Furthermore, *flii* mutants seem to be more severely affected compared to *dus* mutants.

Figure 4.6: Flii deficiency leads to impaired heart function.

A) Measurement of zebrafish ventricular fractional shortening. Heartbeats of animals have been imaged with a spinning disc microscope different time points (here shown 72 hpf). Diastolic and systolic heart phases have been measured as maximal and minimal areas as indicated by the red dotted lines. **B)** Analysis of ventricular fractional shortening. At 48 hpf there is no difference between the measured dus^{tg250} mutant animals (0.48 +/- 0.02 (n=3)) and siblings (0.48 +/- 0.05 (n=4)). At 72 hpf mutants animals show a trend towards reduced fractional shortening (0.34 +/- 0.01 (n=10)) compared to siblings (0.39 +/- 0.02 n=10)).

Mutant animals at 4 dpf also show a trend towards reduced fractional shortening (0.28 +/- 0.03 (n=5)) compared to siblings (0.32 +/- 0.01 (n=5)). **C)** Example for blood flow measurements in the zebrafish dorsal aorta. Individual blood cells have been tracked over time (red and pink dots represent two individual cells, respectively). The red line in the graph on the right panel shows the distance over time. Individual values are listed in the table below. D,E) Calculation of the velocity of the blood cells over time shows the characteristic sinus curve of the heartbeat. Measurements have been performed on 5 individual animals of $dus^{tg250/tg250}$ and $flii^{mi372/mi372}$ mutants and their corresponding siblings at 6

dpf. **D)** dus^{tg250} mutants show reduced maximum blood flow velocity compared to dus^{tg250} siblings. **E)** $flii^{mi372}$ mutants show reduced maximum blood flow velocity compared to $flii^{mi372}$ siblings.

4.1.7 Myofibrillar components and remodeling factors are differentially expressed in *duesentrieb* mutants.

In order to analyze the proteins that might play a role together with Flightless I in the formation of the *duesentrieb* phenotype we performed a mass spectrometric analysis. For this study we employed protein extracts from whole zebrafish larvae at 3 dpf and compared *dus* mutants with siblings (Fig. 4.7). We found that peptides from 2520 proteins were recovered and 146 had statistical significance (> -log10 p-value of 1). Furthermore, 41 proteins were differentially expressed (log$_2$ ratio mutant/sib < 0.7 and > 1.5) and 16 proteins demonstrated muscle expression and are related to heart or skeletal muscle function.
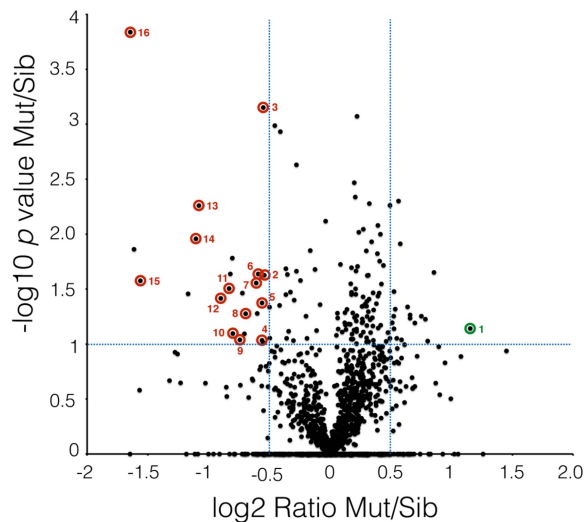

Fig. 4.7 Cofilin-1 is upregulated in dus^{tg250} mutant animals. Volcano plot of log$_2$ ratios representing the log$_2$ fold change of duplicates from dus^{tg250} mutants vs. siblings. Peptides from 2520 proteins were recovered. 146 had statistical significance (> -log10 p-value of 1) 41 proteins were differentially expressed (log$_2$ ratio mutant/sib < 0.7 and > 1.5). 16 proteins show muscle expression and are related to heart or skeletal muscle function. Proteins marked are listed in table ?, in red downregulated proteins. Cofilin-1 (green dot) is significantly upregulated in mutant animals compared to siblings. Dotted lines: upper right corner (≥log$_2$ 0.5 and -log$_{10}$ p value ≥1) and upper left corner (≤log$_2$ -0.5 and -log$_{10}$ p value ≥ 1).

Amongst the upregulated proteins we found the Actin severing protein Cofilin-1 (cfl1). Amongst the downregulated proteins we found myosins, tropomyosins and troponins etc. (Table 4.1). These results confirm the myofibrillar phenotype observed in *duesentrieb* mutants mainly affecting sarcomere building blocks.

Table 4.1: Summary of muscle-related genes from mass spectrometric analysis.

No.	Score	Sequence coverage [%]	Unique peptides	-Log10 p value Mut/Sib	log2 Ratio Mut/Sib	Gene symbols	Gene Names
1	168.67	50.3	6	1.14136	1.15405	*cfl1*	*cofilin 1*
2	61.147	54.6	5	1.62579	-0.541474	*tpm2*	*tropomyosin 2*
3	323.31	62.3	7	3.15263	-0.550676	*mylz3*	*myosin, light polypeptide 3, skeletal muscle*
4	56.78	77.1	6	1.03384	-0.561259	*mylpfb*	*myosin light chain, phosphorylatable, fast skeletal muscle b*
5	57.462	24.9	7	1.37545	-0.561277	*atp2a1l*	*ATPase, Ca++ transporting, cardiac muscle, fast twitch 1 like*
6	323.31	26.9	103	1.63813	-0.592263	*neb*	*nebulin*
7	74.08	38.3	5	1.55554	-0.608715	*myl10*	*myosin, light chain 10, regulatory*
8	228.9	26.8	29	1.27663	-0.695535	*myom1a*	*myomesin 1a (skelemin)*
9	83.819	62.5	5	1.03866	-0.742407	*myhz1.3*	*myosin, heavy polypeptide 1.3, skeletal muscle*
10	134.4	49.3	0	1.09657	-0.800242	*tpm1*	*tropomyosin 1 (alpha)*
11	181.41	62.5	11	1.50431	-0.831029	*tnnc2*	*troponin C type 2 (fast)*
12	77.412	29.4	1	1.41595	-0.900718	*tnnt3b*	*troponin T type 3b (skeletal, fast)*
13	92.734	55.6	0	2.26027	-1.07958	*tpm3*	*tropomyosin 3*
14	115.69	30.7	10	1.95707	-1.10528	*tnni2a.4*	*troponin I type 2a (skeletal, fast), tandem duplicate 4*
15	224.93	31.5	29	1.57673	-1.56141	*ttna*	*titin a*
16	103.15	40.9	11	3.83826	-1.64409	*tnnt3a*	*troponin T type 3a (skeletal, fast)*

4.2 Memo1

4.2.1 Mediator of ErbB2 driven cell motility (Memo1) is expressed in the zebrafish heart.

In order to study the relevance of ErbB2 downstream signaling in trabeculation we analyzed the expression of *memo1* in zebrafish. The analysis of *memo1* temporal expression revealed that it is maternally contributed and expressed throughout embryonic development until 72 hpf (Fig. 4.8, A). Furthermore, we analyzed its spatial expression by *in situ* hybridization. *memo1* was expressed in the zebrafish brain, in the fin buds and in the heart at 4 dpf (Fig. 4.8, B). Partial dissection of the hearts showed that *memo1* is expressed in both cardiac chambers at 7 dpf (Fig. 4.8, C). To get more information we

generated a reporter construct driving EGFP, employing 5 kb of the *memo1* promoter including the ATG start codon (Fig. 4.8, D). Fluorescence microscopy analysis of the *memo1*-reporter revealed expression in the midbrain, hindbrain and in the heart, however expression in the heart was weak compared to the expression in the brain at 80 hpf (Fig. 4.8, E). At a later developmental stage (6 dpf) GFP could still be detected in mid- and hindbrain and reporter expression in the heart appeared increased at this time point. *memo1*-reporter expression can also be found in the liver. Confocal imaging of the hearts indicated that *memo1*-reporter is mainly activated in endocardial cells at 4 and 5 dpf (Fig. 4.8, F).
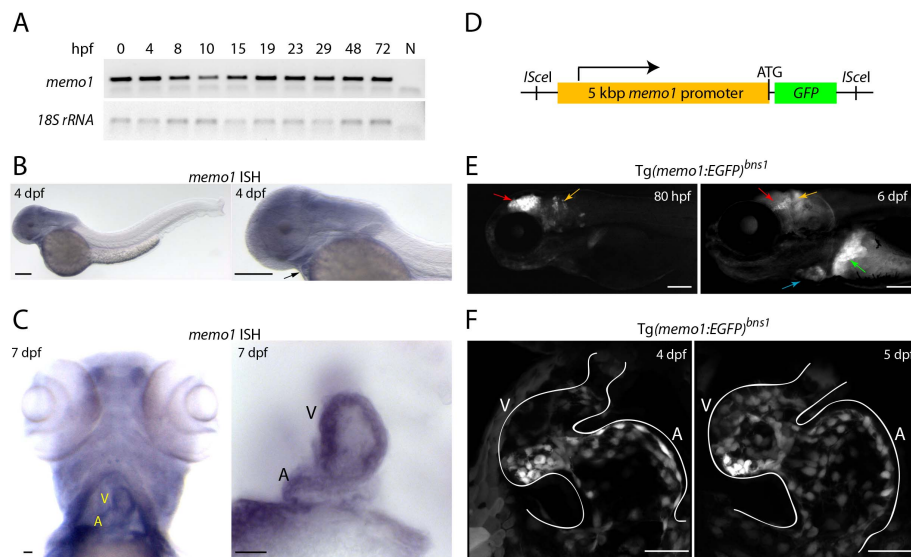

Figure 4.8: *memo1* is expressed in the zebrafish heart, brain and liver.

A) Temporal expression of *memo1* by RT-PCR. *memo1* is maternally contributed and expressed at all developmental time points tested from 4 hpf to 72 hpf. Expression of 18S rRNA has been measured as loading control. **B,C)** *In situ* hybridization for *memo1*. **B)** *memo1* is expressed in the brain and in the heart of zebrafish larvae at 4 dpf. Arrow on magnification denotes position of the heart. Scale bars 250 µm. **C)** *memo1* is expressed in ventricular and atrial chambers of the zebrafish heart at 7 dpf. Scale bars 25 µm. **D)** Scheme of *memo1* reporter construct. 5 kb of the zebrafish *memo1* promoter, including the ATG start-codon, drive expression of GFP. Meganuclease restriction sites *ISce*I have been used to allow insertion of the construct into the zebrafish genome. **E)** Expression of the *memo1* reporter construct *Tg(memo1:EGFP)^bns1* in zebrafish at 80 hpf and 6 dpf respectively. Fluorescence microscopy images of larvae show expression of GFP mainly in the midbrain (red arrow) and the cerebellum (orange arrow) at 80 hpf and in the heart (blue arrow) and the liver (green arrow) at 6 dpf. Scale bars 150 µm. **F)** Confocal projections of *Tg(memo1:EGFP)^bns1* zebrafish hearts at 4 dpf and 5 dpf. *memo1*-reporter expression in the heart can only be detected in the endocardium. Scale bars 25 µm. A=Atrium V=Ventricle

4.2.2 Memo1 might play a role in endo- and myocardial development.

To better understand the function of Memo1 in heart development we designed a morpholino (MO) that binds to an ATG located in the 5' untranslated region (UTR) of the *memo1* mRNA (Fig. 4.9, A). Injection of 0.8 ng of 5' UTR MO led to craniofacial malformations and pericardial edema, suggesting a role for *memo1* in heart development. Injection of a *memo1* MO that binds to the ATG start codon did not cause any obvious phenotypes nor a developmental delay, and has therefore been used as a control MO in further studies. Since we found the *memo1*-reporter to be activated in endocardial cells, we analyzed the endocardium in MO-injected fish by employing the transgenic line expressing EGFP under the *kdrl* promoter. Wt and control MO-injected animals developed normally containing a looped and ballooned heart at 72 hpf (Fig. 4.9, C). The Common Cardinal Vein/Duct of Cuvier (CCV/DC) above the yolk is symmetrically shaped and the hearts contract. 5'UTR MO injected animals however showed an asymmetric CCV/DC with delayed development of the heart, which is was positioned slightly underneath the jaw.
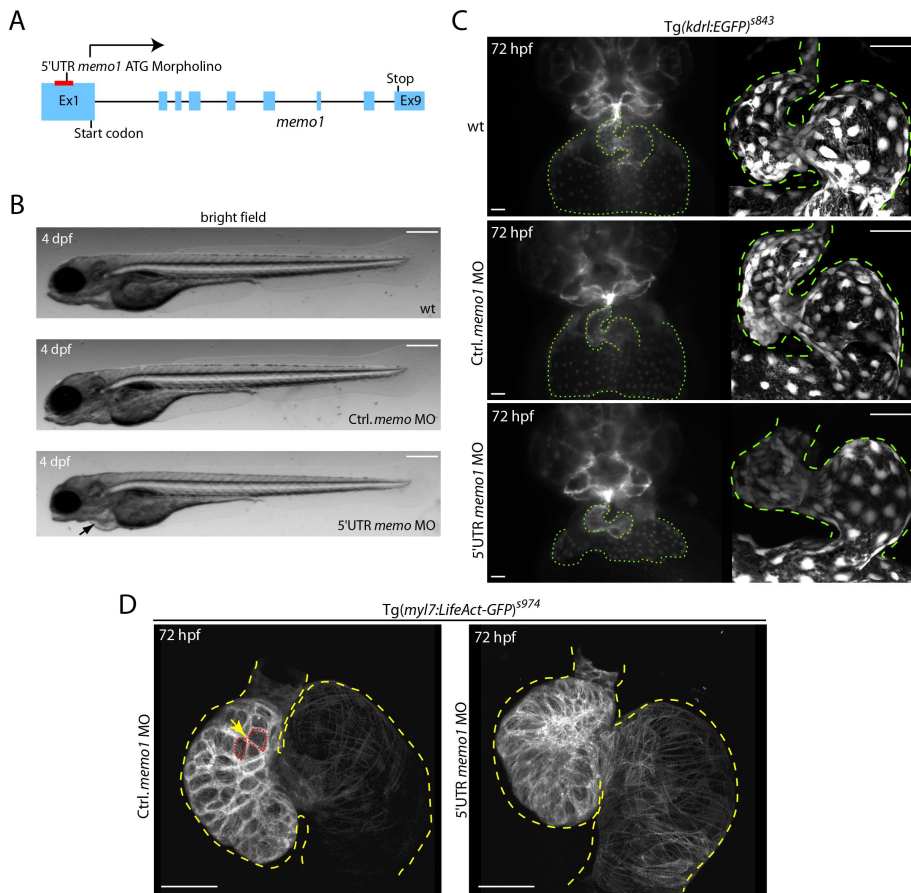

Figure 4.9: Morpholino-mediated knockdown of *memo1* leads to pericardial.

A) Scheme of *memo1* gene. *memo1* is composed of 9 coding exons. The translation blocking morpholino (MO) binds to an ATG in the 5'UTR of *memo1*. **B)** Bright field images of zebrafish larvae at 4 dpf. Animals injected with 0.8 ng of control MO develop

indistinguishable from wt animal. Animals injected with 0.8 ng of *memo1* 5'UTR MO develop a pericardial edema (arrow). Scale bars 250 μm. **C)** Confocal projections of hearts from *Tg(kdrl:EGFP)*[s843] zebrafish larvae at 72 hpf. GFP expressed und the *kdrl* promoter marks endothelial cells. Wt and control MO (0.8 ng) injected animals develop indistinguishable from each other. The hearts are looped and ballooned and the Common Cardinal Vein/Duct of Cuvier (CCV/DC) appears symmetrical. Animals injected with 0.8 ng of *memo1* 5'UTR MO are developmentally delayed. The hearts show delayed looping and the position of the heart in respect to the body axis is different compared to wt and control MO injected animals. The CCV/DC of these animals appears dysmorphic. The green doted lines outline the shape of the heart and the CCV/DC. Scale bars 25 μm. **D)** Confocal projections of hearts from *Tg(myl:LifeAct-GFP)*[s974] zebrafish larvae at 72 hpf. Animals injected with 0.8 ng control MO appear normal. The hearts are looped and ballooned. The shape of the cells is outlined by the subcellular distribution of LifeAct-GFP as schematically shown by the red lines surrounding the cardiomyocytes. Animals injected with 0.8 ng *memo1* 5'UTR MO show delayed looping. The outlines (red doted lines) of individual cardiomyocytes by LifeAct-GFP localization are not as clear in these animals. The yellow doted lines outline the shape of the heart. Scale bars 25 μm.

To evaluate if the myocardium is also affected in *memo1* morphants we analyzed hearts of transgenic fish expressing LifeAct-GFP under the *myl7* promoter. Hearts of control MO-injected animals developed normally and LifeAct-GFP was localized to contractile structures of cardiomyocytes (Fig. 4.9, D). The cell shape can be extrapolated by the subcellular localization of LifeAct-GFP as depicted by the red doted lines. However, *memo1* 5' UTR MO-injected animals exhibited delayed looping. Furthermore the cell shape of the cardiomyocytes can't be seen as clearly as in the controls. These results suggest, that MO-mediated knockdown of *memo1* might cause heart developmental defects affecting the endocardium as well as the myocardium.

4.2.3 Zygotic *memo1* expression is dispensable for zebrafish development.

In order to study the function of Memo1 in heart development we generated a mutant by employing the CRISPR/Cas technology. Memo1 is highly conserved between humans and zebrafish and the protein sequences of these species share 88% identity (Fig. 4.10, A). We designed a gRNA that binds in the first coding exon of the gene, close to the start codon ATG (Fig. 4.10, B). A frame shift mutation at this position would disrupt the gene in front of the conserved Tryptophan 16 (W16) which has been shown to be essential for Memo1 phosphorylated ErbB2 receptor binding (Fig. 4.10, A, B).
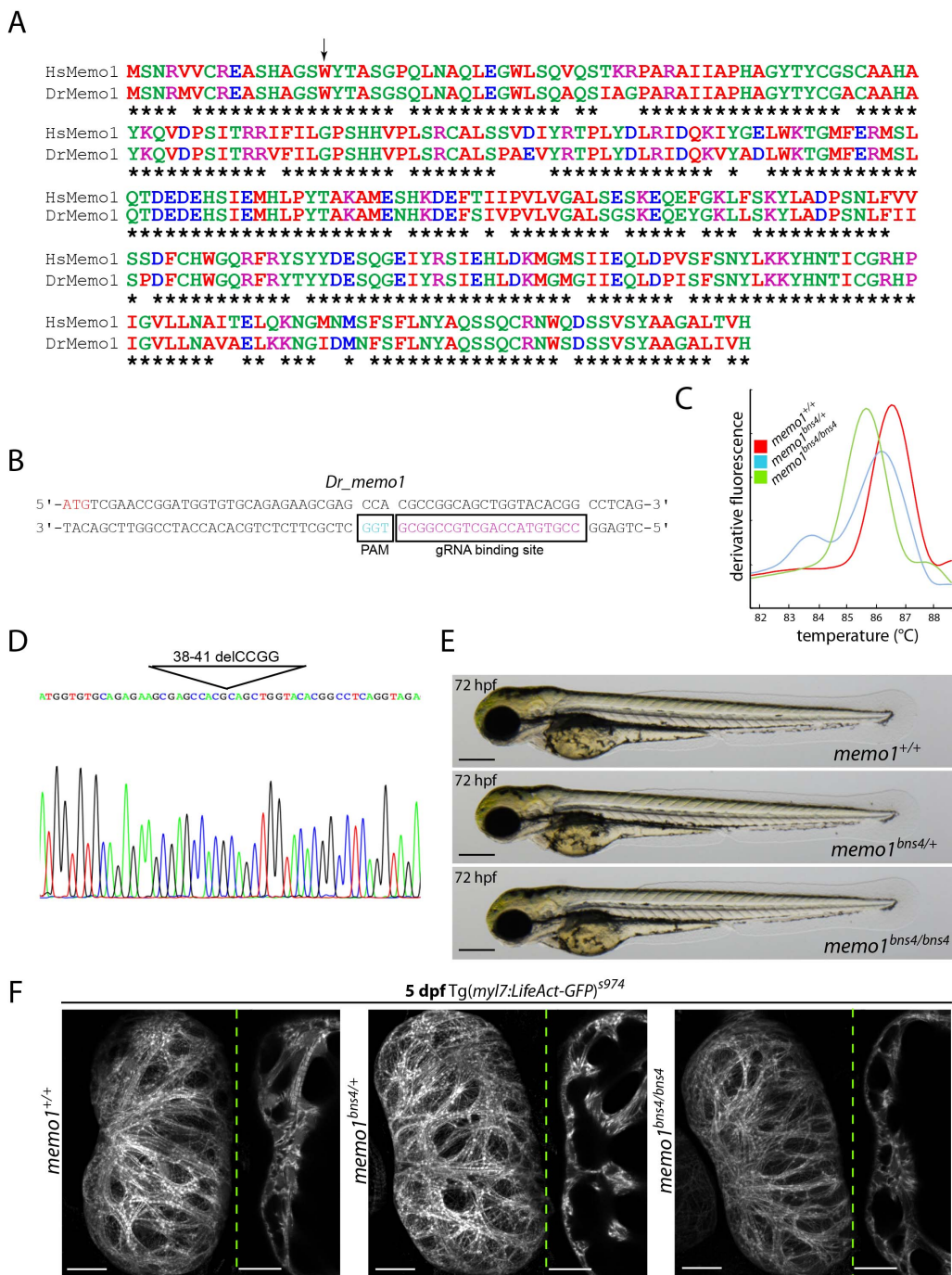
A

```
HsMemo1  MSNRVVCREASHAGSWYTASGPQLNAQLEGWLSQVQSTKRPARAIIAPHAGYTYCGSCAAHA
DrMemo1  MSNRMVCREASHAGSWYTASGSQLNAQLEGWLSQAQSIAGPARAIIAPHAGYTYCGACAAHA
         ****  ********* ************ **  *************** *****
HsMemo1  YKQVDPSITRRIFILGPSHHVPLSRCALSSVDIYRTPLYDLRIDQKIYGELWKTGMFERMSL
DrMemo1  YKQVDPSITRRVFILGPSHHVPLSRCALSPAEVYRTPLYDLRIDQKVYADLWKTGMFERMSL
         *********** ******** ******      ************ *   ***********
HsMemo1  QTDEDEHSIEMHLPYTAKAMESHKDEFTIIPVLVGALSESKEQEFGKLFSKYLADPSNLFVV
DrMemo1  QTDEDEHSIEMHLPYTAKAMENHKDEFSIVPVLVGALSGSKEQEYGKLLSKYLADPSNLFII
         ********************* ***** * ******* ***** *** ***********
HsMemo1  SSDFCHWGQRFRYSYYDESQGEIYRSIEHLDKMGMSIIEQLDPVSFSNYLKKYHNTICGRHP
DrMemo1  SPDFCHWGQRFRYTYYDESQGEIYRSIEHLDKMGMGIIEQLDPISFSNYLKKYHNTICGRHP
         * ********** ********************** ****** ******************
HsMemo1  IGVLLNAITELQKNGMNMSFSFLNYAQSSQCRNWQDSSVSYAAGALTVH
DrMemo1  IGVLLNAVAELKKNGIDMNFSFLNYAQSSQCRNWSDSSVSYAAGALIVH
         *******  ** *** * *************** ********* **
```

B

Dr_memo1

```
5'-ATGTCGAACCGGATGGTGTGCAGAGAAGCGAG CCA CGCCGGCAGCTGGTACACGG CCTCAG-3'
3'-TACAGCTTGGCCTACCACACGTCTCTTCGCTC GGT GCGGCCGTCGACCATGTGCC GGAGTC-5'
                                    PAM    gRNA binding site
```

C

D

38-41 delCCGG

E

F

5 dpf Tg(*myl7:LifeAct-GFP*)^{s974}

Figure 4.10: *memo1* homozygous mutants develop phenotypically normal and are viable to adulthood.

A) Amino acid (aa) sequence alignment of *Homo sapiens* and *Danio rerio* Memo1 protein. The two homologues proteins share 88% identity. The asterisks correspond to aa that are identical in both sequences. The color code is according to the aa side chain characteristics: red are nonpolar, green are polar, blue are acidic and purple are basic. The arrow marks the Tryptophan (W16) that is important for ErbB2 receptor binding. **B)** CRISPR design. Shown is the partial coding sequence of the *memo1* gene including the ATG start-codon. The PAM is boxed and marked in blue and the gRNA-binding site is boxed and marked in pink. **C)** High-resolution-melt-curve HRM of PCRs from a wt (red line), a heterozygous (blue line) and a homozygous mutant (green line) animal. **D)** Sequencing analysis of a homozygous

mutant animal lacking 4 bp corresponding to position 38-41 (Δ_CCGG). **E)** Bright field images of zebrafish larvae at 72 hpf. *memo1*$^{bns4/bns4}$ animals are indistinguishable from their wt and heterozygous siblings. Scale bars 250 μm. **F)** Confocal projections and single planes of *Tg(myl7:LifeAct-GFP)*^{s974} zebrafish heart ventricles at 5 dpf. Ventricles from wt, heterozygous and homozygous mutant *memo1* animals appear morphologically normal. Ventricles of *memo1*$^{+/+}$, *memo1*$^{bns4/+}$ and *memo1*$^{bns4/bns4}$ animals have formed trabeculae, which are visible in the lumen of the chambers. Scale bars are 25 μm.

Genotyping and Sequencing of the injected F_0/F_1 generation revealed founders carrying a 4 bp deletion at position 38-41 (Δ_CCGG) (Fig. 4.10, C, D). This *memo1*^{bns4} mutation causes a frame shift and a premature stop codon at aa position 37. Zygotic F_1 *memo1*^{bns4} animals however, did not show any obvious developmental defects at 72 hpf (Fig. 4.10, E). Since we were interested whether Memo1 was important for trabeculation we analyzed hearts of transgenic animals expressing LifeAct-GFP in the myocardium. Heterozygous as well as homozygous mutant animals develop morphologically normal ventricular chambers and trabeculae compared to *memo1*$^+$ animals (Fig. 4.10, F). Furthermore homozygous mutant animals are viable to adulthood are fertile. These results suggest that zygotic *memo1* expression is dispensable for zebrafish development.

4.2.4 Memo1-GFP localization to sarcomere-like structures requires Tnnt2-dependent sarcomere formation.

Previous studies in keratinocytes have shown that Memo1 translocates from the cytoplasm to the plasma membrane where it specifically binds to phosphorylated ErbB2 receptors in order to recruit proteins that capture microtubules thereby enabling efficient cell migration (Zaoui et al., 2010). In order to better understand the ErbB2-dependent initiation of trabeculation, we were interested to determine whether a GFP-tagged Memo1 (Mediator of ErbB2 driven cell motility) protein could be used to detect activated ErbB2 receptors in live cardiomyocytes prior to trabeculation. To answer this question we designed a transgenic construct driving the expression of Memo1-GFP under the control of the cardiomyocyte-specific *myl7* promoter (Fig. 4.11, B). Surprisingly, transgenic expression of Memo1-GFP shows a sarcomere-like, nuclear and cytoplasmic distribution in ventricular cardiomyocytes at 5 dpf (Fig. 4.11, A, A'). Sections of adult zebrafish hearts show similar Memo1-GFP sarcomere-like localization with some additional structures of unknown identity (Fig. 4.11, C).
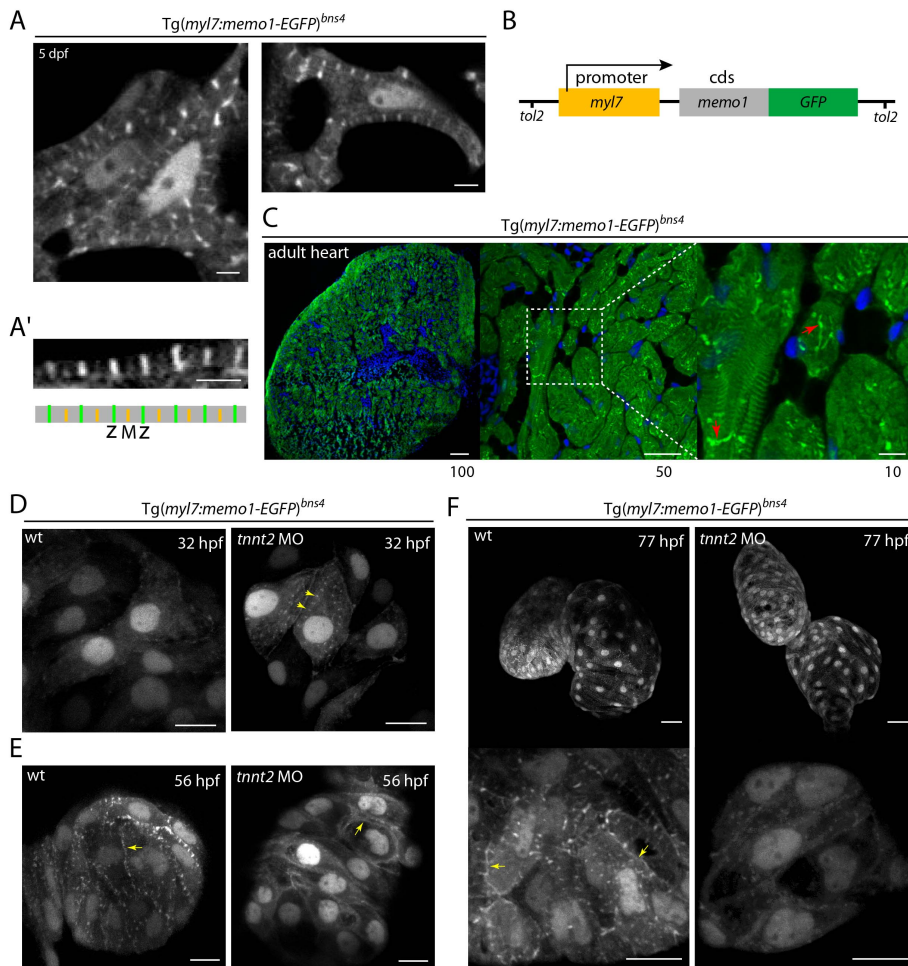
Figure 4.11: Morpholino mediated knockdown for *tnnt2* leads to aberrant localization of Memo1-GFP.
A) Single confocal planes showing subcellular localization of *Tg(myl7:memo1-EGFP)^{bns4}* in zebrafish cardiomyocytes. Memo1-GFP expression is driven by the cardiomyocyte-specific promoter *myl7* and shows a regular striated pattern (A') similar to sarcomeric z-disc (green) and M-band (yellow) (scheme). Memo1-GFP localizes to nuclei. Scale bars are 2.5 µm. **B)** Schematic of *Tg(myl7:memo1-EGFP)^{bns4}* construct. The cardiomyocyte-specific promoter *myl7* (orange box) drives the expression of the coding sequence (cds) of *memo1* (gray box) in frame with GFP (green box). Transposase recognition sites (*tol2*) have been used to allow insertion of the construct into the zebrafish genome. **C)** Expression of *Tg(myl7:memo1-EGFP)^{bns4}* in adult zebrafish hearts. Memo1-GFP in green shows striated pattern. Nuclei stained with DAPI are blue. Scale bars are from left to right: 100 µm, 50 µm and 10 µm, respectively. **D-F)** Confocal projections of *Tg(myl7:memo1-EGFP)^{bns4}* zebrafish at 32 hpf, 56 hpf and 77 hpf. **D)** Memo1 localizes to the nucleus of cardiomyocytes in both *tnnt2* MO (0.5 ng) injected and non-injected animals. *Tnnt2* MO injected animals show dotted Memo1-GFP pattern in the cytoplasm (arrows). Siblings show an even distribution of Memo1-GFP in the cytoplasm. Scale bars 10 µm. **E)** Memo1-GFP localizes to nuclei, cytoplasm and appears to be associated to membrane structures at cell-cell boundaries. *Tnnt2* MO injected animals show similar distribution of Memo1-GFP. Memo1-GFP localization to membrane structures is present in Tnnt2-deficient animals however its distribution appears less punctuated compared to wt animals (arrows) Scale bars 10 µm. **F)** At 77 hpf animals injected with *tnnt2* MO appear dysmorphic compared to wt animals. Magnifications of the ventricular apex show that the Memo1-GFP localization at the cell-cell junctions forms a striated pattern in wt animals. These regular striations seem to be missing in Tnnt2-deficient animals. Scale bars 25 µm.

To determine if the Memo1-GFP localization was dependent on the formation of functional sarcomeres we used a *tnnt2* morpholino-mediated knockdown in the *Tg(myl7:memo1-EGFP)^bns4* transgenic line. At 32 hpf we found that Memo1-GFP localized in the cytoplasm and in nuclei of atrial cardiomyocytes (Fig. 4.11, D). In Tnnt2-deficient atrial cardiomyocytes regular cytoplasmic dots could be observed (Fig. 4.11, D, arrows). At 56 hpf Memo1-GFP was found in the nuclei and the cytoplasm of ventricular cardiomyocytes, but also localized in cell-cell boundaries in a striated pattern (Fig. 4.11, E). Animals, for Tnnt2 failed to form these regular striations but still showed localization of Memo1-GFP in cell-cell boundaries, cytoplasm and nuclei (Fig. 4.11, E, arrow). As expected the overall morphology of Tnnt2-deficient hearts was disturbed and cardiac chambers started to partially collapse at 77 hpf (Fig. 4.11, F). Magnification of ventricular cardiomyocytes showed that Memo1-GFP localized in nuclei, cell-cell junctions and to a sarcomere-like striated structures that appear to connect to the plasma membrane, giving the impression of a stitching. Tnnt2-deficient cardiomyocytes failed to form this regular, striated Memo1-GFP pattern but still showed the nuclear localization and the localization in cell-cell junctions and the cytoplasm (Fig. 4.11, F). These results suggest, that Memo1-GFP localization is dependent on proper sarcomere formation requiring *tnnt2* expression.

4.2.5 Memo1-GFP localization to cell-cell junctions is lost during cardiomyocyte maturation in an ErbB2-dependent manner.

Localization of memo1-GFP to cell-cell junctions could be observed in ventricular cardiomyocytes at the time before trabeculation from 48 hpf until 77 hpf (Fig. 4.12, A, B). At 82 hpf and 96 hpf, when the first trabeculae are formed however, Memo1-GFP localization to cell-cell junctions could no longer be detected (Fig. 4.12, A, B), suggesting, that cardiomyocytes undergo certain changes affecting the cell-cell junctions during this developmental period.
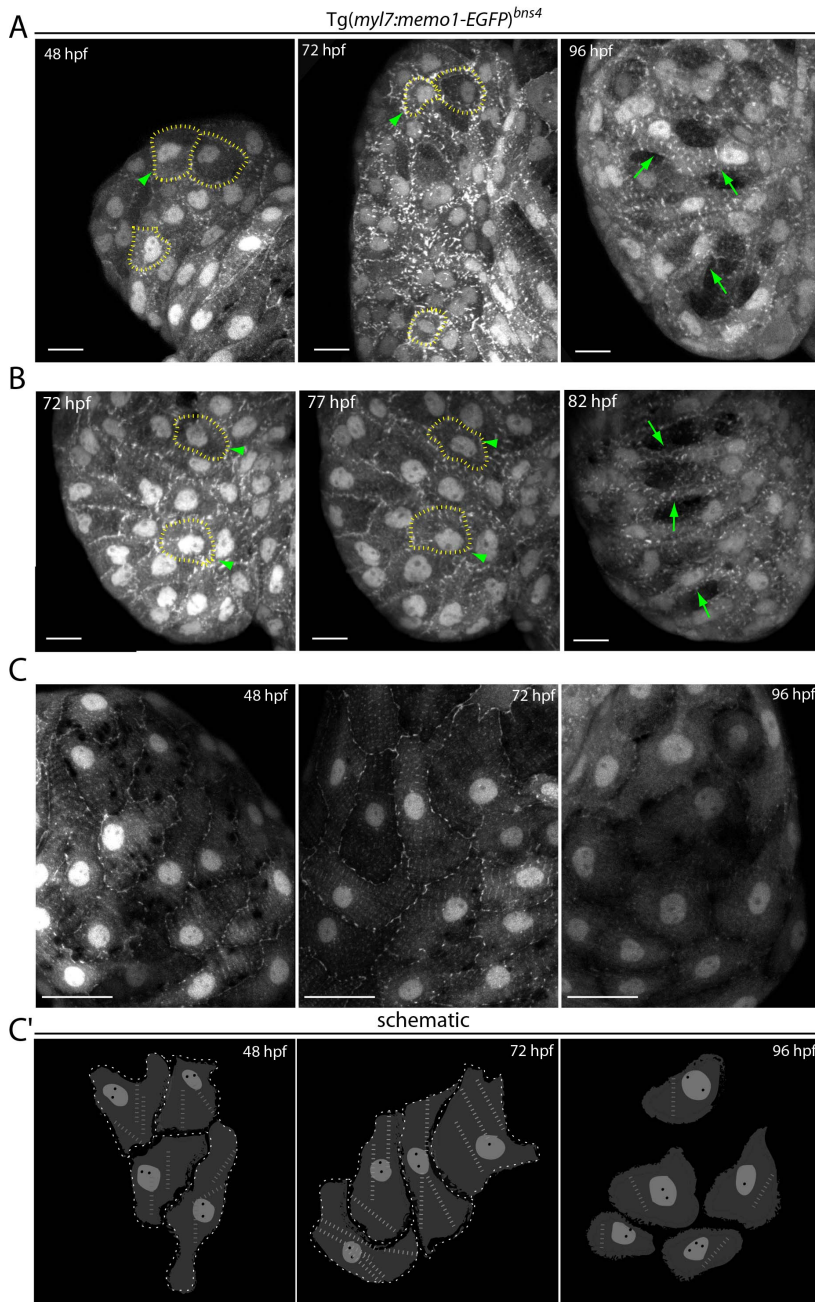
Figure 4.12: Cardiomyocyte-specific Memo1-GFP localization to cell-cell junctions is transient during development.
Confocal projections of *Tg(myl7:memo1-EGFP)*[bns4] zebrafish hearts. **A,B)** Projections of ventricles show that Memo1-GFP localizes to nuclei and cell-cell junctions (red doted lines and green arrowhead) and shows a sarcomere-like striated pattern at 48 hpf and 72 hpf and 77 hpf. Upon trabeculation at 82 hpf and 4 dpf Memo1-GFP localizes to nuclei and sarcomere-like striated structures, but can't be detected at cell-cell boundaries. Green arrows point at trabecular cells. **C)** Projections of atria at 48 and 72 hpf show localization of Memo1-GFP to nuclei and cell-cell junctions and to sarcomere-like striated structures similar to ventricular cardiomyocytes. Memo1-GFP localization to cell-cell boundaries can't be detected at 4 dpf. Scale bars 20 µm. **C')** The schematic of atrial cardiomyocytes shows Memo1-GFP localization to cell-cell boundaries (white doted lines) which are not visible at 4 dpf.

In order to understand if this process is specific to ventricular chambers or if it is a general cardiomyocyte maturation process we analyzed atrial cardiomyocytes. Atrial cardiomyocytes also showed Memo1-GFP localization to nuclei, the cytoplasm and to cell-cell junctions at 48 hpf and 72 hpf (Fig. 4.12, C). In addition an intracellular sarcomere-like striated pattern could be observed in atrial cells, which is less prominent,

but present, in ventricular cardiomyocytes, most probably because the cells of the atrium are much bigger compared to ventricular cardiomyocytes (Fig. 4.12, C, C'). At 96 hpf however the Memo1-GFP localization to the cell-cell junctions is lost also in the atrial cells (Fig. 4.12, C, C').

A previous study has shown, that there is a direct link between ErbB2 activity and myofibril remodeling in ventricular cardiomyocytes (Reischauer et al., 2014). In order to understand if Memo1-GFP relocalization is ErbB2-dependent we treated transgenic fish with ErbB2 inhibitor. Ventricles of inhibitor-treated animals did not show trabeculae in the ventricular lumen at 5 dpf in contrast to DMSO-treated control animals (Fig. 4.12, A green arrows). Only ErbB2 inhibitor-treated animals show Memo1-GFP localization to cell-cell junctions (Fig. 4.12, A, green arrowheads). In order to exclude that the aberrant localization of Memo1-GFP is due a secondary effect of the drug we generated a line that carries the *erbb2*^{st61} mutant allele in a *Tg(myl7:memo1-EGFP)*^{bns4} transgenic background. As expected Memo1-GFP localized to cell-cell junctions at 48 hpf and 72 hpf in ErbB2-deficient animals (Fig. 4.13, B). As observed in ErbB2 inhibitor-treated animals Memo1-GFP still localizes to cell-cell junctions at 96 hpf in contrast to wt animals (Fig. 4.12, A; Fig 4.13, B), suggesting that Memo1-GFP relocalization is ErbB2-dependent. Since atrial cardiomyocytes do not undergo ErbB2-dependent trabeculation we were interested to see if ErbB2-deficient atrial cardiomyocytes also retain Memo1-GFP localization at the cell-cell junctions.
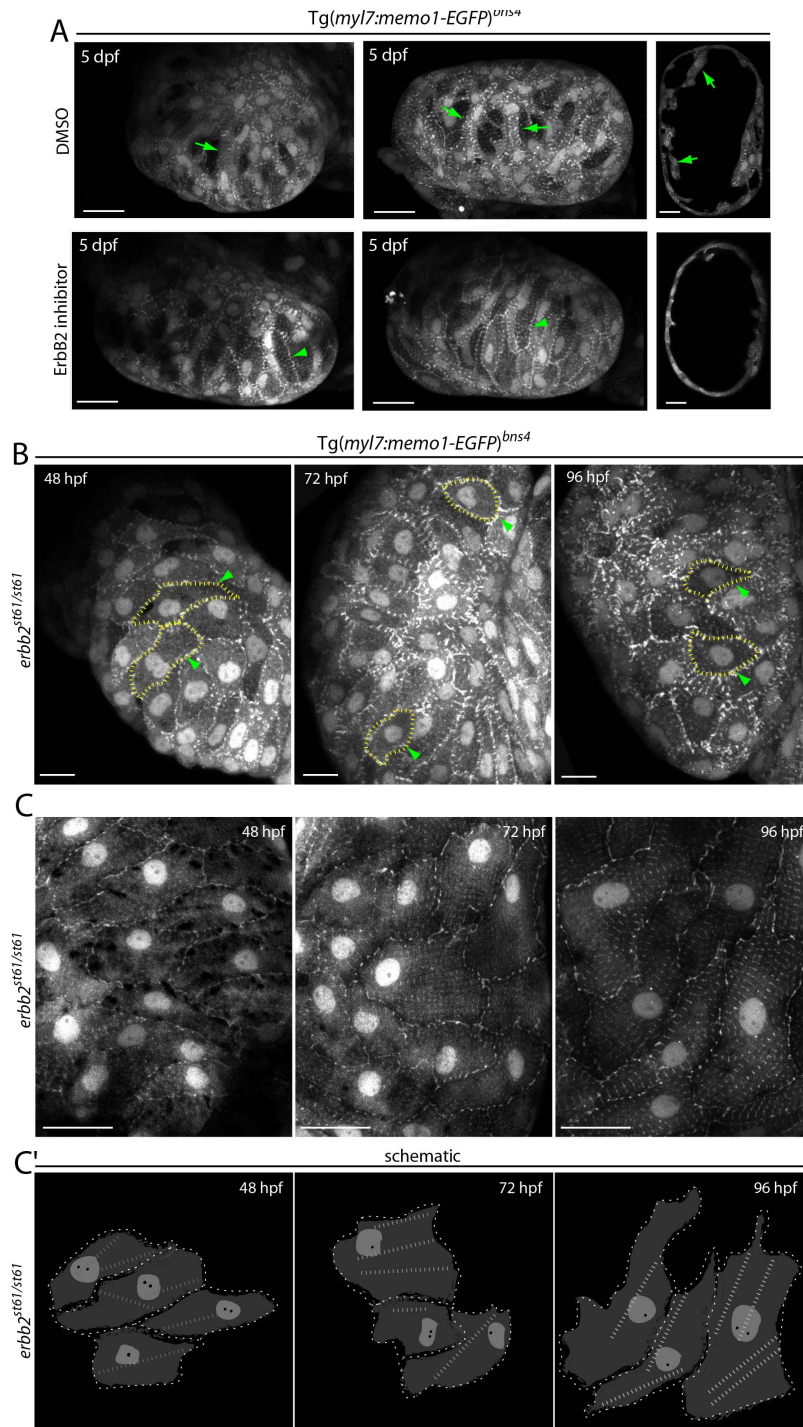
Figure 4.13: Cardiomyocyte-specific Memo1-GFP localization to cell-cell junctions is retained in ErbB2-deficient cells.

Confocal projections of $Tg(myl7:memo1-EGFP)$[bns4] zebrafish hearts. **A)** Projections of ErbB2 inhibitor or DMSO-treated hearts at 5 dpf. Memo1-GFP localizes to nuclei and sarcomere-like striated structures, but is not detected at cell-cell boundaries. Memo1-GFP localizes to nuclei and sarcomere-like striated structures, but can't be detected at cell-cell boundaries in DMSO-treated animals. Green arrows point at trabecular cells. Right panel shows trabeculae (green arrows) in the ventricular lumen. Animals treated with erbb2 inhibitor don't show trabeculae in the ventricular lumen (right panel). As in DMSO-treated animals Memo1-GFP localizes to nuclei and sarcomere-like striated structures in cardiomyocytes. In addition Memo1-GFP localizes to cell-cell junctions of erbb2 inhibitor treated animals. **B)** Memo1-GFP localizes to nuclei and cell-cell junctions (red doted lines and green arrowheads) and shows a sarcomere-like striated pattern in ventricles of erbb2 mutant animals at 48 hpf, 72 hpf and 4 dpf. **C)** Projections of erbb2 mutant atria at 48 hpf, 72 hpf and 4 dpf show localization of Memo1-GFP to nuclei and cell-cell junctions and to sarcomere-like striated structures. **C')** The schematic of atrial cardiomyocytes shows Memo1-GFP localization to cell-cell boundaries (white doted lines) which are still present at 4 dpf. Scale bars are 20 μm.

As in *erbb2$^+$* animals Memo1-GFP localized to cell-cell junctions of *erbb2^{st61}* mutant cardiomyocytes at 48 hpf and 72 hpf. However, as in ventricular cardiomyocytes Memo1-GFP localization was maintained at cell-cell junctions at 96 hpf in *erbb2^{st61}* mutant atria. These results suggest that, ErbB2 signaling might play a role in ventricular and atrial cardiomyocyte maturation in the zebrafish heart.

4.3 Golgi

4.3.1 Cardiomyocyte-specific expressed Golgi marker GalT-mCherry localizes to Golgi-like structures surrounding the nucleus.

In order to study cardiomyocyte polarization we designed a construct, which would enable us to express a cardiomyocyte specific, previously described Golgi marker. We therefore cloned a construct where *myl7* drives the expression of a fragment of the human Galactosyltransferase fused to mCherry (Fig. 4.14, B). The analysis of double transgenic hearts (*Tg(myl7:galT-mCherry)^{bns5}* / *Tg(myl7:memo1-GFP)^{bns4}* revealed that the Golgi marker GalT localizes to trans-Golgi vesicles, surrounding the nuclei (Fig. 4.14, A). Unlike in polarized epithelial cells, where the Golgi forms a classic single-stack, GalT marked several structures per cell, which markedly varied in size, suggesting, that the Golgi is fragmented in cardiomyocytes (Fig. 4.14, C, D). In order to find out if the larger vesicles are located in a specific position in respect to the nucleus we analyzed ventricular cardiomyocytes before trabeculation. The analysis of five consecutive single planes of the ventricular outer curvature revealed that, the Golgi vesicles are located in all dimensions surrounding the nucleus at 72 hpf, forming partial belts to full shells. (Fig. 4.14, E). This result suggests, that the Golgi-apparatus is not localized in a polarized manner in ventricular cardiomyocytes before trabeculation.
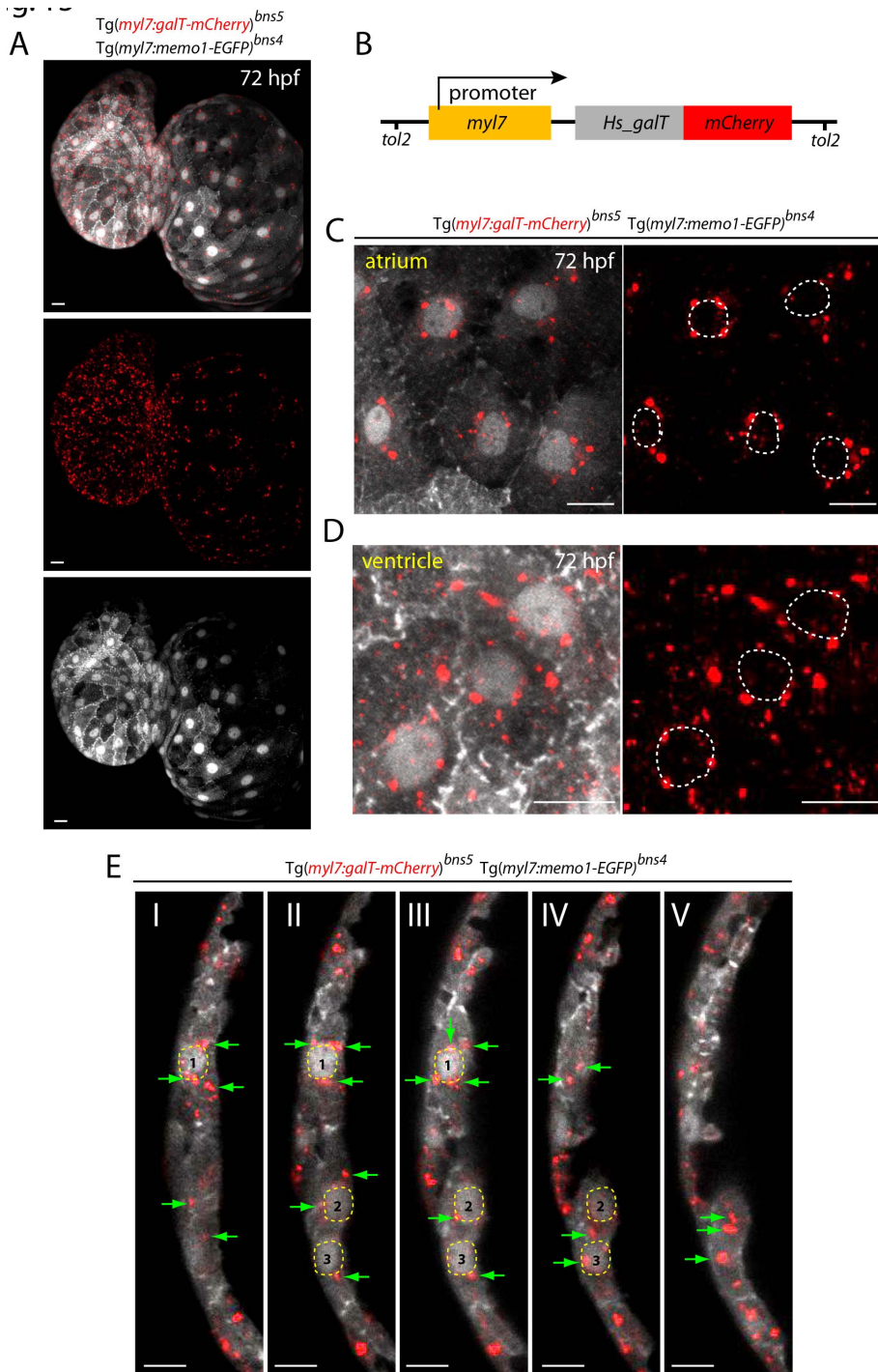
Figure 4.14: Cardiomyocytes specific expressed Golgi marker GalT-mCherry localizes to several vesicular structures.
A,C,D) Confocal projections of *Tg(myl7:galT-mCherry)^bns5* / *Tg(myl7:memo1-EGFP)^bns4* zebrafish at 72 hpf. **A)** The Golgi marker in red shows *myl7* driven expression in cardiomyocytes. **B)** Schematic of *Tg(myl7:galT-mCherry)^bns5* construct. The cardiomyocyte specific promoter *myl7* (orange box) drives the expression of the first 60 amino acids of the human Galactosyltransferase gene (gray box) in frame with mCherry (red box). Transposase recognition sites (*tol2*) have been used to allow insertion of the construct into the zebrafish genome. **C)** Magnification of atrial cardiomyocytes. Right panel shows the red channel. Nuclei (doted lines outline position of nuclei) are surrounded by several big vesicular structures. **D)** Magnification of ventricular cardiomyocytes show several big and small vesicular structures surrounding the nuclei. **E)** Serial single planes (from I ventral to dorsal V) of ventricular outer curvature showing cells of the ventricular compact layer before trabeculation (72 hpf). GalT-mCherry-positive vesicular structures surround the nuclei in all three dimensions. Green arrows point at vesicular structures. Scale bars are 10 µm.

To examine if the Golgi changes its localization during trabeculation we studied single planes of ventricular outer curvatures at 4 dpf (Fig. 4.15, A).
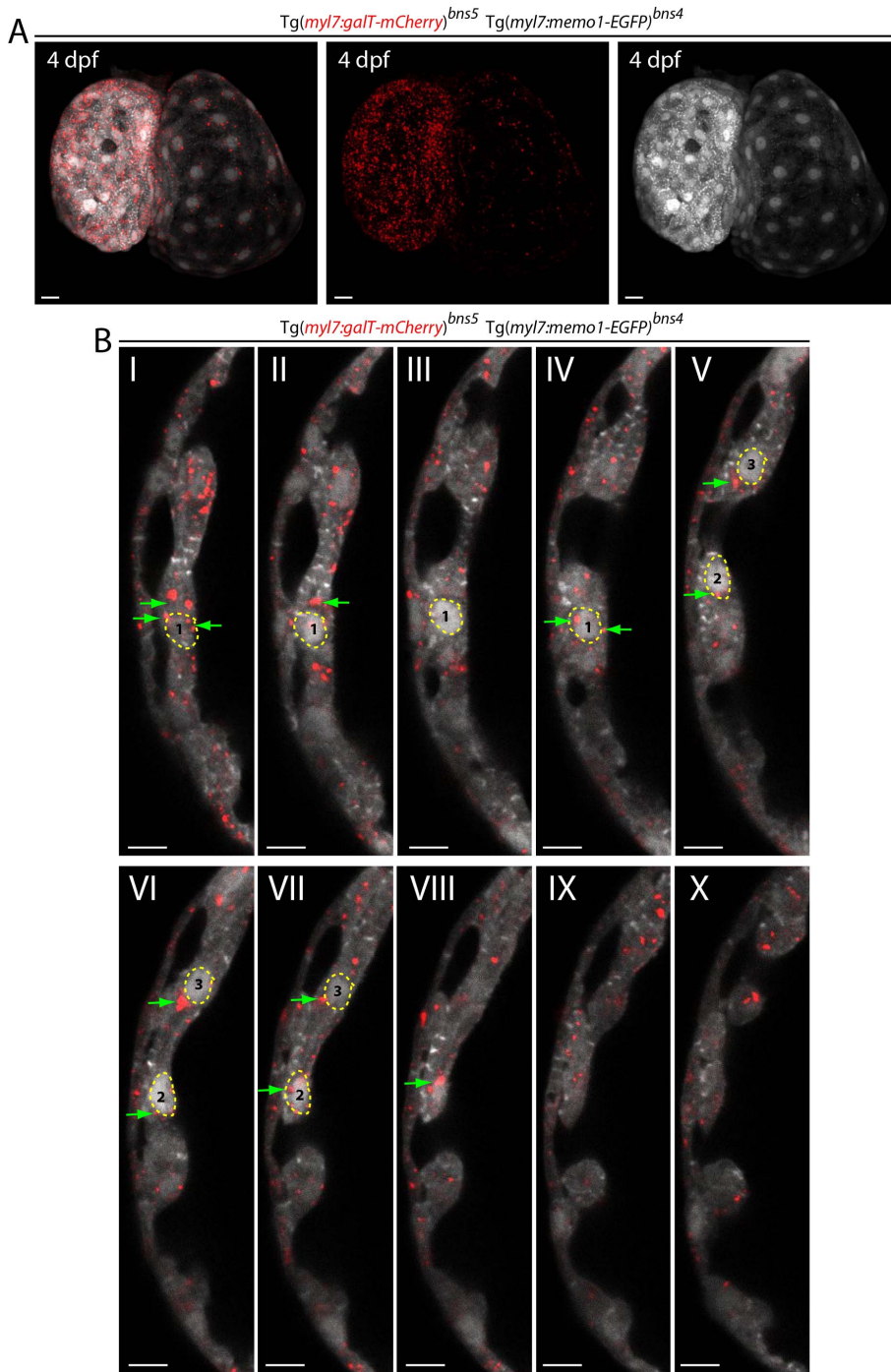

Figure 4.15: The Golgi marker GalT-mCherry marks several vesicular structures in trabecular cardiomyocytes.

A) Confocal projections of *Tg(myl7:galT-mCherry)^{bns5}* / *Tg(myl7:memo1-EGFP)^{bns4}* zebrafish at 4 dpf. **E)** Serial single planes (from I ventral to dorsal x) of ventricular outer curvature showing ventricular cardiomyocytes after initiation of trabeculation (4 dpf). GalT-mCherry-positive vesicular structures surround the nuclei in all three dimensions. Green arrows point at vesicular structures. Scale bars are 10 μm.

Similar to compact layer cardiomyocytes, Golgi vesicles are located in all dimensions surrounding the nucleus in trabeculating cells (Fig. 4.15, B), suggesting that the Golgi is not polarized in cardiomyocytes at the time points analyzed in this study.

5 Discussion

Previous studies have shown a casual relationship between Nrg1 and ErbB2/ErbB4 signaling and trabeculation of the mammalian heart. Further there are indications, that sarcomere stability is a critical factor in cardiac trabeculation. Therefore in this study we analyzed the molecular mechanisms of heart development and trabeculation.

In order to test the hypotheses that **"Flightless I function in cytoskeletal organization and mechanosensation and Memo1 mediated ErbB2 signaling are essential for the initiation of ventricular trabeculation in the zebrafish heart"** we followed these aims:

Aim 1: Analyzing the function of Flii in zebrafish skeletal muscle and heart by studying Flii-deficient animals.

Aim 2: Assessing the function of Memo1 during zebrafish heart development by utilizing Memo1-deficient animals.

Aim 2.1: Determining the subcellular localization of Memo1 in cardiomyocytes.

Aim 3: Studying the Golgi-apparatus in cardiomyocytes.

5.1 Flightless I is essential for fast and slow skeletal muscle development

We have shown that zebrafish carrying a mutation in the Flightless I gene can't develop functional skeletal muscle cells. As previously shown $flii^{mi372}$ mutant animals display a slow-twitch muscle based swimming behavior, which fails to progress to fast-twitch muscle coiling based swimming after 48 hpf (Naganawa and Hirata, 2011). Furthermore they show, that in contrast to fast-twitch fibers, slow-twitch fibers develop normally in mutant animals, suggesting a secondary role for Flii in these cells. However, we have shown that in Flii-deficient animals, slow-twitch muscle fibers of the jaw and a subset of slow-twitch fibers of the trunk display abnormal and undulated myofibrils. One possible explanation why some of the slow-twitch trunk fibers are not affected is that the maternally contributed *flii* mRNA provides sufficient functional Flii protein in this subset of cells to form the contractile apparatus.

Slow-twitch muscle cells differentiate from the so-called adaxial cells, which are located in the presomitic mesoderm located directly adjacent to the notochord, in response to hedgehog signaling. These cells are the first to commit to a myogenic fate prior to somite formation and form a single subcutaneous layer (Coutelle et al., 2001). In a second wave of differentiation the fast-twitch muscle cells are formed in the posterior half of each somite (Weinberg et al., 1996). This temporal separation of fiber type development, with a potentially unequal distribution of maternally contributed *flii* mRNA, could therefore account for the observed proportion of intact slow muscle cells. Another explanation is that the differences in the underlying transcriptional regulatory networks (Elworthy et al., 2008; Roy, 2001; von Hofsten et al., 2008) that control fiber type formation account for the observed phenomenon (Jackson and Ingham, 2013). In the future, one way to study the role of maternal *flii* mRNA could be the analysis of the slow-twitch muscle fibers in mutant animals injected with a translation-blocking morpholino, which would allow the depletion of functional Flii protein before the adaxial cells differentiate. Alternatively, germline-replacement techniques would allow to generate maternal zygotic mutants (Ciruna et al., 2002).

5.2 Flightless I is implicated in focal adhesion and t-tubule formation

We have seen that *flii*-deficiency leads to the lack of transverse tubules and aberrant localization of Vinculin in zebrafish skeletal muscle cells.

Previously, it has been shown, that Flii is a core-complex protein of focal adhesions, co-precipitating with Paxillin and co-localizing with Vinculin in NIH 3T3 cells. Flii knockdown cells showed reduced numbers of Vinculin-positive focal adhesions in migrating cells compared to wt cells (Mohammad et al., 2012). In accordance with these findings, *duesentrieb* mutants showed a lack of Vinculin-GFP localization to costameres and to cell-matrix adhesions at the cell edges, which are known to be focal adhesion-like structures in muscle cells. Furthermore, we could show that a transiently expressed membrane marker failed to localize to specified membrane structures, t-tubules, indicating that Flii-deficient cells are unable to form these structures. Therefore our results suggest, that Flightless I is essential for the development of functional skeletal muscle fibers, being involved in the formation of mechanosensory units and in turn for

the formation of sarcomere-dependent structures like transverse tubules, which are essential for efficient action potential propagation.

Another focal adhesion core complex protein, Paxillin, becomes activated through the phosphorylation by FAK and Src at activated focal adhesion sites facilitating focal adhesion site turnover (Bach et al., 2009). Flii overexpressing primary mouse fibroblasts show decreased levels of total Paxillin and a significantly reduced ratio of p-Paxillin levels compared to wt cells (Kopecki et al., 2011). However, these cells show an increased number of focal adhesions suggesting that overexpression of Flii might inhibit the interaction of Paxillin with other signaling molecules resulting in decreased Paxillin activation and impaired adhesion site turnover. We showed, that *duesentrieb* mutants have slightly increased expression of Paxillin whereas p-Paxillin was unchanged, resulting in a slight reduction of the p-pax/pax ratio in mutants compared to siblings. To understand why Flii-deficient animals show a reduction in p-pax levels, as has been shown for Flii overexpressing cells, and if this slight change is at all relevant for the generation of the observed Flii phenotype would need further investigation.

5.3 Flightless I is essential for cardiac trabeculation and heart performance

We found that Flightless I is essential for cardiac myofibril formation / bundling leading to impaired ventricular trabeculation and reduced cardiac performance. Cardiac myofibrils are aligned and bundled to form thick myofibril bundles, which enable synchronous contractions of cardiomyocytes, building the basis for heart function. The lack of thick myofibrils in ventricular cardiomyocytes and the lack of trabeculae, most likely, account for the reduced cardiac performance measured in *duesentrieb* mutants (Zhang et al., 2013). The alignment of newly formed myofibrils to myofibril bundles is established partially through "sliding" of myofibrils, but mainly through sarcomere reorganization, which involves remodeling of sarcomeres, the cellular cytoskeleton and the surrounding membranes (Raeker et al., 2014). This process is dependent on F-actin disassembly and reassembly. Ventricular cardiomyocytes, which undergo trabeculation, might have an additional requirement for efficient F-actin turnover in order to form protrusions, to undergo shape changes, and to move out of the monolayer (McNally and Dellefave, 2009). Flightless I has been shown to be involved in the regulation of the

Actin assembly activity of Diaphanous-related formins Daam1 (Dishevelled associated activator of morphogenesis) and mDia1 (mammalian Diaphanous homolog 1) in cooperation with active Rho-GTPase. The F-actin assembly activity of C-terminal Daam1 and mDia1 is increased by 40% compared to their activity in Flii-immunodepleted cytosol (Higashi et al., 2010). Therefore it is possible that decreased formin activity in premature cardiomyocytes affect F-actin turnover and therefore account for the defective myofibril bundling and trabeculation in *flii* mutants. Future studies should address whether cardiomyocyte-specific expression of a constitutively active DRF is able to rescue the phenotype in dus mutants.

F-actin "tread milling" is however dependent on two processes: F-actin polymerization and F-actin de-polymerization. Flightless I is a Gelsolin domain-containing protein (Campbell et al., 2002). Unlike Gelsolin itself, Flightless I has not yet been shown to have F-actin severing activity. Despite the lack of evidence for this activity, the myofibril bundling phenotype of the mutants could also be explained by impaired F-actin turnover due to reduced Actin severing, suggesting that flightless may indeed sever Actin. In a mass spectrometric analysis comparing *dus* mutants with siblings, we found that sarcomeric proteins are downregulated in *duesentrieb* mutants, which is in accordance with the observed myofibril disorganization phenotype in skeletal muscle and heart, suggesting that, the contractile apparatus is being disassembled in the mutants. Furthermore, we found that Cofilin1, an Actin severing protein, was upregulated in *dus* mutants, again suggesting a misregulation of the F-actin assembly/disassembly in the mutants.

On one hand, it is possible, that Cofilin1 upregulation is compensatory for a potential loss of Flightless I F-actin severing activity. On the other hand, however, a non-compensatory upregulation of Cofilin1 could be causative for the impaired bundling due to increased severing activity resulting in the lack of stable F-actin fibers available for myofibril formation. The analysis of the phosphorylation status of Cofilin1 in the mutants could provide additional information, since phosphorylated, inactive Cofilin1 inhibits cell migration in migratory adenocarcinoma cells, and could therefore account for the trabeculation phenotype observed (Popow-Wozniak et al., 2012). Future studies should also address whether a dominant negative form of Cofilin1, containing an S3D amino

acid residue which renders it constitutively inactive, is able to rescue the fibril bundling phenotype (Moriyama et al., 1996). Taken together, our findings indicate that Flii-deficiency leads to perturbed thick myofibril formation and in turn this leads to the lack of trabeculation and finally to reduced heart performance.

We found that the mutated mRNA of *flii* and *dus* mutants is stable and slightly upregulated compared to siblings. In *duesentrieb* mutants (C1581A) this mRNA becomes translated and heterozygous adults posses a residual protein fragment encoding the LRR-domain, which is highly expressed in the skeletal muscles of these animals but absent in wt siblings. It is possible, that this truncated protein domain is able to fulfill a partial Flii function. Indeed, this could explain the more severely affected cardiac performance of *flii* compared to *dus* mutants.

In conclusion our data show, that Flightless I function is essential for striated muscle development in zebrafish. Myofibrillar bundling and focal adhesion formation represent the basis for this development, and are ultimately a prerequisite for cardiac trabeculation.

5.4 Zygotic *memo1* expression is dispensable for zebrafish development

Knockout of *Memo1* in mice is lethal at E18.5 due to subcutaneous edema and significant bleeding in embryos starting from E14.5, suggesting a role of *Memo1* in endothelial cells regulating vascular development. We have shown, that in zebrafish *memo1* is expressed in the brain, the heart and fin buds at different developmental stages. We created a *memo1* reporter line (*Tg(memo1:EGFP)^bns1^*) in order to characterize its spatial expression in more detail. We confirmed that *memo1* is expressed in mid- and hindbrain, in the heart and the liver. Expression in the heart was predominant in the endocardium suggesting a role for *memo1* in heart development. Morpholino-mediated knockdown using a 5' UTR ATG binding oligomer caused craniofacial malformation, delayed heart development and pericardial edema in zebrafish larvae. In accordance with the *memo1* expression pattern the endocardium and the Common Cardinal Vein/Duct of Cuvier (CCV/DC) of morphant animals showed signs of delayed and dysmorphic development. Furthermore the myocardium of morphants showed aberrant LifeAct-GFP distribution when compared to control animals. In order to study *memo1* function in more detail, while avoiding

potential *memo1* morpholino toxicity-related phenotypes, we created a mutant memo1 (*memo1^{bns4}*) zebrafish line, carrying a 4 bp deletion leading to a premature stop codon. The characterization of hetero- and homozygous mutant *memo1^{bns4}* animals however revealed no obvious phenotypes in organs that express *memo1* and that were affected in morphants. As such, trabeculation of ventricular cardiomyocytes was not affected in mutant animals. Furthermore *Memo1^{bns4}* homozygous mutant animals develop to adulthood and are fertile, suggesting that zygotic expression of *memo1* is dispensable for zebrafish development. One possible explanation for the discrepancy between morphants and mutants is that the maternally contributed *memo1* mRNA, which is present in homozygous mutant *memo1^{bns4}* animals, is sufficient for normal development. Another possible explanation is that mutant animals are able to genetically compensate for the *memo1* deficiency through a mechanism that is restricted to mutant animals and might not become activated in morphants (Stainier et al., 2015), (Rossi et al. in press), (Deconinck et al., 1997; Hagelkruys et al., 2014). However, we can't exclude the possibility that the morphant phenotype is unspecific due to off target and toxic effects. Future studies should investigate whether maternal zygotic animals, which do not carry maternal contributed *memo1* mRNA, show a developmental defect.

5.5 Ventricular and atrial cardiomyocyte maturation is ErbB2-dependent

We have shown that overexpressed Memo1-GFP in cardiomyocytes localizes to sarcomere-like structures and to cell-cell junctions. Memo1-localization to cell-cell junctions in the ventricle was transient and disappeared between 77 hpf and 82 hpf. This change in cell-cell junctions leading to the loss of memo1 localization might indicate a process of cardiomyocyte maturation, which is timely with the start of ventricular cardiomyocyte trabeculation. Interestingly atrial cardiomyocytes, which do not form trabeculae at this stage, undergo the same cell-cell junction rearrangements between 72 and 96 hpf, suggesting a common maturation process in both cardiomyocyte subtypes. Considering the importance of ErbB2 for trabeculation we investigated cardiomyocyte Memo1-GFP localization in cardiomyocytes of ErbB2-deficient animals. In addition to the trabeculation defect in ErbB2 inhibitor-treated and in ErbB2 mutant fish we found that Memo1-GFP localization is retained in cell-cell junctions strikingly in

cardiomyocytes of both, ventricular and atrial, chambers. These results suggest a common role of ErbB2 in atrial and ventricular cardiomyocyte maturation independent of its function in initiating trabeculation. Indeed it has been shown, that animals carrying the hypomorphic ErbB2 missense mutation die at E12.5-13 due to defects in atrial electrical signal propagation, leading to an atrial-specific conduction block (Tenin et al., 2014). In conclusion, our data show that ErbB2 signaling is not only important for the trabeculation of the ventricular myocardium, but also for cardiomyocyte maturation affecting both cardiac chambers.

5.6 Skeletal muscle-like fragmented Golgi distribution in zebrafish cardiomyocytes

We generated a transgenic line expressing a fragment of the human Galactosyltransferase fused to mCherry in order to study the Golgi complex in live cardiomyocytes. Epithelial cells possessing an apico-basal polarity show polarized localization of the Golgi-apparatus which is lost when cells undergo epithelial to mesenchymal transition (EMT). Trabecular cardiomyocytes undergo similar changes, potentially displaying a partial EMT. To study cell polarization in cardiomyocytes we analyzed the localization of the Golgi-complex. We found that unlike in epithelial cells the Golgi-apparatus of cardiomyocytes is fragmented. We found GalT-mCherry-positive structures surrounding the nuclei as well as smaller trans-Golgi vesicles in the periphery of cardiomyocytes. In skeletal muscle cells the Golgi-complex transitions from a classic (a stack of flattened cisternae next to the nucelus) to an alternative fragmented organization during differentiation (Ralston, 1993; Tassin et al., 1985a; Tassin et al., 1985b). In cultured C2 mouse skeletal muscle cells the Golgi relocalizes dependent on centrosomal proteins and independent of microtubules (Zaal et al., 2011). It appears that zebrafish cardiomyocytes have a similar Golgi-complex distribution suggesting a similar differentiation-dependent re-organization. This striated muscle specific, fragmented Golgi distribution might be an advantage for these cells in order to shuttle vesicles through the densely packed sarcomere structures. However, the question if cells undergoing trabeculation change from a epithelial-like to a "partially"-mesenchymal character remains unsolved.

I Conclusion

In conclusion our data show, that Flightless I function is essential for striated muscle development in zebrafish. Myofibrillar bundling and focal adhesion formation represent the basis for this development, and are ultimately a prerequisite for cardiac trabeculation. Future analysis of Actin polymerization in trabeculation will provide addition knowledge about the sensitivity of the developing and adult heart to a disequilibrium in F-actin versus G-actin availability.

In this study we found a novel ErbB2-dependent cardiomyocyte maturation process which affects both cardiac chambers. It will be of great interest to further study the nature of the Memo1-GFP cell-cell junctions and other junction proteins in order to unravel the significance of this maturation process for heart development.

Interestingly we found, that *memo1*^{*bns4*} homozygous mutant animals, which we generated with CRISPR/Cas9 technology, develop indistinguishable from siblings, suggesting that zygotic *memo1* expression is dispensable for zebrafish development. Future studies will address the question if maternal zygotic *memo1*^{*bns4*} mutants will develop a heart or vascular phenotype as reported form *Memo1* knockout mice or as observed in *memo1* morphants in this study.

In cultured C2 mouse skeletal muscle cells the Golgi-apparatus relocalizes dependent on centrosomal proteins and independent of microtubules. We describe here that zebrafish cardiomyocytes have a similar Golgi-complex distribution suggesting a similar differentiation-dependent reorganization. This striated muscle specific, fragmented Golgi distribution might be an advantage for these cells in order to shuttle vesicles through the densely packed sarcomere structures. Future studies could address the timing of the Golgi-reorganization in cardiomyocytes during development and possibly use this Golgi-zebrafish line as a tool to study cardiomyocyte maturation in disease models and in heart regeneration.

II German Summary

Zusammenfassung

„Molekulare Mechanismen der Herzentwicklung und Trabekulierung"

Einleitung

Herzentwicklung

Während der frühen Embryonalentwicklung von Wirbeltieren kann der Embryo anfangs über Diffusion mit Sauerstoff versorgt werden. Allerdings wird relativ früh eine Blutzirkulation benötigt, um für die weitere Entwicklung des Organismus den essentiellen Sauerstoff zur Verfügung zu stellen. Daher ist das Herz das erste Organ, das sich bildet und seine Funktion aufnimmt. Da die basalen Mechanismen der Herzentwicklung innerhalb des Wirbeltier-Subphylums stark konserviert sind (Burggren and Crossley, 2002; Opitz and Clark, 2000), ist die Nutzung von Modellorganismen zu deren Erforschung möglich. Der Zebrabärbling, *Danio rerio*, hat sich als Modellorganismus in vielen medizinischen und entwicklungsbiologischen Labors durchgesetzt, da sich seine transparenten Embryonen in großer Zahl außerhalb der Mutter entwickeln. Ein weiterer Vorteil des Zebrafisches ist seine Widerstandsfähigkeit gegenüber entwicklungsbedingten Missbildungen, welche es erlaubt Vorgänge in Mutanten zu studieren, die in Säugetieren letal sind.

Die Herzentwicklung im Zebrafisch beginnt in zwei bilateralen Feldern des Mesoderms. Hier werden die ersten herzspezifischen Gene ca. 16 Stunden nach der Fertilisation (hpf, hours post fertilization) exprimiert (Stainier and Fishman, 1992; Yelon, 2001). Diese beiden Herzanlagen vereinigen sich später in der Mittellinie des Embryos und bilden den sogenannten Herzkegel, welcher sich im weiteren Verlauf der Entwicklung dorsoventral zum Herzschlauch verlängert. Dieser beginnt bereits 22 hpf mit peristaltischen Kontraktionen und besteht aus zwei Zelllagen, dem Endokard und dem Myokard, welche durch eine zellfreie Schicht, der Herzgallerte, getrennt sind. In den darauffolgenden 24 Stunden krümmt sich der Herzschlauch und erhält dadurch eine S-

Förmige Morphologie. Weiterführende morphogenetische Prozesse formen die zwei Herzkammern des Zebrafischherzens, das Atrium und den Ventrikel als auch den Atrioventrikulären-Kanal, in welchem später die Herzklappen gebildet werden. In den darauffolgenden Stunden, ab etwa 80 hpf, beginnen einige der ventrikulären Kardiomyozyten in das Kammerlumen einzudringen und bilden dort die sogenannten Trabekuli (Hu et al., 2000).

Molekulare Mechanismen der Trabekulierung

Einblicke in die molekularen Mechanismen der Trabekulierung wurden durch die Erforschung von Signalwegen in mutanten Zebrafischen und Mäusen gewonnen.

Es konnte gezeigt werden, dass Morphogene wie Notch1, welches überwiegend vom Endokard, an der Basis trabekulierender Zellen exprimiert wird, die Expression von BMP10 beeinflusst. BMP10 wiederum stimuliert, ebenfalls im Endokard, die Expression von Neuregulin1 (Nrg1), welches an ErbB2/ErbB4 Rezeptortyrosinkinasen, im Myokard bindet. Die Nrg1-abhängige Aktivierung der Rezeptoren führt dann zur Differenzierung von Kardiomyozyten und zur Initiation der Trabekulierung (Grego-Bessa et al., 2007). Des Weiteren konnte gezeigt werden, dass das Fehlen von Numb/Numblike zu einer starken Erhöhung von BMP10 durch Notch2 führt was letztlich eine Hypertrabekulierung in den Herzen der Mäuse bewirkt (Yang et al., 2012).

Die Inhibition des Nrg1/ErbB2-Signalweges, durch Mutationen im *cloche* bzw. *ErbB2* Gen hingegen, führt zum Verlust von Trabekuli in den Ventrikeln dieser Zebrafisch- und Mausmutanten (Ozcelik et al., 2002; Stainier et al., 1995).

Die Charakterisierung von Zebrafischen, die Mutationen in Genen tragen welche für die Kontraktilität der Zellen verantwortlich sind, haben weitere Einblicke in die Regulation der Trabekulierung erbracht. Ein Beispiel ist die „silent heart" (*sih*) Mutante welche Mutationen im *tnnt2* Gen, trägt welches für den Aufbau von Sarkomeren wichtig ist. Die Herzen dieser Fische sind nicht kontraktil und formen keine Trabekuli (Chi et al., 2008; Sehnert et al., 2002).

Nicht nur die Kontraktilität der Zellen selbst ist wichtig für die morphogenetische Entwicklung des Herzens, sondern auch der Blutfluss durch die Herzkammern spielt eine entscheidende Rolle. Die Zebrafischmutante „weak atrium" (*wea*) trägt eine Mutation im

amhc Gen, (Berdougo et al., 2003) welches für die Kontraktilität des Atriums verantwortlich ist. Diese Mutanten haben kontraktile Ventrikel zeigen aber reduzierte Blutzirkulation und sind ebenfalls nicht in der Lage ventrikuläre-Trabekuli zu bilden.

Während des gesamten Prozesses der Trabekulierung bleiben die Kardiomyozyten kontraktil. Das Zytoskelett und der kontraktile Apparat dieser Zellen muss deshalb ein hohes Maß an Flexibilität aufweisen, um die fortlaufende Reorganisation der Sarkomere und Zellformveränderung während der Zellmigration zu ermöglichen. F-Aktin Polymerisation und Depolymerisation spielen hierbei eine entscheidende Rolle, und werden von zwei Proteingruppen katalysiert. Sogenannte Formine, wie beispielsweise Daam1 und mDia1, katalysieren die F-Aktin Polymerisation, während Cofilin-1 F-Aktin depolymerisiert. Die Feinabstimmung dieser beiden Prozesse ist essentiell, da sie Zellen ermöglicht sich an verändernde Bedingungen anzupassen, was insbesondere für trabekulierende Kardiomyozyten von Bedeutung ist.

Des Weiteren müssen diese Zellen ihre Zelladhäsionen während der Zellbewegung ständig erneuern. Muskelzellen bilden deshalb spezialisierte Fokale Adhäsionen, sogenannte Costamere, über welche sie ihren kontraktilen-Apparat in der Basalmembran verankern. Diese Strukturen verleihen mechanische Stabilität und ermöglichen Mechanorezeption. Letztere ist im Speziellen wichtig für sich entwickelnde Muskelzellen, da sich diese an hämodynamische Veränderungen nur so anpassen können. Störungen in der Verankerung und der Mechanorezeption dieser Zellen führen zu muskulären Erbkrankheiten wie Muskeldystrophien und dilatativen Kardiomyopathien (Deconinck et al., 1997; Hoffman et al., 1987; Raeker et al., 2014). Es konnte gezeigt werden, dass die Interaktion des Aktin bindenden Proteins Flightless I (Flii) mit Daam1 und mDia1 die Polymerisation von Aktin katalysiert. Darüber hinaus ist Flii ein Kernbestandteil von Fokalen Adhäsionen und ein negativer Regulator der Wundheilung in Mäusen (Higashi et al., 2010; Kopecki et al., 2011; Mohammad et al., 2012). Mutationen in diesem Gen in Zebrafischen führen zu Missbildungen des Skelettmuskels sowie zu verminderter Schwimmfähigkeit (Granato et al., 1996; Naganawa and Hirata, 2011). Ein Rolle von Flii in der Entwicklung des Herzmuskels ist nicht bekannt.

4D Beobachtungen von schlagenden Herzen, vor und während der Trabekulierung haben gezeigt, dass Kardiomyozyten ihre Zell-Zell Kontakte erneuern, indem sie

luminale Zellfortsätze entlang benachbarter Zell-Zell Kontakte aussenden (Staudt et al., 2014). Daraufhin beginnen diese Zellen ihre apikale Oberfläche zu verkleinern und bewegen ihre Zellkörper ins ventrikuläre Lumen. Diese Beobachtung deutet an, dass ErbB2-aktivierte, trabekulierende Kardiomyozyten einige ihre Epithel-Charakteristika verlieren. In Krebszellen bewirkt die Aktivierung von ErbB2-Rezeptoren die Initiation einer Epithelial-mesenchymalen Transition (EMT), welche zum Verlust der apiko-basalen Zellpolarisation führt, und die damit einhergehende Relokalisation des Golgi-Apparates nach sich zieht (Aranda et al., 2006).

Kardiomyozyten von Zebrafischherzen zeigen Unterschiede in der Verteilung von Myofibrillen innerhalb der Zellen. So variiert die Myofibrillen-Architektur zwischen der basalen Seite, welche hauptsächlich dicke, kortikale Myofibrillen enthält, und der apikalen Seite, welche aus feinen Fibrillen besteht. Diese Beobachtung deutet auf eine apiko-basale Zellpolarisation von Kardiomyozyten während der Zebrafischentwicklung hin (Reischauer et al., 2014). Ob Kardiomyozyten eine Art EMT vollziehen und wie die Aktivierung von ErbB2 zur Trabekulierung führt, ist derzeit noch unbekannt.

Memo1 „Mediator of ErbB2-driven cell motility 1" ist ein Protein welches in migrierenden Zellen als Sensor für aktivierte ErbB2-Rezeptoren fungiert (Marone et al., 2004; Zaoui et al., 2010). Hier bindet es spezifisch an phosphorylierte Rezeptoren und bewirkt dadurch die Relokalisation von Proteinkomplexen an die Zellmembran. Dies erlaubt eine gezielte Reaktion auf einen extrazellulären Stimulus. Die darauffolgende Memo1-abhängige Verankerung von Mikrotubuli (MT) an der Zellmembrane erlaubt dann die effiziente Migration in Richtung des Stimulus. Ob die Aktivierung von ErbB2-Rezeptoren auch in Kardiomyozyten zu einer Memo1-abhängigen Zellmigration führt ist bislang nicht bekannt.

Hypothese

Die Organisation des Zytoskeletts und die Bildung von Fokalen Adhäsionen durch Flightless I, sowie die Memo1-vermittelte ErbB2-Signalantwort, sind essentiell für die Initiation der ventrikulären Trabekulierung im Zebrafischherzen.

Um diese Hypothese zu untersuchen haben wir uns folgende Ziele gesetzt:

Ziel 1: Die Analyse der Flightless I Funktion im Skelettmuskel und Herz von Flightless I Zebrafischmutanten.

Ziel 2: Die Analyse der subzellulären Lokalisation von Memo1 in Zebrafischkardiomyozyten.

Ziel 3: Die Untersuchung von Memo1-defizienten Zebrafischherzen zur Erforschung der Memo1 Funktion während der Trabekulierung.

Ziel 4: Die Erforschung des Golgi-Apparates in Zebrafischkardiomyozyten.

Ergebnisse und Diskussion

Fehlende Trabekulierung aufgrund von dysfunktionaler Myofibrillenbündelung und Fokaler Adhäsions-(Neu)-Bildung in *duesentrieb* Mutanten.

In vorhergehenden Studien wurde gezeigt, dass das Protein Flightless I eine wichtige Rolle in der Entwicklung des Skelettmuskels in der Fruchtfliege und im Zebrafisch spielt (Campbell et al., 1993; Naganawa and Hirata, 2011). Dir Ergebnisse dieser Studie zeigen, dass *flii* mRNA maternal beigesteuert wird und während der gesamten Embryonalentwicklung exprimiert wird. Die Untersuchung der spatio-temporalen Verteilung zeigt, das *flii* mRNA vor allem im Herzen, im Gehirn und in den Flossenanlagen von Larven bei 72 hpf exprimiert wird. Während der späteren Entwicklung, bei 7 Tagen nach Fertilisation (dpf, days post fertilization) kann die *flii* Expression noch immer im Herzen detektiert werden, während die Expression im Gehirn stark reduziert ist.

Homozygote *flightless I*-Mutanten für die beiden Allele, $flii^{mi372}$ und dus^{tg250}, zeigen Rumpf und Kiefer „slow-twitch" (S-Faser) und „fast-twitch" (F-Faser) Muskelfehlbildungen. Überdies entwickeln sich die mutanten Larven fast ununterscheidbar von ihren Geschwistern, sind aber nach 6 dpf nicht dazu in der Lage sich weiterzuentwickeln, da sie keine Schwimmblase ausbilden. Zur Untersuchung der Rolle von Flii in der Bildung von Fokalen Adhäsionen haben wir die Lokalisation von Vinculin-GFP in Skelettmuskelzellen des Rumpfes studiert. Vinculin interagiert mit einer Reihe von Proteinen um das Aktin-Zytoskelett an der Zellmembran zu verankern und spielt somit eine Rolle in der Formation von Fokalen Adhäsionen. In Muskelzellen

lokalisiert Vinculin an Costameren sowie an „Somit-Grenzen" welche spezialisierte muskelspezifische Fokale Adhäsionen darstellen (Samarel, 2005). Die Lokalisation von Vinculin-GFP an diese spezialisierten Adhäsionen ist in *dus*-Mutanten, im Vergleich zu Geschwistern gestört. Stattdessen ist es im gesamten Zytoplasma diffus detektierbar. Um eine weitere Analyse dieser Membran-assoziierten Strukturen durchzuführen, haben wir die Präsenz von sogenannten transversale-Röhren, welche vom Sarkolemma (Muskelzellmembran) gebildet werden, in Skelettmuskelzellen des Rumpfes untersucht. Diese Strukturen sind für die effiziente Weiterleitung von Aktionspotentialen notwendig und überlagern mit Costameren und Z-Scheiben (Brette and Orchard, 2003). *Dus*-Mutanten zeigen, im Vergleich zu Geschwistertieren, keine Lokalisation des membranständigen-Fluoreszenzproteins zu diesen Strukturen, was daraufhin deutet, dass Flii-defiziente Zellen keine transversale-Röhren ausbilden können. Zusammengefasst zeigen diese Ergebnisse, dass Flii essentiell für die Entwicklung von Skelettmuskelzellen ist, und dabei eine besondere Rolle in der Ausbildung von spezialisierten Fokalen Adhäsionen und transversale-Röhren spielt.

Als nächstes haben wir uns die Funktion von Flightless I im Zebrafischherzen angeschaut. Um die Herzfunktion in *dus*-Mutanten zu untersuchen, haben wir uns einer indirekten Methode bedient, bei welcher die Geschwindigkeit der Blutzellen in der dorsalen Aorta im Zebrafisch gemessen wird. Mutanten beider Allele, *dus* und *flii,* zeigen eine Reduktion der maximalen Blutzellgeschwindigkeit im Vergleich zu Geschwistern. Diese Reduktion lässt auf eine verminderte Herzfunktion in den Zebrafischmutanten schließen.

Um herauszufinden ob Herzmuskelzellen wie auch Skelettmuskelzellen myofibrilläre Missbildungen entwickeln, haben wir Herzen, welche ein Aktin-bindendes GFP exprimieren (LifeAct-GFP), mittels konfokaler Mikroskopie untersucht. *Dus*-Mutanten können Sarkomere sowie Myofibrillen bilden, zeigen jedoch, im Unterschied zu Geschwistern, nur feine Myofibrillenbündel. Das Fehlen von starken, gebündelten Myofibrillen könnte geschwächte Zellkontraktionen und dadurch die reduzierte Herzfunktion in den *dus*-Mutanten nach sich ziehen.

Eine nähere Analyse der Ventrikel von *dus*-Mutanten zeigt, dass Zellen der ventrikulären-Wand nicht in das Ventrikellumen hineinragen, und deutet somit darauf

hin, dass *dus*-Mutanten keine Trabekuli bilden können. Das Bündeln wie auch das Reorganisieren von Myofibrillen in trabekulierenden Zellen bedingt den Abbau und Wiederaufbau von Sarkomeren. Dieser hochkomplexe Vorgang wiederum basiert unter anderem auf der Polymerisation und Depolymerisation von F-Aktin. Die reduzierte Effizienz der F-Aktin Polymerisation durch das Fehlen von Flii könnte ein Grund für die verminderte Bündelung der Myofibrillen aber auch für das Fehlen von Trabekuli sein.

Die Untersuchung des Gesamtproteins aus 3 dpf Zebrafischlarven mittels Massenspektrometrie zeigt in den Mutanten eine Reduktion von muskelspezifischen Proteinen, die für den Aufbau von Sarkomeren notwendig sind. Dieses Ergebnis deutet auf eine allgemeine Reduktion der Skelettmuskelapparates in den Flii-defizienten Tieren hin. Desweitern konnte eine Erhöhung des Proteins Cofilin-1 in den Mutanten gemessen werden, was ebenfalls auf eine potentielle Störung des F-Aktin Auf- bzw. Abbaus hindeutet.

Zusammenfassend schlussfolgern wir, dass die Funktion von Flightless I eine essentielle Rolle in der Entwicklung von quergestreiften Muskelfasern im Zebrafisch spielt, welche maßgeblich von der Funktion von Fokalen Adhäsionen und der Formation starker Myofibrillen abhängig ist, und letztlich eine Voraussetzung für die Bildung von ventrikulären Trabekuli darstellt.

Kardiomyozyten-Maturation ist ErbB2-abhängig

Um ein besseres Verständnis für die intrazellulären Vorgänge zu erlangen, welche nach der ErbB2-Rezeptor Aktivierung zur Trabekulierungs-Initiation führen, haben wir eine Zebrafischlinie generiert, welche Memo1-GFP exprimiert. Mit Hilfe dieses Konstrukts haben wir untersucht, ob die Kardiomyozyten-spezifische Expression von Memo1-GFP als Reporter für aktivierte Rezeptoren vor und während der Trabekulierung genutzt werden kann.

Unsere Ergebnisse zeigen, dass das Fusionsprotein Memo1-GFP zu Zellkernen, Sarkomerartigen, quergestreiften Strukturen, und zu Zell-Zell Kontakten in ventrikulären und atrialen Kardiomyozyten nach 48 und 72 hpf lokalisiert. Nach der Initiation der Trabekulierung bei 96 hpf lokalisiert Memo1-GFP noch immer zu Zellkernen und Sarkomerartigen Strukturen. Die Lokalisation zu Zell-Zell Kontakten ist jedoch weder in

trabekulierenden noch in nicht-trabekulierenden Kardiomyozyten detektierbar. Atriale Kardiomyozyten erfahren den gleichen Verlust der Memo1-GFP Lokalisation zu Zell-Zell Kontakten nach 96 hpf, was darauf schließen lässt, dass diese Veränderung einem generellen Reifungsprozess der Kardiomyozyten entspricht.

Da Memo1, spezifisch, an aktivierte ErbB2-Rezeptoren bindet, haben wir die Lokalisation von Memo1-GFP in Kardiomyozyten von *erbb2*-Mutanten untersucht. Wie auch im Wildtyp (wt) lokalisiert Memo1-GFP zu Zellkernen, Sarkomerartigen Strukturen und zu Zell-Zell Kontakten in ventrikulären und atrialen Kardiomyozyten nach 48 und 72 hpf. Im Gegensatz zu wt Zebrafischen jedoch, bleibt die Lokalisation zu Zell-Zell Kontakten in ErbB2-defizienten Tieren nach 96 hpf Stunden erhalten. Dieses Ergebnis legt nahe, dass Kardiomyozyten beider Herzkammern eine ErbB2-abhängige Zell-Zell Kontakt-„Reifung" durchlaufen, welche zeitlich mit dem Beginn der Trabekulierung übereinstimmt aber unabhängig davon zu sein scheint.

Zygotische *memo1* Expression ist für die Zebrafischentwicklung entbehrlich

Um die Funktion von Memo1 in Herzen zu studieren, haben wir zunächst dessen Expression im Zebrafisch untersucht. *Memo1* wird maternal beigesteuert und während der gesamten Embryonalentwicklung bis 72 hpf exprimiert. Die spatiale Analyse mittels *in situ*-Hybridisierung zeigt *memo1* Expression im Gehirn, in den Flossenanlagen und im Herzen bei 4 dpf. Die Sektion von 7 dpf alten Herzen zeigt, dass *memo1* in beiden Herzkammern exprimiert wird.

Um eine genauere Analyse durchzuführen, haben wir ein Reporterkonstrukt generiert, das es uns erlaubt, die *memo1* Expression über dessen Promoter Aktivität zu untersuchen. Die fluoreszenzmikroskopische Analyse von Embryonen bei 80 hpf zeigt, dass der *memo1*-Reporter im Mittel- und Kleinhirn und im Herzen exprimiert wird. Bei 6 dpf ist die Expression im Mittel- und Kleinhirn noch immer vorhanden, jedoch ist die Expression im Herzen zu diesem Zeitpunkt deutlich stärker. Die genauere Analyse von Herzen bei 4 und 5 dpf mittels konfokaler Mikroskopie zeigt, dass *memo1* hauptsächlich im Endokard exprimiert wird.

Zum Zweck der funktionellen Analyse von Memo1 in Zebrafischherzen haben wir ein Morpholino (MO) eingesetzt welches spezifisch an die *memo1* mRNA bindet und

deren Translation verhindert. Die Injektion von bereits 0,8 ng dieses MOs führt zu kraniofacialen Missbildungen, und peri-kardialen Ödemen. Des Weiteren konnten wir beobachten, dass das Myokard sowie das Endokard und die Common Cardinal Vein/Duct of Cuvier (CCV/DV) entwicklungsbiologische Verzögerungen und Missbildungen aufweisen. Zusammengefasst lassen diese Ergebnisse darauf schließen, dass *memo1* eine Rolle in der Zebrafischentwicklung des Herzens spielt.

Um sicherzustellen, dass die beobachteten Phänotypen *memo1*-spezifisch sind, haben wir mit Hilfe der CRISPR/Cas9 Technologie eine *memo1*-Mutante generiert. Die Sequenzanalyse der F_0 und F_1 Generation zeigte eine 4-Basenpaar Deletion an Stelle 38-41 (Δ:CCGG). Um die Funktion von Memo1 während der Trabekulierung zu studieren, haben wir LifeAct-GFP-positive Herzmuskeln in Mutanten im Vergleich zu Geschwistern untersucht. Heterozygote sowie homozygote *memo1*-Mutanten zeigen morphologisch ununterscheidbare Herzen. Auch sind diese Tiere dazu in der Lage Trabekuli in den ventrikulären Herzkammern zu bilden. Homozygote *memo1*-Mutanten entwickeln sich ununterscheidbar von ihren heterozygoten und wt Geschwistern und sind fertil. Diese Ergebnisse legen nahe, dass die zygotische *memo1* Expression für die Zebrafischentwicklung entbehrlich ist.

Ein möglicher Grund für die Diskrepanz zwischen den *memo1*-Mutanten und den Morphanten ist die maternal beigetragene mRNA welche in den Mutanten translatiert werden und zu einer Rettung des Phänotyps führen könnte. Auch ist es möglich, dass die Mutanten, durch einen unbekannten Mechanismus/Signalweg dazu in der Lage sind die Mutation zu kompensieren und dass diese Kompensation in den Morphanten nicht stattfindet (Deconinck et al., 1997; Hagelkruys et al., 2014; Stainier et al., 2015); (Rossi et al. in press). Wir können jedoch die Möglichkeit nicht ausschließen, dass der MO-induzierte Phänotyp unspezifisch ist und durch sogenannte „off-targets" oder durch Toxizität des MO's verursacht wird. Zukünftige Untersuchungen der maternal-zygotischen Mutanten, welche keine maternal beigetragene mRNA tragen, werden weiteren Aufschluss über die Funktion von Memo1 im Zebrafisch geben.

Fragmentierter Golgi-Apparat in Zebrafischkardiomyozyten

Um zu untersuchen ob Kardiomyozyten eine Zellpolarisation aufweisen haben wir ein Konstrukt generiert, welches die Lokalisation des Golgi-Apparates erlaubt. Die Kardiomyozyten-spezifische Expression eines Fragments der humanen Galaktosyltransferase als Fusionsprotein mit dem Fluoreszenzprotein mCherry (GalT-mCherry), diente bei dieser Studie als Golgi-Marker. Die konfokal-mikroskopische Analyse ergab, dass GalT-mCherry in Kardiomyozyten exprimiert wird und in atrialen wie auch ventrikulären Zellen mehrere vesikuläre Strukturen markiert. Diese Golgi-Vesikel befinden sich hauptsächlich in der Nähe der Zellkerne und umgeben diese. Im Unterschied zu polarisierten, epithelartigen Zellen, die einen „klassischen" Golgi-Apparat aufweisen, welcher aus einem einzigen Membranstapel pro Zelle besteht, zeigen Kardiomyozyten mehrere Golgi-Vesikel. Diese Beobachtung legt dar, dass der Golgi-Apparat in Kardiomyozyten fragmentiert ist. Um herauszufinden ob diese Golgi-Vesikel eine gewisse Position im Bezug zum Zellkern in 3D aufweisen, haben wir konsekutive optische Ebenen von Ventrikeln vor bzw. während der Trabekulierung analysiert. Golgi-Vesikel umgeben die Zellkerne in allen Dimensionen und zeigen keinerlei Orientierung. Weder in Zellen der ventrikulären Wand vor bzw. während der Trabekulierung noch trabekulierenden Zellen zeigen eine Orientierung des Golgi-Apparates aus. Diese Ergebnisse zeigen, dass der Golgi-Apparat in Kardiomyozyten von der „klassischen" epithelialen Form abweicht und darüber hinaus keinerlei Polarisation anzeigt.

Es konnte gezeigt werden, dass sich der Golgi-Apparat in C2-Skelettmuskelzellen während der Zelldifferenzierung verändert (Zaal et al., 2011). Der zu Beginn „klassische" Golgi –Apparat fragmentiert und relokalisiert, wenn diese Zellen beginnen ihren kontraktilen Apparat auszubilden (Ralston, 1993; Tassin et al., 1985b). Die Fragmentierung des Golgi-Apparates zu mehreren kleineren Organellen in Muskelzellen wie auch in Kardiomyozyten, ist möglicherweise ein Weg, wie diese Zellen den Vesikeltransport durch das kompakte Myofibrillengerüst erleichtern. Die Frage ob Kardiomyozyten eine Zellpolarisation aufweisen und ob sich diese während der Trabekulierung verändert, kann durch die subzelluläre Lokalisation des Golgi-Apparates nicht untersucht werden und bleibt daher unbeantwortet.

III References

Alexander, J. and Stainier, D. Y. (1999). A molecular pathway leading to endoderm formation in zebrafish. *Current biology : CB* **9**, 1147-1157.

Aranda, V., Haire, T., Nolan, M. E., Calarco, J. P., Rosenberg, A. Z., Fawcett, J. P., Pawson, T. and Muthuswamy, S. K. (2006). Par6-aPKC uncouples ErbB2 induced disruption of polarized epithelial organization from proliferation control. *Nature cell biology* **8**, 1235-1245.

Auman, H. J., Coleman, H., Riley, H. E., Olale, F., Tsai, H. J. and Yelon, D. (2007). Functional modulation of cardiac form through regionally confined cell shape changes. *PLoS biology* **5**, e53.

Baarlink, C., Brandt, D. and Grosse, R. (2010). SnapShot: Formins. *Cell* **142**, 172, 172 e171.

Bach, C. T., Creed, S., Zhong, J., Mahmassani, M., Schevzov, G., Stehn, J., Cowell, L. N., Naumanen, P., Lappalainen, P., Gunning, P. W., et al. (2009). Tropomyosin isoform expression regulates the transition of adhesions to determine cell speed and direction. *Molecular and cellular biology* **29**, 1506-1514.

Berdougo, E., Coleman, H., Lee, D. H., Stainier, D. Y. and Yelon, D. (2003). Mutation of weak atrium/atrial myosin heavy chain disrupts atrial function and influences ventricular morphogenesis in zebrafish. *Development* **130**, 6121-6129.

Bornens, M. (1991). Cell polarity: intrinsic or externally imposed? *The New biologist* **3**, 627-636.

Brette, F. and Orchard, C. (2003). T-tubule function in mammalian cardiac myocytes. *Circulation research* **92**, 1182-1192.

Brown, M. C. and Turner, C. E. (2004). Paxillin: adapting to change. *Physiological reviews* **84**, 1315-1339.

Burggren, W. and Crossley, D. A., 2nd (2002). Comparative cardiovascular development: improving the conceptual framework. *Comparative biochemistry and physiology. Part A, Molecular & integrative physiology* **132**, 661-674.

Campbell, H. D., Fountain, S., McLennan, I. S., Berven, L. A., Crouch, M. F., Davy, D. A., Hooper, J. A., Waterford, K., Chen, K. S., Lupski, J. R., et al. (2002). Fliih, a gelsolin-related cytoskeletal regulator essential for early mammalian embryonic development. *Molecular and cellular biology* **22**, 3518-3526.

Campbell, H. D., Schimansky, T., Claudianos, C., Ozsarac, N., Kasprzak, A. B., Cotsell, J. N., Young, I. G., de Couet, H. G. and Miklos, G. L. (1993). The Drosophila melanogaster flightless-I gene involved in gastrulation and muscle degeneration encodes gelsolin-like and leucine-rich repeat domains and is conserved in Caenorhabditis elegans and humans. *Proceedings of the National Academy of Sciences of the United States of America* **90**, 11386-11390.

Cardamone, M., Darras, B. T. and Ryan, M. M. (2008). Inherited myopathies and muscular dystrophies. *Seminars in neurology* **28**, 250-259.

Carisey, A., Tsang, R., Greiner, A. M., Nijenhuis, N., Heath, N., Nazgiewicz, A., Kemkemer, R., Derby, B., Spatz, J. and Ballestrem, C. (2013). Vinculin regulates the recruitment and release of core focal adhesion proteins in a force-dependent manner. *Current biology : CB* **23**, 271-281.

Chan, R., Hardy, W. R., Laing, M. A., Hardy, S. E. and Muller, W. J. (2002). The catalytic activity of the ErbB-2 receptor tyrosine kinase is essential for embryonic development. *Molecular and cellular biology* **22**, 1073-1078.

Chawla, J. (2011). Stepwise approach to myopathy in systemic disease. *Frontiers in neurology* **2**, 49.

Chen, H., Zhang, W., Sun, X., Yoshimoto, M., Chen, Z., Zhu, W., Liu, J., Shen, Y., Yong, W., Li, D., et al. (2013). Fkbp1a controls ventricular myocardium trabeculation and compaction by regulating endocardial Notch1 activity. *Development* **140**, 1946-1957.

Chen, J. N., van Eeden, F. J., Warren, K. S., Chin, A., Nusslein-Volhard, C., Haffter, P. and Fishman, M. C. (1997). Left-right pattern of cardiac BMP4 may drive asymmetry of the heart in zebrafish. *Development* **124**, 4373-4382.

Chi, N. C., Shaw, R. M., Jungblut, B., Huisken, J., Ferrer, T., Arnaout, R., Scott, I., Beis, D., Xiao, T., Baier, H., et al. (2008). Genetic and physiologic dissection of the vertebrate cardiac conduction system. *PLoS biology* **6**, e109.

Ciruna, B., Weidinger, G., Knaut, H., Thisse, B., Thisse, C., Raz, E. and Schier, A. F. (2002). Production of maternal-zygotic mutant zebrafish by germ-line replacement. *Proceedings of the National Academy of Sciences of the United States of America* **99**, 14919-14924.

Coutelle, O., Blagden, C. S., Hampson, R., Halai, C., Rigby, P. W. and Hughes, S. M. (2001). Hedgehog signalling is required for maintenance of myf5 and myoD expression and timely terminal differentiation in zebrafish adaxial myogenesis. *Developmental biology* **236**, 136-150.

Deconinck, N., Tinsley, J., De Backer, F., Fisher, R., Kahn, D., Phelps, S., Davies, K. and Gillis, J. M. (1997). Expression of truncated utrophin leads to major functional improvements in dystrophin-deficient muscles of mice. *Nature medicine* **3**, 1216-1221.

Edwards, M., Zwolak, A., Schafer, D. A., Sept, D., Dominguez, R. and Cooper, J. A. (2014). Capping protein regulators fine-tune actin assembly dynamics. *Nature reviews. Molecular cell biology* **15**, 677-689.

Elworthy, S., Hargrave, M., Knight, R., Mebus, K. and Ingham, P. W. (2008). Expression of multiple slow myosin heavy chain genes reveals a diversity of zebrafish slow twitch muscle fibres with differing requirements for Hedgehog and Prdm1 activity. *Development* **135**, 2115-2126.

Epstein, H. F. and Fischman, D. A. (1991). Molecular analysis of protein assembly in muscle development. *Science* **251**, 1039-1044.

Fishman, M. C. and Chien, K. R. (1997). Fashioning the vertebrate heart: earliest embryonic decisions. *Development* **124**, 2099-2117.

Gautel, M. (2011). The sarcomeric cytoskeleton: who picks up the strain? *Current opinion in cell biology* **23**, 39-46.

Ginzburg, I. (1991). Neuronal polarity: targeting of microtubule components into axons and dendrites. *Trends in biochemical sciences* **16**, 257-261.

Glickman, N. S. and Yelon, D. (2002). Cardiac development in zebrafish: coordination of form and function. *Semin Cell Dev Biol* **13**, 507-513.

Goldmann, W. H. (2014). Mechanosensation: a basic cellular process. *Progress in molecular biology and translational science* **126**, 75-102.

Goley, E. D. and Welch, M. D. (2006). The ARP2/3 complex: an actin nucleator comes of age. *Nature reviews. Molecular cell biology* **7**, 713-726.

Goode, B. L. and Eck, M. J. (2007). Mechanism and function of formins in the control of actin assembly. *Annual review of biochemistry* **76**, 593-627.

Granato, M., van Eeden, F. J., Schach, U., Trowe, T., Brand, M., Furutani-Seiki, M., Haffter, P., Hammerschmidt, M., Heisenberg, C. P., Jiang, Y. J., et al. (1996). Genes controlling and mediating locomotion behavior of the zebrafish embryo and larva. *Development* **123**, 399-413.

Grego-Bessa, J., Luna-Zurita, L., del Monte, G., Bolos, V., Melgar, P., Arandilla, A., Garratt, A. N., Zang, H., Mukouyama, Y. S., Chen, H., et al. (2007). Notch signaling is essential for ventricular chamber development. *Developmental cell* **12**, 415-429.

Hagelkruys, A., Lagger, S., Krahmer, J., Leopoldi, A., Artaker, M., Pusch, O., Zezula, J., Weissmann, S., Xie, Y., Schofer, C., et al. (2014). A single allele of Hdac2 but not Hdac1 is sufficient for normal mouse brain development in the absence of its paralog. *Development* **141**, 604-616.

Higashi, T., Ikeda, T., Murakami, T., Shirakawa, R., Kawato, M., Okawa, K., Furuse, M., Kimura, T., Kita, T. and Horiuchi, H. (2010). Flightless-I (Fli-I) regulates the actin assembly activity of diaphanous-related formins (DRFs) Daam1 and mDia1 in cooperation with active Rho GTPase. *The Journal of biological chemistry* **285**, 16231-16238.

Hirata, H., Sokabe, M. and Lim, C. T. (2014). Molecular mechanisms underlying the force-dependent regulation of actin-to-ECM linkage at the focal adhesions. *Progress in molecular biology and translational science* **126**, 135-154.

Hoffman, E. P., Brown, R. H., Jr. and Kunkel, L. M. (1987). Dystrophin: the protein product of the Duchenne muscular dystrophy locus. *Cell* **51**, 919-928.

Hopkinson, S. B., Hamill, K. J., Wu, Y., Eisenberg, J. L., Hiroyasu, S. and Jones, J. C. (2014). Focal Contact and Hemidesmosomal Proteins in Keratinocyte Migration and Wound Repair. *Advances in wound care* **3**, 247-263.

Hove, J. D., Kofoed, K. F., Wu, H. M., Holm, S., Friberg, L., Meyer, C., Aldershvile, J., Hesse, B. and Kelbaek, H. (2003). Simultaneous cardiac output and regional myocardial perfusion determination with PET and nitrogen 13 ammonia. *Journal of nuclear cardiology : official publication of the American Society of Nuclear Cardiology* **10**, 28-33.

Hu, N., Sedmera, D., Yost, H. J. and Clark, E. B. (2000). Structure and function of the developing zebrafish heart. *The Anatomical record* **260**, 148-157.

Icardo, J. M. and Fernandez-Teran, A. (1987). Morphologic study of ventricular trabeculation in the embryonic chick heart. *Acta anatomica* **130**, 264-274.

Inoue, S. (1981). Cell division and the mitotic spindle. *The Journal of cell biology* **91**, 131s-147s.

Inoue, S. and Sato, H. (1967). Cell motility by labile association of molecules. The nature of mitotic spindle fibers and their role in chromosome movement. *The Journal of general physiology* **50**, Suppl:259-292.

Israeli-Rosenberg, S., Manso, A. M., Okada, H. and Ross, R. S. (2014). Integrins and integrin-associated proteins in the cardiac myocyte. *Circulation research* **114**, 572-586.

Jackson, H. E. and Ingham, P. W. (2013). Control of muscle fibre-type diversity during embryonic development: the zebrafish paradigm. *Mechanisms of development* **130**, 447-457.

Jiang, K., Yang, Z., Cheng, L., Wang, S., Ning, K., Zhou, L., Lin, J., Zhong, H., Wang, L., Li, Y., et al. (2013). Mediator of ERBB2-driven cell motility (MEMO) promotes extranuclear estrogen receptor signaling involving the growth factor receptors IGF1R and ERBB2. *The Journal of biological chemistry* **288**, 24590-24599.

Judice, C. C., Marin, T. M. and Franchini, K. G. (2009). Calcium and the mechanotransduction in cardiac myocytes. *Frontiers in bioscience* **1**, 189-199.

Kondo, S., Bottos, A., Allegood, J. C., Masson, R., Maurer, F. G., Genoud, C., Kaeser, P., Huwiler, A., Murakami, M., Spiegel, S., et al. (2014). Memo has a novel role in S1P signaling and is [corrected] crucial for vascular development. *PloS one* **9**, e94114.

Kopecki, Z., O'Neill, G. M., Arkell, R. M. and Cowin, A. J. (2011). Regulation of focal adhesions by flightless i involves inhibition of paxillin phosphorylation via a Rac1-dependent pathway. *The Journal of investigative dermatology* **131**, 1450-1459.

Kuo, C. T., Morrisey, E. E., Anandappa, R., Sigrist, K., Lu, M. M., Parmacek, M. S., Soudais, C. and Leiden, J. M. (1997). GATA4 transcription factor is required for ventral morphogenesis and heart tube formation. *Genes & development* **11**, 1048-1060.

Lamouille, S., Xu, J. and Derynck, R. (2014). Molecular mechanisms of epithelial-mesenchymal transition. *Nature reviews. Molecular cell biology* **15**, 178-196.

Le Garrec, J. F., Ragni, C. V., Pop, S., Dufour, A., Olivo-Marin, J. C., Buckingham, M. E. and Meilhac, S. M. (2013). Quantitative analysis of polarity in 3D reveals local cell coordination in the embryonic mouse heart. *Development* **140**, 395-404.

Lee, K. F., Simon, H., Chen, H., Bates, B., Hung, M. C. and Hauser, C. (1995). Requirement for neuregulin receptor erbB2 in neural and cardiac development. *Nature* **378**, 394-398.

Leung, C., Lu, X., Liu, M. and Feng, Q. (2014). Rac1 signaling is critical to cardiomyocyte polarity and embryonic heart development. *Journal of the American Heart Association* **3**, e001271.

Liu, J., Bressan, M., Hassel, D., Huisken, J., Staudt, D., Kikuchi, K., Poss, K. D., Mikawa, T. and Stainier, D. Y. (2010). A dual role for ErbB2 signaling in cardiac trabeculation. *Development* **137**, 3867-3875.

Lyons, I., Parsons, L. M., Hartley, L., Li, R., Andrews, J. E., Robb, L. and Harvey, R. P. (1995). Myogenic and morphogenetic defects in the heart tubes of murine embryos lacking the homeo box gene Nkx2-5. *Genes & development* **9**, 1654-1666.

Manninen, A. (2015). Epithelial polarity - Generating and integrating signals from the ECM with integrins. *Experimental cell research* **334**, 337-349.

Marchionni, M. A. (1995). Cell-cell signalling. neu tack on neuregulin. *Nature* **378**, 334-335.

Marone, R., Hess, D., Dankort, D., Muller, W. J., Hynes, N. E. and Badache, A. (2004). Memo mediates ErbB2-driven cell motility. *Nature cell biology* **6**, 515-522.

McNally, E. and Dellefave, L. (2009). Sarcomere mutations in cardiogenesis and ventricular noncompaction. *Trends in cardiovascular medicine* **19**, 17-21.

Meira, M., Masson, R., Stagljar, I., Lienhard, S., Maurer, F., Boulay, A. and Hynes, N. E. (2009). Memo is a cofilin-interacting protein that influences PLCgamma1 and cofilin activities, and is essential for maintaining directionality during ErbB2-induced tumor-cell migration. *Journal of cell science* **122**, 787-797.

Meyer, D., Yamaai, T., Garratt, A., Riethmacher-Sonnenberg, E., Kane, D., Theill, L. E. and Birchmeier, C. (1997). Isoform-specific expression and function of neuregulin. *Development* **124**, 3575-3586.

Millarte, V. and Farhan, H. (2012). The Golgi in cell migration: regulation by signal transduction and its implications for cancer cell metastasis. *TheScientificWorldJournal* **2012**, 498278.

Mitchison, T. and Kirschner, M. (1984). Dynamic instability of microtubule growth. *Nature* **312**, 237-242.

Mitchison, T. J. (1986). The role of microtubule polarity in the movement of kinesin and kinetochores. *Journal of cell science. Supplement* **5**, 121-128.

Mohammad, I., Arora, P. D., Naghibzadeh, Y., Wang, Y., Li, J., Mascarenhas, W., Janmey, P. A., Dawson, J. F. and McCulloch, C. A. (2012). Flightless I is a focal adhesion-associated actin-capping protein that regulates cell migration. *FASEB journal : official publication of the Federation of American Societies for Experimental Biology* **26**, 3260-3272.

Molkentin, J. D., Lin, Q., Duncan, S. A. and Olson, E. N. (1997). Requirement of the transcription factor GATA4 for heart tube formation and ventral morphogenesis. *Genes & development* **11**, 1061-1072.

Moriyama, K., Iida, K. and Yahara, I. (1996). Phosphorylation of Ser-3 of cofilin regulates its essential function on actin. *Genes to cells : devoted to molecular & cellular mechanisms* **1**, 73-86.

Naganawa, Y. and Hirata, H. (2011). Developmental transition of touch response from slow muscle-mediated coilings to fast muscle-mediated burst swimming in zebrafish. *Developmental biology* **355**, 194-204.

Nelson, W. J. (1991). Cytoskeleton functions in membrane traffic in polarized epithelial cells. *Seminars in cell biology* **2**, 375-385.

Nicklas, R. B. (1971). Mitosis. *Advances in cell biology* **2**, 225-297.

Nogales, E., Wolf, S. G. and Downing, K. H. (1998). Structure of the alpha beta tubulin dimer by electron crystallography. *Nature* **391**, 199-203.

Olmsted, J. B. and Borisy, G. G. (1973). Microtubules. *Annual review of biochemistry* **42**, 507-540.

Opitz, J. M. and Clark, E. B. (2000). Heart development: an introduction. *American journal of medical genetics* **97**, 238-247.

Otterbein, L. R., Graceffa, P. and Dominguez, R. (2001). The crystal structure of uncomplexed actin in the ADP state. *Science* **293**, 708-711.

Ozcelik, C., Erdmann, B., Pilz, B., Wettschureck, N., Britsch, S., Hubner, N., Chien, K. R., Birchmeier, C. and Garratt, A. N. (2002). Conditional mutation of the ErbB2 (HER2) receptor in cardiomyocytes leads to dilated cardiomyopathy. *Proceedings of the National Academy of Sciences of the United States of America* **99**, 8880-8885.

Pelham, R. J. and Chang, F. (2002). Actin dynamics in the contractile ring during cytokinesis in fission yeast. *Nature* **419**, 82-86.

Pollard, T. D. (2007). Regulation of actin filament assembly by Arp2/3 complex and formins. *Annual review of biophysics and biomolecular structure* **36**, 451-477.

Popow-Wozniak, A., Mazur, A. J., Mannherz, H. G., Malicka-Blaszkiewicz, M. and Nowak, D. (2012). Cofilin overexpression affects actin cytoskeleton organization and migration of human colon adenocarcinoma cells. *Histochemistry and cell biology* **138**, 725-736.

Raeker, M. O., Shavit, J. A., Dowling, J. J., Michele, D. E. and Russell, M. W. (2014). Membrane-myofibril cross-talk in myofibrillogenesis and in muscular dystrophy pathogenesis: lessons from the zebrafish. *Frontiers in physiology* **5**, 14.

Ralston, E. (1993). Changes in architecture of the Golgi complex and other subcellular organelles during myogenesis. *The Journal of cell biology* **120**, 399-409.

Reischauer, S., Arnaout, R., Ramadass, R. and Stainier, D. Y. (2014). Actin binding GFP allows 4D in vivo imaging of myofilament dynamics in the zebrafish heart and the identification of Erbb2 signaling as a remodeling factor of myofibril architecture. *Circulation research* **115**, 845-856.

Rogalski, A. A. and Singer, S. J. (1984). Associations of elements of the Golgi apparatus with microtubules. *The Journal of cell biology* **99**, 1092-1100.

Roy, A. L. (2001). Biochemistry and biology of the inducible multifunctional transcription factor TFII-I. *Gene* **274**, 1-13.

Samarel, A. M. (2005). Costameres, focal adhesions, and cardiomyocyte mechanotransduction. *American journal of physiology. Heart and circulatory physiology* **289**, H2291-2301.

Schaller, M. D. (2004). FAK and paxillin: regulators of N-cadherin adhesion and inhibitors of cell migration? *The Journal of cell biology* **166**, 157-159.

Schier, A. F., Neuhauss, S. C., Helde, K. A., Talbot, W. S. and Driever, W. (1997). The one-eyed pinhead gene functions in mesoderm and endoderm formation in zebrafish and interacts with no tail. *Development* **124**, 327-342.

Sedmera, D., Reckova, M., Rosengarten, C., Torres, M. I., Gourdie, R. G. and Thompson, R. P. (2005). Optical mapping of electrical activation in the developing heart. *Microscopy and microanalysis : the official journal of Microscopy Society of America, Microbeam Analysis Society, Microscopical Society of Canada* **11**, 209-215.

Sedmera, D. and Thomas, P. S. (1996). Trabeculation in the embryonic heart. *BioEssays : news and reviews in molecular, cellular and developmental biology* **18**, 607.

Sehnert, A. J., Huq, A., Weinstein, B. M., Walker, C., Fishman, M. and Stainier, D. Y. (2002). Cardiac troponin T is essential in sarcomere assembly and cardiac contractility. *Nature genetics* **31**, 106-110.

Sorrentino, V. and Gerli, R. (2003). Structure and molecular organisation of the sarcoplasmic reticulum of skeletal muscle fibers. *Italian journal of anatomy and embryology = Archivio italiano di anatomia ed embriologia* **108**, 65-76.

Stainier, D. Y. and Fishman, M. C. (1992). Patterning the zebrafish heart tube: acquisition of anteroposterior polarity. *Developmental biology* **153**, 91-101.

Stainier, D. Y., Kontarakis, Z. and Rossi, A. (2015). Making sense of anti-sense data. *Developmental cell* **32**, 7-8.

Stainier, D. Y., Lee, R. K. and Fishman, M. C. (1993). Cardiovascular development in the zebrafish. I. Myocardial fate map and heart tube formation. *Development* **119**, 31-40.

Stainier, D. Y., Weinstein, B. M., Detrich, H. W., 3rd, Zon, L. I. and Fishman, M. C. (1995). Cloche, an early acting zebrafish gene, is required by both the endothelial and hematopoietic lineages. *Development* **121**, 3141-3150.

Staudt, D. and Stainier, D. (2012). Uncovering the molecular and cellular mechanisms of heart development using the zebrafish. *Annual review of genetics* **46**, 397-418.

Staudt, D. W., Liu, J., Thorn, K. S., Stuurman, N., Liebling, M. and Stainier, D. Y. (2014). High-resolution imaging of cardiomyocyte behavior reveals two distinct steps in ventricular trabeculation. *Development* **141**, 585-593.

Tanaka, M., Chen, Z., Bartunkova, S., Yamasaki, N. and Izumo, S. (1999). The cardiac homeobox gene Csx/Nkx2.5 lies genetically upstream of multiple genes essential for heart development. *Development* **126**, 1269-1280.

Tassin, A. M., Maro, B. and Bornens, M. (1985a). Fate of microtubule-organizing centers during myogenesis in vitro. *The Journal of cell biology* **100**, 35-46.

Tassin, A. M., Paintrand, M., Berger, E. G. and Bornens, M. (1985b). The Golgi apparatus remains associated with microtubule organizing centers during myogenesis. *The Journal of cell biology* **101**, 630-638.

Telley, I. A. and Denoth, J. (2007). Sarcomere dynamics during muscular contraction and their implications to muscle function. *Journal of muscle research and cell motility* **28**, 89-104.

Tenin, G., Clowes, C., Wolton, K., Krejci, E., Wright, J. A., Lovell, S. C., Sedmera, D. and Hentges, K. E. (2014). Erbb2 is required for cardiac atrial electrical activity during development. *PloS one* **9**, e107041.

Tidball, J. G. (1991). Force transmission across muscle cell membranes. *Journal of biomechanics* **24 Suppl 1**, 43-52.

Vavylonis, D., Yang, Q. and O'Shaughnessy, B. (2005). Actin polymerization kinetics, cap structure, and fluctuations. *Proceedings of the National Academy of Sciences of the United States of America* **102**, 8543-8548.

von Hofsten, J., Elworthy, S., Gilchrist, M. J., Smith, J. C., Wardle, F. C. and Ingham, P. W. (2008). Prdm1- and Sox6-mediated transcriptional repression specifies muscle fibre type in the zebrafish embryo. *EMBO reports* **9**, 683-689.

Watanabe, T., Noritake, J. and Kaibuchi, K. (2005). Regulation of microtubules in cell migration. *Trends in cell biology* **15**, 76-83.

Weinberg, E. S., Allende, M. L., Kelly, C. S., Abdelhamid, A., Murakami, T., Andermann, P., Doerre, O. G., Grunwald, D. J. and Riggleman, B. (1996). Developmental regulation of zebrafish MyoD in wild-type, no tail and spadetail embryos. *Development* **122**, 271-280.

Woychik, R. P., Maas, R. L., Zeller, R., Vogt, T. F. and Leder, P. (1990). 'Formins': proteins deduced from the alternative transcripts of the limb deformity gene. *Nature* **346**, 850-853.

Yang, J., Bucker, S., Jungblut, B., Bottger, T., Cinnamon, Y., Tchorz, J., Muller, M., Bettler, B., Harvey, R., Sun, Q. Y., et al. (2012). Inhibition of Notch2 by Numb/Numblike controls myocardial compaction in the heart. *Cardiovascular research* **96**, 276-285.

Yeaman, C., Grindstaff, K. K. and Nelson, W. J. (1999). New perspectives on mechanisms involved in generating epithelial cell polarity. *Physiological reviews* **79**, 73-98.

Yelon, D. (2001). Cardiac patterning and morphogenesis in zebrafish. *Developmental dynamics : an official publication of the American Association of Anatomists* **222**, 552-563.

Yelon, D., Horne, S. A. and Stainier, D. Y. (1999). Restricted expression of cardiac myosin genes reveals regulated aspects of heart tube assembly in zebrafish. *Developmental biology* **214**, 23-37.

Yelon, D. and Stainier, D. Y. (1999). Patterning during organogenesis: genetic analysis of cardiac chamber formation. *Semin Cell Dev Biol* **10**, 93-98.

Zaal, K. J., Reid, E., Mousavi, K., Zhang, T., Mehta, A., Bugnard, E., Sartorelli, V. and Ralston, E. (2011). Who needs microtubules? Myogenic reorganization of MTOC, Golgi complex and ER exit sites persists despite lack of normal microtubule tracks. *PloS one* **6**, e29057.

Zaoui, K., Benseddik, K., Daou, P., Salaun, D. and Badache, A. (2010). ErbB2 receptor controls microtubule capture by recruiting ACF7 to the plasma membrane of migrating cells. *Proceedings of the National Academy of Sciences of the United States of America* **107**, 18517-18522.

Zhang, W., Chen, H., Qu, X., Chang, C. P. and Shou, W. (2013). Molecular mechanism of ventricular trabeculation/compaction and the pathogenesis of

the left ventricular noncompaction cardiomyopathy (LVNC). *American journal of medical genetics. Part C, Seminars in medical genetics* **163C**, 144-156.

Acknowledgements

I take the honor to thank

all my colleagues and friends for their support and motivation during my training as a research technician, as a biology student and during my Ph.D. studies.

Prof. Dr. Felix B. Engel and Prof Dr. Didier Stainier for giving me the opportunity to perform my thesis work at the Max Planck Institute for Heart and Lung Research.

My doctoral supervisor Prof. Dr. Felix B. Engel for his kind guidance. I would like to thank him for his encouragement and motivation. I am especially thankful for his very positive way of being and his believe in my research and me.

Prof. Dr. Didier Stainier for the opportunity to continue my Ph.D. research in his lab and for his constant guidance. I want to specially thank him for his honest criticism, which helped me to find my way.

My colleagues and friends in Prof. Dr. Felix B. Engel's laboratory for their help, motivation and inspiration while doing science but also for the best coffee breaks ever. I would like to thank Amna Sajjad, Subhajit Ghosh, Machteld J. van Amerongen, Tatyana Novoyatleva, Ingrid Hauck-Schmalenberger, Ajit Magadum, Marina Leone, David Zebrovski, Petra Freund and Chinmoy Patra.

Chinmoy Patra who taught me a lot about zebrafish and who has an unbreakable love for science which made it a pleasure to work with him.

My colleagues and friends in Prof. Dr. Didier Stainier's laboratory for their help and expertise with challenging experiments. I would like to thank Alethia Villasenor, Oliver Stone, Sven Reischauer, Carol Yang, Pourya Sarvari, Bilge Reischauer, Seyed Javad Rasouli, Radhan Ramadass, Marianne Ploch, Silvia Parajes, Brian Njaine, Sophie Mucenieks, Sharon Meaney-Gardian, Matsuoka Ryota, Jason Lai, Hyouk-Bum Kwon, Zacharias Kontarakis, Ziba Jaberansari, Almary Guerra Rodriguez, Gerri Claudia, Sebastien Gauvrit, Sabine Fischer, Deepika Dogra, Michelle Collins, Anoop Cherian, Markus Bussen, Carmen Buettner, Avdesh Avdesh, Suchit Ahuja and in particular Jenny Pestel.

Prof. Dr. Georg Auburger who always supported me during the time in his laboratory as a research technician and who motivated me to pursue my dream of becoming a developmental biologist.

My colleagues and friends in Prof. Dr. Georg Auburger's laboratory for a really good time and for teaching me almost everything. I would like to thank Suzana Gispert-Sanchez, Joachim Nowock, Alexander Kurz, Birgitt Meseck-Selchow, Marina Talamini,

Curriculum Vitae

Curriculum Vitae

Filomena Ricciardi

geboren am 05.07.1982, in Frankfurt am Main

Schnurstrasse 34, 61231 Bad Nauheim, Hessen
phone: +49 0160 944 25463,
email: ricciardi.filomena@gmail.com

BERUF UND AUSBILDUNG:

05/2011-heute Doktorandin	**Max Planck Institut für Herz- und Lungenforschung**, **Bad Nauheim, Deutschland** In den Laboratorien von Prof. Felix B. Engel und Prof. Didier Stainier Erforschung von muskulären kontraktilen Strukturen und Zellpolarisation während der Herztrabekulation mit Hilfe der CRISPR/CAS Technologie und der Herstellung von transgenen Zebrafisch Linien sowie Charakterisierung von Phänotypen durch Konfokal- und Spinning-Disc Mikroskopie.
10/2006-04/2011 Diplom Student	**Goethe Universität, Frankfurt am Main, Deutschland** Diplomarbeit am Max Planck Institut für Herz- und Lungenforschung Im Laboratorium von Prof. Felix B. Engel Beschreibung der Funktion des HDAC-Komplex Gens Fam60A während der Herz und Hirn Entwicklung in TALEN-induzierten Zebrafischmutanten, im Knockdown-Modell und mit Hilfe von Überexpressionsversuchen. Untersuchung von Zelldifferenzierung und Zellmigration durch *in situ* Hybridisierung, Micro Array Genexpressions-Analysen und Konfokale Mikroskopie.
11/2001-03/2010 Anstellung	**Goethe Universität, Frankfurt am Main, Deutschland** Biologisch Technische Assistentin (BTA) Im Laboratorium von Prof. Georg Auburger Charakterisierung der Proteinfunktion der mitochondrialen Serin/Threonin Kinase Pink1 (PARK6 Gen) durch

Etablierung einer Methode zur Aufreinigung von Proteinen aus *E. coli* für die Durchführung von Kinase-Autophosphorylations Versuchen und zur Herstellung von Antikörpern.

08/1999-07/2001	**Fresenius Fachhochschule, Idstein**
Ausbildung	Beruflische Asubildung zur BTA

PRAKTIKA:

07/2009-9/2009	**Praktikum Genetik an der Goethe Universität,** Prof. Osiewacz
	Herstellung von Glyoxalase defizienten *Podospora anserina* Stämmen durch Homologe Rekombination

05/2009-6/2009	**Praktikum Zellbiologie an der Goethe Universität,** Prof. Bereiter-Hahn
	Quantifizierung des mitochondrialen Membranpotentials durch Zellfärbungen mit TMRM (Tetramethylrhodamine methyl ester) und Fluoreszenz-Intensitäts-Messungen von Fluoreszenzmikroskopischen Aufnahmen.

01/2009-03/2009	**Praktikum Neurobiologie an der Goethe University,** Prof. Auburger
	Genomweite SNP-Analyse in Dystonia type2 (DYT2) Patienten und Sequenzierung des potentiellen Krankheitsgens Dopamine Decarboxylase (DDC).

08/2001-10/2001	**Hoechst Biochemie (Novartis), Frankfurt am Main**
	Verbesserung der mikrobiellen Antibiotika Produktion durch Testung von verschiedenen Filtrationsmethoden.

PUBLIKATIONEN (in Vorbereitung):

Cardiac trabeculation is dependent on Flightless I mediated focal adhesion formation and myofibril bundling.
Filomena Ricciardi, Michael P. Housley, Felix B. Engel, Didier Y.R. Stainier, Sven Reischauer (in preparation)

Cavin4/Murc is required for skeletal muscle development and function in zebrafish.
Michael P. Housley, **Filomena Ricciardi**, Oliver A. Stone, Sawa Kostin, and Didier Y.R. Stainier (in preparation)

Centrosome disassembly promotes a post-mitotic state in mammalian cardiomyocytes.
David C. Zebrowski, Silvia Vergarajauregui, Robert Becker, **Filomena Ricciardi**, Nathalie Falk, Andreas Giess, Felix B. Engel (submitted)

PUBLIKATIONEN:

Organ-specific function of adhesion G protein-coupled receptor GPR126 is domain dependent.
Patra C, van Amerongen MJ, Ghosh S, **Ricciardi F**, Sajjad A, Novoyatleva T, Mogha A, Monk KR, Muhlfeld C, Engel FB.
Proc Natl Acad Sci USA. 2013 Oct; 15;110(42):16898-903.

The functional properties of nephronectin: an adhesion molecule for cardiac tissue engineering.
Patra C, **Ricciardi F**, Engel FB.
Biomaterials. 2012 Jun;33(17):4327-35.

Modulation of the glyoxalase system in the aging model Podospora anserina: effects on growth and lifespan. Scheckhuber CQ, Mack SJ, Strobel I, **Ricciardi F**, Gispert S, Osiewacz HD.
Aging (Albany NY). 2010 Dec;2(12):969-80.

Genome-wide association study of intracranial aneurysm identifies three new risk loci.
Yasuno K, Bilguvar K, Bijlenga P, Low SK, Krischek B, Auburger G, Simon M, Krex D, Arlier Z, Nayak N, Ruigrok YM, Niemelä M, Tajima A, von und zu Fraunberg M, Dóczi T, Wirjatijasa F, Hata A, Blasco J, Oszvald A, Kasuya H, Zilani G, Schoch B, Singh P, Stüer C, Risselada R, Beck J, Sola T, **Ricciardi F**, Aromaa A, Illig T, Schreiber S, van Duijn CM, van den Berg LH, Perret C, Proust C, Roder C, Ozturk AK, Gaál E, Berg D, Geisen C, Friedrich CM, Summers P, Frangi AF, State MW, Wichmann HE, Breteler MM, Wijmenga C, Mane S, Peltonen L, Elio V, Sturkenboom MC, Lawford P, Byrne J, Macho J, Sandalcioglu EI, Meyer B, Raabe A, Steinmetz H, Rüfenacht D, Jääskeläinen JE, Hernesniemi J, Rinkel GJ, Zembutsu H, Inoue I, Palotie A, Cambien F, Nakamura Y, Lifton RP, Günel M.
Nat Genet. 2010 May;42(5):420-5.

Enhanced vulnerability of PARK6 patient skin fibroblasts to apoptosis induced by proteasomal stress.
Klinkenberg M, Thurow N, Gispert S, **Ricciardi F**, Eich F, Prehn JH, Auburger G, Kögel D.
Neuroscience. 2010 Mar 17;166(2):422-34.

The mitochondrial kinase PINK1, stress response and Parkinson's disease.
Jendrach M, Gispert S, **Ricciardi F**, Klinkenberg M, Schemm R, Auburger G.
J Bioenerg Biomembr. 2009 Dec;41(6):481-6. Review.

Parkinson phenotype in aged PINK1-deficient mice is accompanied by progressive mitochondrial dysfunction in absence of neurodegeneration.
Gispert S, **Ricciardi F**, Kurz A, Azizov M, Hoepken HH, Becker D, Voos W, Leuner K, Müller WE, Kudin AP, Kunz WS, Zimmermann A, Roeper J, Wenzel D, Jendrach M, García-Arencíbia M, Fernández-Ruiz J, Huber L, Rohrer H, Barrera M, Reichert AS, Rüb U, Chen A, Nussbaum RL, Auburger G.
PLoS One. 2009 Jun 3;4(6):e5777.

Parkinson patient fibroblasts show increased alpha-synuclein expression.
Hoepken HH, Gispert S, Azizov M, Klinkenberg M, **Ricciardi F**, Kurz A, Morales-Gordo B, Bonin M, Riess O, Gasser T, Kögel D, Steinmetz H, Auburger G.
Exp Neurol. 2008 Aug;212(2):307-13.